

# ATHEROSCLEROTIC PLAQUE AND SHEAR STRESS IN CAROTID ARTERIES

*Harald Groen*

ISBN: 978-90-9025711-2

Printed by PrintPartners Ipskamp

Cover design by Harald Groen, Hanke Matlung, Hans Groen and Ton Everaers

Layout by Ton Everaers



The research described in this thesis (project number 044.01) was financially supported by the Interuniversity Cardiology Institute of the Netherlands, an institute of the Royal Dutch Academia of Science.

Financial support by the Netherlands Heart Foundation for the publication of this thesis is gratefully acknowledged.

The financial support for the publication of this thesis by Merck Sharp & Dohme B.V. and Hamamatsu Photonics Deutschland GmbH is gratefully acknowledged.

© 2010 H.C. Groen, Leiden, The Netherlands

All rights reserved. No part of this thesis may be reproduced or transmitted in any form or by any means, electronic or mechanical, including photocopying, recording, or any information storage and retrieval system, without prior written permission from the copyright owner.

# ATHEROSCLEROTIC PLAQUE AND SHEAR STRESS IN CAROTID ARTERIES

## *Aderverkalking en afschuifspanning in de halsslagader*

*Proefschrift*

ter verkrijging van de graad van doctor aan de  
Erasmus Universiteit Rotterdam  
op gezag van de  
Rector Magnificus

Prof.dr. H.G. Schmidt,

en volgens besluit van het College voor Promoties.

De openbare verdediging zal plaatsvinden op  
*woensdag 10 november 2010* om 13:30 uur

door

**Harald Christian Groen**  
geboren te Haarlem



## PROMOTIECOMMISSIE

*Promotor* Prof.dr.ir. A.F.W. van der Steen

*Co-promotoren* Dr.ir. J.J. Wentzel  
Dr. A. van der Lugt

*Overige Leden* Prof.dr. W.J. Niessen  
Prof.dr.ir J.H.C. Reiber  
Prof.dr. P.J. de Feyter

# CONTENTS

1	Introduction	7
2	Atherosclerotic plaque surface morphology in the carotid bifurcation assessed with multidetector computed tomography angiography	27
3	Atherosclerotic plaque rupture in carotid arteries is associated with higher wall shear stress and plaque thickness	47
4	Plaque rupture in the carotid artery is localized at the high shear stress region: a case report	63
5	Three-dimensional registration of histology of human atherosclerotic carotid plaques to <i>in vivo</i> imaging	71
6	Calcification locates to transglutaminases in advanced human atherosclerotic lesions	89
7	MRI-based quantification of outflow boundary conditions for computational fluid dynamics of stenosed human carotid arteries	105
8	Short-term flow increase destabilizes advanced plaques in ApoE <sup>-/-</sup> mice by increasing lipid content	125
9	General discussion	143
	Summary	156
	Samenvatting	160
	List of publications	164
	Dankwoord	168
	Curriculum Vitae	172
	PhD Portfolio	174



CHAPTER

# 1

INTRODUCTION

## INTRODUCTION

The human is a very sophisticated organism in which adaptation is the key to its survival [1]. During a lifetime, the human body is exposed to a wide variety of stimuli. Some of them are self-inflicted while others arise from the environment and nature itself. Communication plays an important role in the response to these stimuli. The main signal transduction in the human body is organized by electrical signals through nerves or by transportation of biomolecular signals through blood vessels. These blood vessels also provide the organs with nutrients and oxygen. When these communication channels are compromised, the human body will try to repair them or find alternative channels.

Atherosclerosis is an inflammatory disease affecting the arterial blood vessels. The prevalence of atherosclerosis leading to cardiovascular disease is 36.3% [2] and the disease is at the top of the list of the 15 leading causes of death in the USA [3]. If the carotid arteries (which supply the brain with blood) are affected the disease can lead to a stroke, which is the third most common cause of death [3] and is also responsible for 5 million permanently disabled persons per year world wide [4]. Removal of the obstructing atherosclerotic plaque in the carotid bifurcation has reduced the risk of a stroke [5-10], but more knowledge on the development of atherosclerotic disease is required to improve treatment.

### *Atherosclerosis*

Atherosclerosis is a systemic disease, which is characterized by thickening of the arterial wall with accumulation of cholesterol in the intima (Figure 1-1). In a later stage of the disease calcifications are observed. Although the first publications on atherosclerosis were published more than 100 years ago [11], the ancient Egyptians were reported to suffer from the disease [12]. In 1913, Nikolai Anitschkow showed that cholesterol-fed rabbits had changes in the vessel wall eventually leading to atherosclerosis [13]. This finding prompted the search for additional factors that are responsible for, or contribute to, the initiation and progression of the disease. Currently a large number of systemic risk factors are known, i.e. high levels of low density lipid (LDL) cholesterol, high blood pressure, smoking, diabetes, obesity, physical inactivity, age and family history [4]. Apart



from these biological factors, biomechanical forces are also involved in the initiation and development of the plaque.

### *Plaque growth and wall shear stress*

If plaques develop in a patient, these plaques are localized at the inner curves of vessels and at bifurcations [14-16]. At these specific locations, the dragging force of the flowing blood acting on the vessel wall, called the wall shear stress (WSS), is low and/or oscillating [17]. This low WSS results in dysfunctional endothelial cells which, combined with systemic risk factors, results in atherosclerosis at these specific geometrical locations [18-21], and even at a young age [22,23].

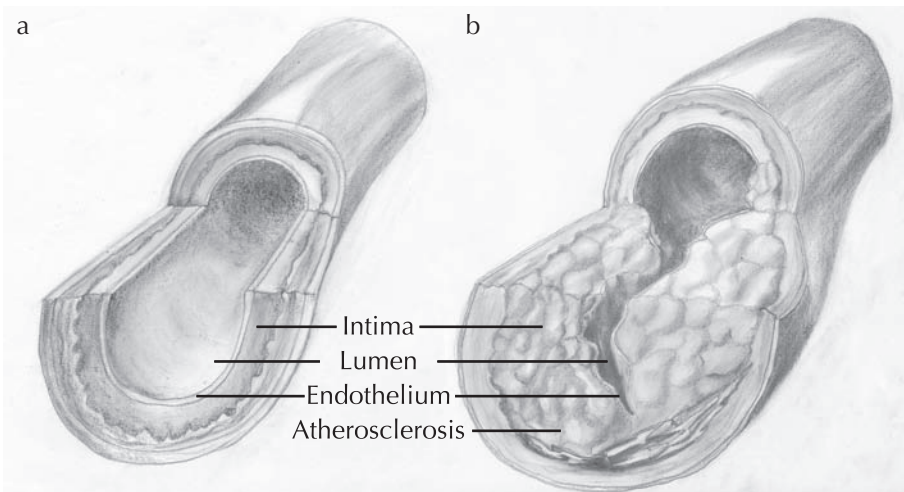


**Figure 1-1:** a) Normal vessel wall; b) Atherosclerotic thickening of the vessel wall. © J.M.Groen

Normally, averaged WSS is around 1.2 Pa in healthy human carotid arteries [24], a very small value compared to tensile stresses induced by the blood pressure that are 10,000 times higher. Despite this small value, endothelial cells covering the inside of the vessels (Figure 1-1b) are thought to be the main sensors for the WSS [25]. Endothelial cells respond to variations in WSS by regulating vascular tone and dimension of the blood vessels (remodeling), aiming to maintain a healthy physiological WSS value [26-28]. This regulation of the endothelium is performed by production of local or systemic vasodilators, such as nitric oxide (NO) and endothelial-derived hyperpolarizing factor (EDHF), and vasoconstrictors like endothelin 1 (ET-1) [29].

Healthy endothelial cells are quiescent and align in the direction of the flow. Dysfunctional endothelial cells are no longer in a healthy polygonal shape, but are activated and recruit monocytes [30]. Furthermore, both the apoptotic rate and oxidative stress of the endothelial cells are increased [20]. It is at these dysfunctional locations that LDL particles can enter the vessel wall and, once oxidized, enhance the inflammatory response and stimulate the migration and proliferation of smooth muscle cells into the growing lesion [31-33]. As such, dysfunctional endothelial cells are considered to be responsible for the initial phase of atherosclerosis in regions with low and/or oscillating WSS. Since the influx of material is larger than the efflux, the atherosclerotic plaque becomes larger, containing cell debris (necrotic core), lipids, cholesterol crystals, macrophages and, at a later stage, calcified areas [34-36].

The vessel wall initially compensates for the plaque accumulation by outward remodeling [37] to maintain a sufficient blood supply to downstream organs; a mechanism known to be regulated by the local WSS [38]. This compensatory enlargement of the lumen continues until 40% of the internal elastic lamina area is occupied by the atherosclerotic lesion, after which the plaque will grow into the lumen; a process which is potentially accelerated by subclinical plaque ruptures [39]. Moreover, due to the outward compensation of the vessel, the WSS patterns remain in favor of plaque build-up [40]. Thus, atherosclerotic plaque build-up continues without leading to vessel obstruction and subsequent clinical symptoms.

### *Vulnerable plaque and wall shear stress*

If plaque growth is accommodated by the vessel wall because of positive remodeling, the shear stress remains the same regardless of the extent of plaque growth. If vascular remodeling is excessive, it overcompensates for plaque growth and can result in larger lumen areas than the initial state before plaque growth. In fact, if the flow remains the same, the WSS will decrease in such vessels. This WSS decrease is thought to further stimulate pro-atherogenic processes and as such could aggravate plaque destabilisation [41].

With the currently available techniques it is impossible to identify in advance the plaque that will lead to clinical symptoms. However, a number of histological characteristics have been identified which are associ-

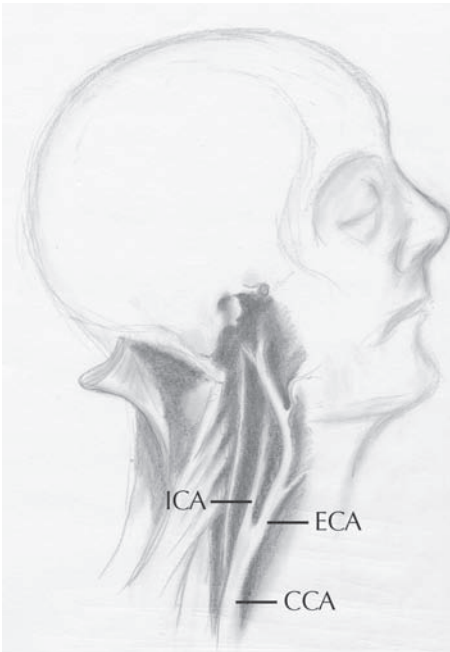


**Figure 1-2:** The carotid bifurcation with the external carotid artery (ECA) supplying the head and neck with blood, and the internal carotid artery (ICA) supplying the brain with blood, both branching off from the common carotid artery (CCA). © J.M. Groen

ated with rupture-prone plaques, called “vulnerable plaques” [42]. Vulnerable plaques are expansively remodeled, contain a large, lipid-rich atheromatous core and are covered by a thin, macrophage and lymphocyte infiltrated cap with a decreased number of smooth muscle cells [35,42-44]. If these plaques rupture, the contents of the plaque cause local thrombus formation: blocking either the entire vessel or leading to embolisation of thrombus and subsequent occlusion of more distally located vessels. If atherosclerotic plaque rupture in carotid arteries (Figure 1-2), this results in a transient ischemic attack (TIA) or stroke.

When lumen narrowing occurs, the upstream part of the plaque is exposed to a high WSS while the downstream part is still exposed

to low WSS. Thus, the change in lumen diameter due to plaque growth will influence the blood flow pattern and therefore the WSS [40]. Even in an inflammatory environment, endothelial cells are capable of responding to signals induced by the WSS [45,46]. Therefore, the low shear stress region of the plaque will remain athero-prone while the high shear stress region is thought to activate alternative signaling pathways leading to matrix degradation and eventually resulting in destabilization of the cap covering the plaque [47]. Weakening of the cap will eventually result in plaque rupture.

Understanding the development of the vulnerable plaque and the role of WSS in the progression of disease requires both the visualization of the atherosclerotic disease and the measurement or calculation of wall shear stress.

### *Imaging atherosclerosis*

Preferably, imaging of atherosclerosis is performed non-invasively to minimize potential damage to the patient due to the imaging procedure itself. Different techniques are available which depend either on the propagation of sound (ultrasound: US), or the absorbance of radiation (computed tomography: CT), or on the magnetic properties of tissue (magnetic resonance imaging: MRI). Each technique has its own advantages and disadvantages for imaging atherosclerosis. Since, in this thesis, plaques located in the carotid bifurcation are investigated, only the imaging methods used to assess atherosclerosis in carotid arteries are discussed.

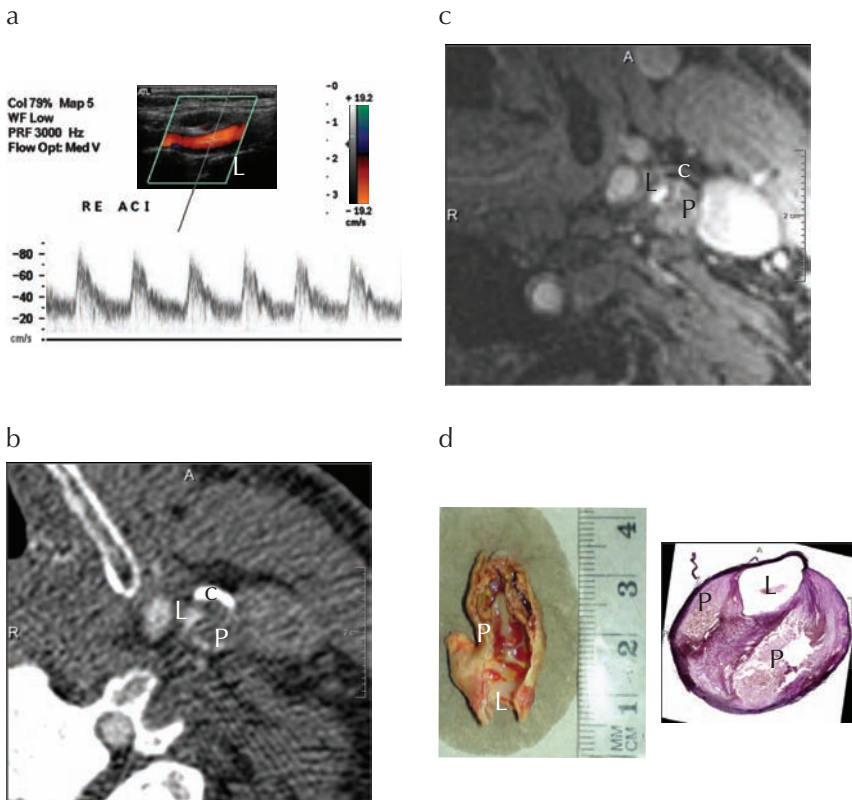


**Figure 1-3:** Overview of imaging modalities visualizing carotid atherosclerosis illustrated by a stenosed plaque in the right internal carotid artery. **a)** Color-doppler ultrasound using an ATL HDI 3000 device and a 12 Mhz transducer; **b)** Computed tomography angiography using the Siemens Sensation 64 CT scanner; **c)** 3DT1-weighted Magnetic Resonance Imaging using a 3-Tesla GE medical system; **d)** Image of the plaque after removal by the vascular surgeon, together with a histological slice stained with Elastin van Gieson. L=Lumen, P=Plaque, c=Calcification.

### *Ultrasound*

Ultrasound has a high temporal and spatial resolution depending on the frequency, i.e. a 7.5 MHz probe has a resolution up to 0.5 mm axial and 0.6 mm lateral with the focal spot at 3.0 cm depth [48]. Ultrasound systems are available in both 2D and 3D and are relatively inexpensive. Ultrasound cannot penetrate dense structures like bone and dense calcifications; the tissue behind these structures is masked. This technique can only be used to image superficial vessels with atherosclerosis, such as the carotid arteries (Figure 1-3a) and femoral arteries, while part of the plaque cannot be evaluated accurately. Using ultrasound, global measures of the diseased artery can be made, i.e. the intima thickness as well as the degree of area stenosis. Currently, identification of carotid plaque components using ultrasound shows a high level of intra- and interobserver variability [49]. However, recent advances in semi-automatic image analysis allowed to assess the relation between global plaque echogenicity and the presence of risk factors [50,51].

### *Computed Tomography (CT)*

Computed tomography, which is based on rotational X-ray images, allows better visualization behind dense structures compared with ultrasound. The spatial resolution is reasonable, i.e. for a 64-slice MDCTA scanner; 0.5 x 0.5 x 0.5 mm, but the temporal resolution is limited, mainly due to minimization of radiation exposure. A disadvantage of this technique is that the patients receive a radiation dose of approximately 3.4 mSv, and dense structures in the body (like bone) can cause beam hardening, blooming and streak artifacts. Visualization of the vessels is performed by administration of iodine contrast material to the blood, i.e. computed tomography angiography: CTA (Figure 1-3b). As such, CT is able to measure the vessel diameter and assess plaque morphology [52]. Apart from the calcifications and the degree of lumen stenosis, the amount of lipids and fibrous tissue inside carotid plaques can also be quantified using CT [53-55].

### *Magnetic Resonance Imaging (MRI)*

MRI does not involve radiation and is therefore considered safer for the patient than CTA. Unfortunately temporal resolution is limited and, in practice, spatial resolution is in the range of 1.0-0.7 mm using dedicated

surface coils for depiction of the carotid arteries. A relatively long scan time is needed to obtain a good signal-to-noise-ratio which, combined with sequential scan sequences, can cause moving artifacts and will further reduce the actual resolution. With MRI it is possible to use different sequences, which allows visualization of different plaque components, such as lipid, intra-plaque hemorrhage, calcifications and fibrous tissue (Figure 1-3c). In addition, the amount of inflammation in the carotid plaque can be measured with contrast agents [56-58]. Furthermore, MRI is able to measure the actual blood flow, which can provide additional information about the perfusion of e.g. the brain [59,60].

### *Histology*

The highest resolution for assessment of plaque components is obtained by histological examination. However, this requires that the actual plaque be excised, either at autopsy or during an operational procedure (Figure 1-3d). A common procedure for plaque removal from the carotid bifurcation is carotid endarterectomy (CEA), performed on symptomatic patients with more than 70% lumen stenosis, to prevent recurrent strokes [7,8]. Using classical histological processing techniques, high-resolution 2D information can be obtained where multiple stains can be used to detect and quantify different tissue types and cells. Unfortunately during tissue processing, tissue distortions and shrinkage occur affecting both the size and shape of the tissue, limiting its use for validation of imaging techniques. Obviously, this technique cannot be used to screen patients or to perform follow-up studies for evaluation of the natural history of atherosclerosis.

### *Wall shear stress assessment*

In practice, it is impossible to measure WSS *in vivo* since the very small force (i.e. around 1 Pa) has to be measured accurately exactly at the lumen border. On the other hand, WSS can be calculated by the derivative of the velocity perpendicular to the vessel wall times the viscosity of the blood. As such, the velocities very close to the wall have to be measured, from which the derivative needs to be calculated. Ultrasound measurements of the common carotid artery are able to assess the velocities close to the vessel wall [61,62]. The disadvantage of this method is that the WSS is only measured at one specific location; it would be practically impos-

sible to assess the total 3D WSS pattern of a carotid bifurcation. In MRI studies the velocity profile in the vessel has been measured and, based on this profile, the slope of the velocity at the vessel wall has been estimated [63,64]. The disadvantage of this method for estimation of the velocities near the vessel wall in the carotid bifurcation is the low resolution and partial volume effects, especially at the site of the stenosis.

### *Computational fluid dynamics (CFD)*

Another way to estimate WSS is by using computational fluid dynamics (CFD). This method simulates the flowing blood through the vessel and is able to estimate the WSS at each location on the vessel wall. This simulation is based on solving the Navier-Stokes equations, describing the viscous behavior of a fluid. For blood flow simulation, the viscosity is preferably modeled as a shear-thinning fluid [65], as this takes into account the non-Newtonian behavior of blood. Boundaries specify the domain in which the simulation is performed. In order to reduce computational time, the boundaries are defined close to the region of interest.

For the carotid bifurcation, the domain is defined by the vessel wall, inflow through the common carotid artery (CCA) and outflow through the internal carotid arteries (ICA) and external carotid arteries (ECA) (Figure 1-2). For the finite element method, the volume is enclosed by these boundaries and filled with either linear or quadratic elements (bricks or tetrahedrals). Appropriate conditions of the boundaries have to be specified, i.e. no-slip of the vessel wall and correct measurements or assumptions of the inflows and outflows. Finally, at each nodal point in the domain, the CFD software estimates the solution of the Navier-Stokes equations, which results in a velocity value in the x, y and z direction as well as a pressure value. Using post-processing software, the derivative of the velocity at the vessel wall can be calculated and, subsequently, the values of the WSS by multiplying this value by the blood viscosity.

The advantage of this method is that the boundaries can be obtained by segmentation of either 3D MRI or CTA images and with appropriate boundary conditions they provide good estimations of the WSS [66-68].

### ***Problem definition and hypothesis***

A remarkable observation of ruptured plaques in the carotid arteries, visible as a cavity filled with blood outside the lumen (ulcers), is the predominately upstream location with respect to the minimal lumen diameter [69-71]. No explanation for this predilection site of plaque rupture is currently available, although there is evidence that the composition of the upstream part of the plaque is different from the downstream site [71-74]. Upstream, more macrophages and less smooth muscle cells are present, indicative of more inflammation and less matrix synthesis upstream. Due to the narrowing of the vessel, the upstream region of the plaque is exposed to higher WSS than the downstream region. Elevated WSS is known to cause vessel wall atrophy of an established neointima [75]. As such, upstream matrix breakdown by plasmin, matrix metalloproteinase and smooth muscle cell apoptosis could be driven by the upstream high WSS, resulting in a biological deterioration of the cap covering the plaque [47]. Indeed, high WSS was found to co-localize with the highest strain in coronary atherosclerosis, suggesting that the strength of the cap is weakened by high WSS [76]. Therefore, we hypothesized that high WSS is involved in plaque destabilization and subsequent plaque rupture.

Although non-invasive MRI and CT imaging can determine the 3D geometry of the vessel for WSS assessment and can measure the presence of lipids, calcifications and inflammation [54,77-79], these modalities cannot be used to reveal biological processes. While those detailed plaque analyses are possible using histological slices of the plaques, these slices cannot be used to assess the WSS. Combining these two techniques enables analysis of both WSS and high-resolution plaque composition. Because of the heterogeneous distribution of plaque components [80,81], accurate 3D spatial registration of histological slices to *in vivo* images is essential for this type of analysis.

Traditionally, this registration to CT or MRI is performed by manually selecting the 2D image slice that best matches a histological cross-section [54,78,82,83]. Using this method, the out-of-plane angulations, shrinkage and non-rigid deformations that may have occurred during processing of the carotid specimens are not taken into account. More advanced registration methods including in-plane rotation, translation and/or non-rigid registration, of histology to *ex vivo* modalities have been developed for brain



tissue [84-87] and vessels [88,89]. However, a framework for registering *in vivo* modalities to the histological slices of atherosclerotic plaques has not yet been developed or validated.

Such a registration framework can be used for studies relating *in vivo* WSS values with plaque composition determined by histology.

The aim of this thesis is to study the relation between WSS, plaque composition and plaque rupture. For this, three lines of research were explored:

1. The relationship between the location of plaque rupture and WSS;
2. Development of a method to study plaque composition by histology and WSS assessment based on non-invasive *in vivo* imaging;
3. The relationship between plaque composition and increased WSS.

## OUTLINE

To study plaque ruptures *in vivo*, modern 3D imaging is required that can visualize and characterize plaque ruptures. Chapter 2 describes plaque surface analysis of the carotid arteries using CTA and investigates the location of plaque rupture. Chapter 3 reports on WSS calculations based on CTA data and describes the relationship with the location of plaque rupture as assessed by CTA.

Chapter 4 describes a serial MRI dataset of a carotid plaque, imaged before and after rupture. The location of plaque rupture is analyzed with respect to the WSS values before rupture, calculated based on the geometry of the carotid artery prior to plaque rupture.

To study the relation between WSS and plaque composition in greater detail (on a tissue and cell type level), Chapter 5 presents a multi-modality registration method for carotid plaques. By obtaining different image modalities during tissue processing, distortions of the histological slices are reduced and the slices are positioned into the 3D space, as imaged pre-operatively using CTA.

In Chapter 6 a sub-section of the registration method described in Chapter 5 is used to investigate the colocalization and activity of tissue type transglutaminase (TG2) and plasma transglutaminase factor XIIIa with calcifications and macrophages in human atherosclerotic plaques.

In patients with atherosclerosis in the carotid bifurcation, different degrees of stenosis are found. Chapter 7 addresses the empirical relation between the degree of stenosis and the amount of flow through the bifurcation. This relationship can be used to estimate flow and flow division at the bifurcation for studies using CFD in the carotid arteries if no flow information is available.

To explore the causal role of high WSS and increased plaque vulnerability, Chapter 8 presents an animal study in which the flow is artificially increased at the location of a vulnerable plaque.

Finally, Chapter 9 presents a general conclusion and discussion of this work, as well as some recommendations and perspectives for the future.

## REFERENCES

1. Darwin, On the origin of species by means of natural selection, or the preservation of favoured races in the struggle for life. 5th ed, ed. J. Murray. Vol. 5th ed. 1869, London.
2. Lloyd-Jones D, et al., Heart disease and stroke statistics--2009 update: a report from the American Heart Association Statistics Committee and Stroke Statistics Subcommittee. *Circulation*, 2009. 119(3): p. 480-6.
3. Heron M, et al., Deaths: final data for 2006. *National Vital Statistics Reports*, 2009. 57(14): p. 1-134.
4. Mackay J, et al., *The Atlas of Heart Disease and Stroke*. 2004. 112.
5. Barnett HJ, et al., Causes and severity of ischemic stroke in patients with internal carotid artery stenosis. *the Journal of the American Medical Association*, 2000. 283(11): p. 1429-36.
6. Halliday A, et al., Prevention of disabling and fatal strokes by successful carotid endarterectomy in patients without recent neurological symptoms: randomised controlled trial. *Lancet*, 2004. 363(9420): p. 1491-502.
7. Beneficial effect of carotid endarterectomy in symptomatic patients with high-grade carotid stenosis. *North American Symptomatic Carotid Endarterectomy Trial Collaborators. the New England Journal of Medicine*, 1991. 325(7): p. 445-53.
8. MRC European Carotid Surgery Trial: interim results for symptomatic patients with severe (70-99%) or with mild (0-29%) carotid stenosis. *European Carotid Surgery Trialists' Collaborative Group. Lancet*, 1991. 337(8752): p. 1235-43.

9. Goldstein LB, et al., Primary prevention of ischemic stroke: a guideline from the American Heart Association/American Stroke Association Stroke Council: cosponsored by the Atherosclerotic Peripheral Vascular Disease Interdisciplinary Working Group; Cardiovascular Nursing Council; Clinical Cardiology Council; Nutrition, Physical Activity, and Metabolism Council; and the Quality of Care and Outcomes Research Interdisciplinary Working Group: the American Academy of Neurology affirms the value of this guideline. *Stroke*, 2006. 37(6): p. 1583-633.
10. Sacco RL, et al., Guidelines for prevention of stroke in patients with ischemic stroke or transient ischemic attack: a statement for healthcare professionals from the American Heart Association/American Stroke Association Council on Stroke: co-sponsored by the Council on Cardiovascular Radiology and Intervention: the American Academy of Neurology affirms the value of this guideline. *Stroke*, 2006. 37(2): p. 577-617.
11. Marchand F, Ueber Atherosclerosis. *Verhandlung der Kongresse fuer Innere Medizin. 21 Kongresse*, 1904.
12. Allam AH, et al., Computed tomographic assessment of atherosclerosis in ancient Egyptian mummies. *the Journal of the American Medical Association*, 2009. 302(19): p. 2091-4.
13. Anitschkow N and Chaladow S, Über experimentelle Cholesterinsteatose und ihre Bedeutung für die Entstehung einiger pathologischer Prozesse. *Zentralblatt für allgemeine Pathologie und pathologische Anatomie*, 1913. 24: p. 1-9.
14. VanderLaan PA, Reardon CA, and Getz GS, Site specificity of atherosclerosis: site-selective responses to atherosclerotic modulators. *Arteriosclerosis, Thrombosis, and Vascular Biology*, 2004. 24(1): p. 12-22.
15. Sabbah HN, et al., Blood velocity in the right coronary artery: relation to the distribution of atherosclerotic lesions. *the American Journal of Cardiology*, 1984. 53(8): p. 1008-12.
16. Zarins CK, et al., Carotid bifurcation atherosclerosis. Quantitative correlation of plaque localization with flow velocity profiles and wall shear stress. *Circulation Research*, 1983. 53(4): p. 502-14.
17. Ku DN, et al., Pulsatile flow and atherosclerosis in the human carotid bifurcation. Positive correlation between plaque location and low oscillating shear stress. *Arteriosclerosis*, 1985. 5(3): p. 293-302.
18. Cheng C, et al., Atherosclerotic lesion size and vulnerability are determined by patterns of fluid shear stress. *Circulation*, 2006. 113(23): p. 2744-53.
19. Dai G, et al., Distinct endothelial phenotypes evoked by arterial waveforms derived from atherosclerosis-susceptible and -resistant regions of human vasculature. *Proceedings of the National Academy of Sciences of the United States of America*, 2004. 101(41): p. 14871-6.

20. Malek AM, Alper SL, and Izumo S, Hemodynamic shear stress and its role in atherosclerosis. *Journal of the American Medical Association*, 1999. 282(21): p. 2035-42.
21. Brooks AR, Lelkes PI, and Rubanyi GM, Gene expression profiling of human aortic endothelial cells exposed to disturbed flow and steady laminar flow. *Physiological Genomics*, 2002. 9(1): p. 27-41.
22. Enos WF, Holmes RH, and Beyer J, Coronary disease among United States soldiers killed in action in Korea; preliminary report. *Journal of the American Medical Association*, 1953. 152(12): p. 1090-3.
23. Sary HC, Macrophages, macrophage foam cells, and eccentric intimal thickening in the coronary arteries of young children. *Atherosclerosis*, 1987. 64(2-3): p. 91-108.
24. Cheng C, et al., Large variations in absolute wall shear stress levels within one species and between species. *Atherosclerosis*, 2007. 195(2): p. 225-35.
25. Davies PF, Flow-mediated endothelial mechanotransduction. *Physiological Reviews*, 1995. 75(3): p. 519-60.
26. Furchgott RF and Zawadzki JV, The obligatory role of endothelial cells in the relaxation of arterial smooth muscle by acetylcholine. *Nature*, 1980. 288(5789): p. 373-6.
27. Kamiya A, et al., Roles of fluid shear stress in physiological regulation of vascular structure and function. *Biorheology*, 1988. 25(1-2): p. 271-8.
28. Kamiya A and Togawa T, Adaptive regulation of wall shear stress to flow change in the canine carotid artery. *the American Journal of Physiology*, 1980. 239(1): p. H14-21.
29. Sima AV, Stancu CS, and Simionescu M, Vascular endothelium in atherosclerosis. *Cell and Tissue Research*, 2009. 335(1): p. 191-203.
30. Libby P, Atherosclerosis: the new view. *Scientific American*, 2002. 286(5): p. 46-55.
31. Orr AW, et al., The subendothelial extracellular matrix modulates NF-kappaB activation by flow: a potential role in atherosclerosis. *Journal of Cell Biology*, 2005. 169(1): p. 191-202.
32. Cheng C, et al., Shear stress-induced changes in atherosclerotic plaque composition are modulated by chemokines. *the Journal of Clinical Investigation*, 2007. 117(3): p. 616-26.
33. Liu Y, et al., Shear stress activation of SREBP1 in endothelial cells is mediated by integrins. *Arteriosclerosis, Thrombosis, and Vascular Biology*, 2002. 22(1): p. 76-81.
34. Kapustin A and Shanahan CM, Targeting vascular calcification: softening-up a hard target. *Current Opinion in Pharmacology*, 2009. 9(2): p. 84-9.
35. Virmani R, et al., Lessons from sudden coronary death : A comprehensive morphological classification scheme for atherosclerotic lesions. *Arteriosclerosis, Thrombosis, and Vascular Biology*, 2000. 20(5): p. 1262.

36. Sary HC, et al., A definition of initial, fatty streak, and intermediate lesions of atherosclerosis. A report from the Committee on Vascular Lesions of the Council on Arteriosclerosis, American Heart Association. *Circulation*, 1994. 89(5): p. 2462-78.
37. Glagov S, et al., Compensatory enlargement of human atherosclerotic coronary arteries. *the New England Journal of Medicine*, 1987. 316(22): p. 1371-5.
38. Zarins CK, et al., Shear stress regulation of artery lumen diameter in experimental atherogenesis. *Journal of Vascular Surgery*, 1987. 5(3): p. 413-20.
39. Burke AP, et al., Healed plaque ruptures and sudden coronary death: evidence that subclinical rupture has a role in plaque progression. *Circulation*, 2001. 103(7): p. 934-40.
40. Slager C, et al., The role of shear stress in the generation of rupture-prone vulnerable plaques. *Nature Clinical Practice Cardiovascular Medicine*, 2005. 2(8): p. 401-7.
41. Chatzizisis YS, et al., Prediction of the localization of high-risk coronary atherosclerotic plaques on the basis of low endothelial shear stress: an intravascular ultrasound and histopathology natural history study. *Circulation*, 2008. 117(8): p. 993-1002.
42. Schaar JA, et al., Terminology for high-risk and vulnerable coronary artery plaques. Report of a meeting on the vulnerable plaque, June 17 and 18, 2003, Santorini, Greece. *European Heart Journal*, 2004. 25(12): p. 1077-82.
43. Virmani R, et al., Pathology of the Vulnerable Plaque. *Journal of the American College of Cardiology*, 2006. 47(8): p. C13-C18.
44. Pasterkamp G, et al., Relation of arterial geometry to luminal narrowing and histologic markers for plaque vulnerability: the remodeling paradox. *Journal of the American College of Cardiology*, 1998. 32(3): p. 655-62.
45. Tricot O, et al., Relation between endothelial cell apoptosis and blood flow direction in human atherosclerotic plaques. *Circulation*, 2000. 101(21): p. 2450-3.
46. Dimmeler S, et al., Upregulation of superoxide dismutase and nitric oxide synthase mediates the apoptosis-suppressive effects of shear stress on endothelial cells. *Arteriosclerosis, Thrombosis, and Vascular Biology*, 1999. 19(3): p. 656-64.
47. Slager C, et al., The role of shear stress in the destabilization of vulnerable plaques and related therapeutic implications. *Nature Clinical Practice Cardiovascular Medicine*, 2005. 2(9): p. 456-64.
48. Schulte-Altdorneburg G, et al., Accuracy of in vivo carotid B-mode ultrasound compared with pathological analysis: intima-media thickening, lumen diameter, and cross-sectional area. *Stroke*, 2001. 32(7): p. 1520-4.
49. Sztajzel R, Ultrasonographic assessment of the morphological characteristics of the carotid plaque. *Swiss Med Wkly*, 2005. 135(43-44): p. 635-43.

50. Andersson J, et al., The carotid artery plaque size and echogenicity are related to different cardiovascular risk factors in the elderly: the Prospective Investigation of the Vasculature in Uppsala Seniors (PIVUS) study. *Lipids*, 2009. 44(5): p. 397-403.
51. Prah U, et al., Percentage white: a new feature for ultrasound classification of plaque echogenicity in carotid artery atherosclerosis. *Ultrasound in Medicine & Biology*, 2010. 36(2): p. 218-26.
52. Goddard AJ, Mendelow AD, and Birchall D, Computed tomography angiography in the investigation of carotid stenosis. *Clinical Radiology*, 2001. 56(7): p. 523-34.
53. Wintermark M, et al., High-resolution CT imaging of carotid artery atherosclerotic plaques. *American Journal of Neuroradiology*, 2008. 29(5): p. 875-82.
54. de Weert TT, et al., In vivo characterization and quantification of atherosclerotic carotid plaque components with multidetector computed tomography and histopathological correlation. *Arteriosclerosis, Thrombosis, and Vascular Biology*, 2006. 26(10): p. 2366-72.
55. deWeert TT, et al., Assessment of atherosclerotic carotid plaque volume with multidetector computed tomography angiography. *the International Journal of Cardiovascular Imaging*, 2008. 24(7): p. 751-9.
56. Clarke S, et al., Quantitative assessment of carotid plaque composition using multicontrast MRI and registered histology. *Magnetic Resonance in Medicine*, 2003. 50(6): p. 1199-1208.
57. Saam T, et al., Quantitative evaluation of carotid plaque composition by in vivo MRI. *Arteriosclerosis, Thrombosis, and Vascular Biology*, 2005. 25(1): p. 234-9.
58. Adame I, et al., Automatic segmentation and plaque characterization in atherosclerotic carotid artery MR images. *Magnetic Resonance Materials in Physics, Biology and Medicine*, 2004. 16(5): p. 227-34.
59. Poels MM, et al., Total cerebral blood flow in relation to cognitive function: the Rotterdam Scan Study. *Journal of Cerebral Blood Flow and Metabolism*, 2008. 28(10): p. 1652-5.
60. Vernooij MW, et al., Total cerebral blood flow and total brain perfusion in the general population: the Rotterdam Scan Study. *Journal of Cerebral Blood Flow and Metabolism*, 2008. 28(2): p. 412-9.
61. Brands PJ, et al., A noninvasive method to estimate wall shear rate using ultrasound. *Ultrasound in Medicine & Biology*, 1995. 21(2): p. 171-85.
62. Samijo SK, et al., Reproducibility of shear rate and shear stress assessment by means of ultrasound in the common carotid artery of young human males and females. *Ultrasound in Medicine & Biology*, 1997. 23(4): p. 583-90.
63. Wentzel J, et al., Does shear stress modulate both plaque progression and regression in the thoracic aorta? Human study using serial magnetic resonance imaging. *Journal of the American College of Cardiology*, 2005. 45(6): p. 846-54.

64. Oyre S, et al., Accurate noninvasive quantitation of blood flow, cross-sectional lumen vessel area and wall shear stress by three-dimensional paraboloid modeling of magnetic resonance imaging velocity data. *Journal of the American College of Cardiology*, 1998. 32(1): p. 128-34.
65. Gijzen FJ, van de Vosse FN, and Janssen JD, The influence of the non-Newtonian properties of blood on the flow in large arteries: steady flow in a carotid bifurcation model. *Journal of Biomechanics*, 1999. 32(6): p. 601-8.
66. Steinman D, et al., Reconstruction of carotid bifurcation hemodynamics and wall thickness using computational fluid dynamics and MRI. *Magnetic Resonance in Medicine*, 2001. 47(1): p. 149-59.
67. Marshall I, MRI and CFD studies of pulsatile flow in healthy and stenosed carotid bifurcation models. *Journal of Biomechanics*, 2004. 37(5): p. 679-87.
68. Thomas J, et al., Reproducibility of image-based computational fluid dynamics models of the human carotid bifurcation. *Annals of Biomedical Engineering*, 2003. 31(2): p. 132-41.
69. Lovett J and Rothwell P, Site of Carotid Plaque Ulceration in Relation to Direction of Blood Flow: An Angiographic and Pathological Study. *Cerebrovascular Diseases*, 2003. 16(4): p. 369-75.
70. Masawa N, et al., Three-dimensional analysis of human carotid atherosclerotic ulcer associated with recent thrombotic occlusion. *Pathology International*, 1994. 44(10-11): p. 745-52.
71. Fagerberg B, et al., Differences in Lesion Severity and Cellular Composition between in vivo Assessed Upstream and Downstream Sides of Human Symptomatic Carotid Atherosclerotic Plaques. *Journal of Vascular Research*, 2009. 47(3): p. 221-30.
72. Dirksen MT, et al., Distribution of inflammatory cells in atherosclerotic plaques relates to the direction of flow. *Circulation*, 1998. 98(19): p. 2000-3.
73. Segers D, et al., Gelatinolytic activity in atherosclerotic plaques is highly localized and is associated with both macrophages and smooth muscle cells in vivo. *Circulation*, 2007. 115(5): p. 609-16.
74. Yilmaz A, et al., Accumulation of immune cells and high expression of chemokines/chemokine receptors in the upstream shoulder of atherosclerotic carotid plaques. *Experimental and Molecular Pathology*, 2007. 82(3): p. 245-55.
75. Mattsson EJ, et al., Increased blood flow induces regression of intimal hyperplasia. *Arteriosclerosis, Thrombosis, and Vascular Biology*, 1997. 17(10): p. 2245-9.
76. Gijzen FJ, et al., Strain distribution over plaques in human coronary arteries relates to shear stress. *American Journal of Physiology - Heart and Circulatory Physiology*, 2008. 295(4): p. H1608-14.

77. Rozie S, et al., Atherosclerotic plaque volume and composition in symptomatic carotid arteries assessed with multidetector CT angiography; relationship with severity of stenosis and cardiovascular risk factors. *European Radiology*, 2009. 19(9):2294-301.
78. Liu F, et al., Automated in vivo segmentation of carotid plaque MRI with Morphology-Enhanced probability maps. *Magnetic Resonance in Medicine*, 2006. 55(3): p. 659-68.
79. Tang TY, et al., The ATHEROMA (Atorvastatin Therapy: Effects on Reduction of Macrophage Activity) Study. Evaluation using ultrasmall superparamagnetic iron oxide-enhanced magnetic resonance imaging in carotid disease. *Journal of the American College of Cardiology*, 2009. 53(22): p. 2039-50.
80. Lovett J, Gallagher P, and Rothwell P, Reproducibility of Histological Assessment of Carotid Plaque: Implications for Studies of Carotid Imaging. *Cerebrovascular Diseases*, 2004. 18(2): p. 117-23.
81. Lovett JK, Redgrave JN, and Rothwell PM, A critical appraisal of the performance, reporting, and interpretation of studies comparing carotid plaque imaging with histology. *Stroke*, 2005. 36(5): p. 1091-7.
82. Kaazempur-Mofrad MR, et al., Characterization of the atherosclerotic carotid bifurcation using MRI, finite element modeling, and histology. *Annals of Biomedical Engineering*, 2004. 32(7): p. 932-46.
83. Wintermark M, et al., Semi-automated computer assessment of the degree of carotid artery stenosis compares favorably to visual evaluation. *Journal of the Neurological Sciences*, 2008. 269(1-2): p. 74-9.
84. Dauguet J, et al., Three-dimensional reconstruction of stained histological slices and 3D non-linear registration with in-vivo MRI for whole baboon brain. *Journal of Neuroscience Methods*, 2007. 164(1): p. 191-204.
85. Yelnik J, et al., A three-dimensional, histological and deformable atlas of the human basal ganglia. I. Atlas construction based on immunohistochemical and MRI data. *Neuroimage*, 2007. 34(2): p. 618-38.
86. Meyer CR, et al., A methodology for registration of a histological slide and in vivo MRI volume based on optimizing mutual information. *Molecular Imaging*, 2006. 5(1): p. 16-23.
87. Uberti M, et al. Registration of in vivo MR to histology of rodent brains using blockface imaging. in *Medical Imaging 2009: Biomedical Applications in Molecular, Structural, and Functional Imaging*. 2009. Lake Buena Vista, FL, USA SPIE.
88. Lowder LM, et al., Correction of distortion of histologic sections of arteries. *Journal of biomechanics*, 2007. 40(2): p. 445-50.
89. Clarke S, Validation of Automatically Classified Magnetic Resonance Images for Carotid Plaque Compositional Analysis. *Stroke*, 2005. 37(1): p. 93-7.







CHAPTER

# 2

**ATHEROSCLEROTIC PLAQUE SURFACE  
MORPHOLOGY IN THE CAROTID BIFURCATION  
ASSESSED WITH MULTIDETECTOR COMPUTED  
TOMOGRAPHY ANGIOGRAPHY**

Thomas de Weert, Sander Cretier, Harald Groen, Pieter Homburg,  
Hamit Cakir, Jolanda Wentzel, Diederik Dippel, Aad van der Lugt

*Published in: Stroke 2009, 40(4):1334-40*

### ***Background***

Complicated (irregular or ulcerated) carotid plaques have proven to be independent predictors of stroke. We analyzed the frequency and location of plaque irregularities in a large cohort of patients with ischemic cerebrovascular disease, and the relation with severity of stenosis, cardiovascular risk factors and symptomatology.

### ***Methods***

Multidetector computed tomography angiography (MDCTA) images from 406 patients were evaluated. Plaque surface morphology was classified as smooth, irregular or ulcerated. The location of the ulceration was defined as proximal or distal to the point of maximum stenosis.

### ***Results***

Atherosclerotic plaques with an open lumen were present in 448 carotid arteries, these plaque were classified as: smooth: 276(62%), irregular: 99(22%) and ulcerated: 73(16%). Sixty-two(69%) of the ulcerations were located proximal to the point of maximum luminal stenosis. Complicated plaques were significantly ( $p < 0.001$ ) more common in carotid arteries with stenosis  $> 30\%$ , than in those with stenosis  $< 30\%$ . There is an association between complicated plaques and hypercholesterolemia (OR 3.0) and a trend towards an association with smoking (OR 1.9). Complicated plaques are more often present in the symptomatic carotid artery than in the contralateral asymptomatic carotid artery, however this is fully attributed to a significantly higher degree of stenosis in the symptomatic arteries.

### ***Conclusion***

MDCTA allows the classification of atherosclerotic carotid plaque surface. Complicated plaques are frequent in atherosclerotic carotid disease, especially with higher stenosis degree. Ulcerations are mostly located in the proximal part of the atherosclerotic plaque. Hypercholesterolemia and smoking are related with the presence of complicated plaques.

## INTRODUCTION

Cerebral infarction is one of the most important causes of death and the greatest cause of disability in the western world. About 20%-30% of the infarcts can be related to carotid artery stenosis [1,2]. The severity of stenosis is an important predictor of (recurrent) ischemic cerebrovascular events and is used in therapeutic decision-making: patients with symptomatic or asymptomatic carotid stenosis above a certain degree are considered candidates for carotid intervention, such as carotid endarterectomy or stent placement.

Besides the severity of stenosis, plaque ulceration on intra-arterial contrast angiography is a strong independent predictor of stroke [3,4]. It is current opinion that atherosclerotic plaque rupture plays an important role in acute events, like transient ischemic accidents (TIA) and stroke [5]. Rupture-prone plaques have specific morphological features: the most frequently seen vulnerable plaque type has a large lipid-rich core with a thin fibrous cap [5] and has proved to be an independent predictor of ischemic cerebrovascular events [6,7]. With microscopic evaluation of the plaque it became clear that angiographic ulceration and irregularities were strongly associated with the presence of plaque rupture, plaque hemorrhage, a large lipid core size and less fibrous tissue, i.e. features that are all closely related with the concept of a vulnerable plaque [8]. Plaque ulceration has been more frequently observed proximal to the point of maximum luminal stenosis [9], which is exposed to higher wall shear stress [10].

The accuracy of digital subtraction angiography (DSA) in the detection of ulceration, with surgical observations as reference, has been reported to be low (sensitivity 46% and specificity 74%) [11]. The first reports on the accuracy of computed tomography angiography (CTA) compared with DSA in the assessment of plaque ulcers were disappointing, but this might be explained by the rather thick slice thickness used with single section computed tomography (CT) [12]. A later report demonstrated that CTA was superior to DSA in the detection of plaque irregularities and ulcerations [13]. Walker and colleagues evaluated 165 CTA studies, compared them with endarterectomy specimens, and reported a sensitivity of 60% and a specificity of 74% [14]. A recent multi-detector CTA (MDCTA) study reported an even higher sensitivity and specificity for the detection of ulcerations (94% and 99%, respectively) [15].

The purpose of this study was to assess atherosclerotic plaque surface morphology in the carotid arteries with MDCTA in a large consecutive cohort of patients with ischemic cerebrovascular disease. Plaque surface morphology was related to severity of stenosis, cardiovascular risk factors, and type of ischemic cerebrovascular symptoms.

## METHODS

### *Study population*

Consecutive patients (n=406) with ischemic cerebrovascular disease including amaurosis fugax or focal cerebral ischemia (TIA and minor ischemic stroke) were prospectively studied. Patients were enrolled from the neurology department's specialized TIA/stroke outpatient clinic or neurology ward. Patients underwent neurological examination on admission. Medical history was recorded from all patients. All patients underwent multidetector CT (MDCT) of the brain and MDCTA of the carotid arteries. In all patients MDCTA has been performed as part of a research protocol that was approved by the Institutional Review Board and all patients had given written informed consent. The inclusion period ranged from November 2002 to January 2005.

### *Scanning and image reconstruction*

Scanning was performed on a 16-slice MDCT scanner (Siemens, Sensation 16, Erlangen, Germany) with a standardized optimized contrast-enhanced protocol (120 kVp, 180 mAs, collimation 16 x 0.75 mm, pitch 1) [16,17]. The MDCTA scan range reached from the ascending aorta to the intracranial circulation (2 cm above the sella turcica). All patients received 80 ml contrast material (Iodixanol 320 mg/ml, Visipaque, Amersham Health, Little Chalfont, UK), followed by 40 ml saline bolus chaser, both with an injection rate of 4 ml/sec. Synchronization between the passage of contrast material and data acquisition was achieved by real time bolus tracking at the level of the ascending aorta. The trigger threshold was set at an increase in attenuation of 75 Hounsfield Units (HU) above baseline attenuation ( $\approx$  150 HU in absolute HU value).

Image reconstructions were made with field of view 100 mm, matrix size 512 x 512 (real in-plane resolution 0.6 x 0.6 mm), slice thickness

1.0 mm, increment 0.6 mm and with an intermediate reconstruction algorithm [18].

### ***Analysis of the atherosclerotic plaque***

The MDCTA images were sent to a stand-alone workstation (Leonardo–Siemens Medical Solutions, Forchheim, Germany) with dedicated 3D analysis software. On the workstation both carotid bifurcations were evaluated with multi-planar reformatting (MPR) software. With this software oblique planes can be adjusted in order to evaluate the carotid bifurcation in multiple reformations in the short axis and long axes with respect to the carotid artery.

Firstly, the presence of an atherosclerotic plaque was evaluated. The criterion used for the presence of an atherosclerotic lesion was: the presence of a calcification and/or thickening of the vessel wall. If a plaque was visible, the surface of the plaque was evaluated and classified as ulcerated, irregular or smooth (Figure 2-1). Plaques were classified as ulcerated if extension of contrast material was present beyond the vascular lumen into

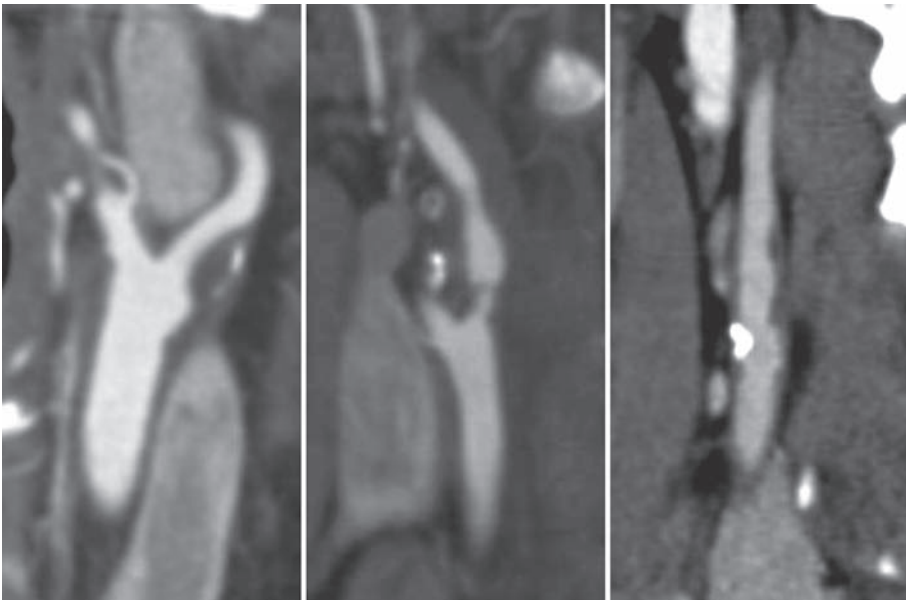


**Figure 2-1:** Multiplanar reformat images of smooth atherosclerotic carotid plaque surface and irregular plaque surface.

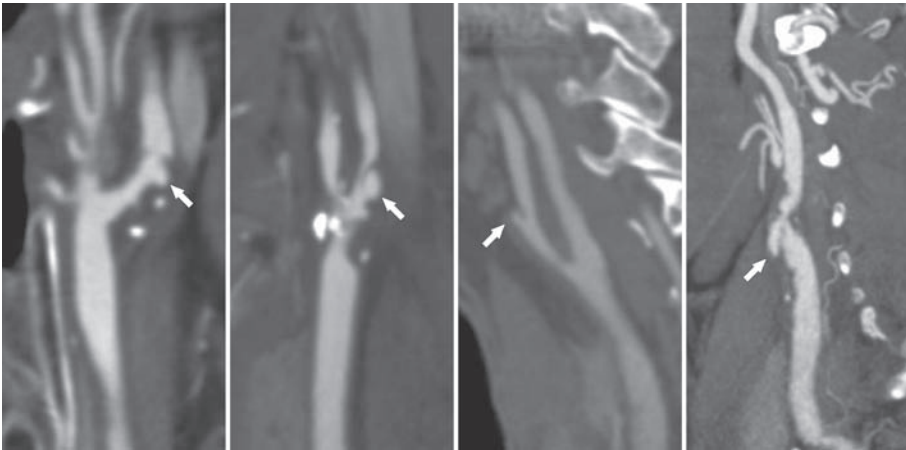


**Figure 2-2:** Multiplanar reformat images of the different types of atherosclerotic carotid plaque ulceration. From left to right: Type 1, type 2, type 3 and type 4.

the surrounding plaque. Ulcerated plaques were categorized according to the shape of the ulcer as type 1 to 4 (Figure 2-2), as previously described by Lovett et al. [8]. Type 1 is an ulcer that points out perpendicular to the lumen; type 2 has a narrow neck, and points out proximally and distally; type 3 has an ulcer neck proximally and points out distally, and type 4 has an ulcer neck distally and points out proximally. The location of the ulcer was defined as proximal or distal to the point of maximum luminal stenosis. Plaques were classified as irregular if pre- or post-stenotic dilatation was present and/or if the plaque surface morphology showed irregularities without any sign of ulceration. If the plaque was not ulcerated or irregular, it was classified as smooth. To calculate interobserver reproducibility a second observer reassessed 100 consecutive MDCTA scans.

### *Severity of stenosis*

The severity of stenosis on CTA was measured according to the North American Symptomatic Carotid Endarterectomy Trial (NASCET) criteria [19]. Oblique MPR images, parallel to the central lumen line were used for measurements. The severity of stenosis was defined as the remaining lumen at the site of stenosis as percentage of the normal lumen distal to the stenosis, and categorized into 0-29%, 30-49%, 50-69%, 70-99% and 100%.



### ***Cardiovascular risk factors***

Clinical measures and information on risk factors and medication were obtained at admission to the hospital. Subjects were categorized as current, past and never smokers. Hypertension was defined as systolic blood pressure over 140 mmHg and/or diastolic blood pressure over 90 mmHg during two episodes of at least 15 minutes of continuous non-invasive blood pressure measurement or treatment with antihypertensive medication. Blood pressure lowering drugs comprised ACE inhibitors, calcium antagonists, beta-blockers and diuretics.

Hypercholesterolemia was defined as fasting cholesterol over 5.0 mmol/l, or on treatment with cholesterol-lowering drugs. Diabetes was defined as fasting serum glucose levels over 7.9 mmol/l, nonfasting serum glucose levels over 11.0 mmol/l, or use of antidiabetic medication.

Information on previous cardiovascular disease (myocardial infarction, atrial fibrillation, angina pectoris, chronic heart failure, coronary artery bypass grafting) and previous ischemic cerebrovascular disease (TIA or ischemic stroke other than the event for which the patient was currently evaluated) was collected.

### ***Symptoms***

Amaurosis fugax was defined as a sudden, focal neurological deficit that was presumed to be of vascular origin and confined to the eye. TIA was defined as a sudden, focal neurological deficit that was presumed to be of vascular origin and was confined to an area of the brain perfused by a specific artery and that lasted less than 24 hours. In addition, no relevant infarct (one that explains the deficit) should be seen on the CT scan. An ischemic stroke was defined as a sudden focal neurologic deficit which lasted more than 24 hours or which was accompanied by a relevant infarct on the CT scan.

### ***Statistics***

Data are presented as mean  $\pm$  standard deviation. Analysis was performed for complicated (irregular or ulcerated) plaques. Reliability of assessment of plaque surface morphology was measured using the kappa statistics. Differences between categorical data and continuous data were analysed with a Chi-squared test and a Mann-Whitney test or Student's t-test,

respectively. In an exploratory analysis we evaluated the association between the presence of complicated plaque and possible determinants (severity of stenosis and cardiovascular risk factors (smoking, hypertension, hypercholesterolemia, diabetes, previous cardiovascular disease, previous ischemic cerebrovascular disease)). All determinants were included in a multiple logistic regression model to assess their association with complicated plaque independently from other determinants. No stepwise procedures were used. The associations were expressed as odds ratios with 95% confidence intervals, which implies we used  $p < 0.05$  as the value for statistical significance. The same analysis was repeated for ulcerated plaques only. Finally, in the patients with symptoms in territory of the carotid arteries the association between the presence of complicated plaque and symptomatic side was evaluated with a logistic regression model after adjustment for severity of stenosis. All calculations were made with SPSS 14.0 for Windows.

## RESULTS

The MDCTA images and medical histories of 406 patients were evaluated. Two patients were excluded because of poor image quality due to dental artifacts. General patient characteristics are shown in Table 2-I. With respect to age, the symptomatic artery, and ischemic cerebrovascular disease, there were no significant differences between men and women. However, men were more frequently smokers and had more frequently experienced previous cardiac disease, while women had more frequently hypercholesterolemia.

In 142 patients (35%) both carotid arteries were free of atherosclerosis, in 68 patients (17%) presence of atherosclerosis was determined in one of the carotid arteries, in 190 patients (47%) both carotid arteries showed atherosclerosis, in 21 patients at least one of the carotid arteries was occluded. Overall, from the 808 studied arteries, 337 (42%) were normal without atherosclerotic plaque, 448 (55%) were diseased, and 23 (3%) were occluded. Table 2-II shows the plaque surface morphology characteristics of the remaining 448 (55%) carotid arteries with atherosclerotic plaque. We found 90 ulcers in 73 carotid arteries of 61 patients. Both carotid arteries were ulcerated in 12 patients, and some patients had multiple (up to 4) ulcerations

**Table 2-I:** Baseline characteristics of the study population.

	Patients 404	Men 242 (60%)	Women 162 (40%)	p-value
Age (mean $\pm$ SD; years)	62 $\pm$ 14	62 $\pm$ 13	62 $\pm$ 14	0.57
<b>Symptomatic artery</b>				
Carotid	350 (87%)	212 (88%)	138 (85%)	0.48
Vertebrobasilar	54 (13%)	30 (12%)	24 (15%)	
<b>Cerebrovascular symptoms</b>				
Amaurosis fugax	83 (21%)	50 (21%)	33 (20%)	0.94
Transient ischemic attack	122 (30%)	72 (30%)	50 (31%)	0.81
Minor stroke	199 (49%)	120 (50%)	79 (49%)	0.87
<b>Risk factors</b>				
Smoking	195 (48%)	136 (56%)	59 (36%)	<0.01
Hypertension	288 (71%)	177 (73%)	111 (69%)	0.31
Diabetes	61 (15%)	38 (16%)	23 (14%)	0.68
Hypercholesterolemia	317 (78%)	177 (73%)	140 (86%)	<0.01
Previous cardiac disease	107 (26%)	73 (30%)	34 (21%)	0.04
Previous cerebrovascular disease	105 (26%)	70 (29%)	35 (21%)	0.10

in the same carotid artery. The prevalence of ulceration among the patients with at least one atherosclerotic carotid artery (n=258) was 24%. Most of the ulcerations (69%) were located proximal to the point of maximum stenosis, and ulcer type 1 and ulcer type 3 were most frequently observed. An irregular plaque was demonstrated in 22% of the carotid arteries with atherosclerotic disease. The two observers agreed on the presence of complicated plaque in 93% of the cases ( $\kappa = 0.84$ ; 95%CI = 0.70-0.97), on the presence of ulcerated plaque in all cases ( $\kappa = 1$ ; 95%CI = 0.86-1.00), on the location of plaque ulceration in 96% of the cases ( $\kappa = 0.91$ ; 95% = 0.54-1.00) and on the types of plaque ulceration in 98-100% of the cases ( $\kappa = 0.98$ -1.00; 95%CI = 0.89-1.00).

Table 2-III shows a cross-table with the degree of stenosis compared with the plaque surface morphology. It can be observed that ulcerated and irregular plaques are significantly ( $p < 0.001$ ) more common, and smooth plaques less common among carotid arteries with a higher degree of stenosis (30-99%). There were not enough ulcerated plaques to determine significant differences in the distribution of ulcer type among the different degrees of stenosis.

**Table 2-II:** Plaque surface morphology characteristics of 448 atherosclerotic carotid arteries with number, type (Type 1-4) and location of plaque ulceration.

<b>Carotid arteries with atherosclerosis</b>	
Smooth surface	276 (62%)
Irregular surface	99 (22%)
Ulcerated surface	73 (16%)
Number of ulcerations per carotid artery	
1	61 (84%)
2	8 (11%)
3	3 (4%)
4	1 (1%)
Type of ulceration	
1	43 (48%)
2	12 (13%)
3	24 (27%)
4	11 (12%)
Location of ulceration	
Proximal	62 (69%)
Distal	28 (31%)

The odds ratio for the association between complicated plaques and severity of stenosis (per 10% increase) adjusted for age and gender is 2.3 (95%CI 1.9-2.9). The odds ratio for the association between ulcerated plaques and severity of stenosis (per 10% increase) adjusted for age and gender is 1.5 (95%CI 1.3-1.7).

The multivariable adjusted odds ratios for the association between cardiovascular risk factors and complicated plaque in one of the carotid arteries

**Table 2-III:** Cross-Table with the degree of stenosis according to the NASCET criteria compared with plaque surface morphology of 448 atherosclerotic carotid arteries. The presence of irregular and ulcerated plaques is significantly different between the lowest degree of stenosis (0-29%) and the higher degrees of stenosis (30-99%) (p-value for both <0.001).

	Number of carotids	Smooth	Irregular	Ulcerated
0% - 29%	346	265 (77%)	49 (14%)	32 (9%)
30% - 49%	48	8 (17%)	23 (48%)	17 (35%)
50% - 69%	29	1 (3%)	13 (45%)	15 (52%)
70% - 99%	25	2 (8%)	14 (56%)	9 (36%)
Total	448	276	99	73

**Table 2-IV: a)** The multivariable adjusted odds ratios for associations between the complicated carotid plaques and cardiovascular risk factors for all patients with atherosclerosis (n=258). **b)** The multivariable adjusted odds ratios for associations between the ulcerated carotid plaques and cardiovascular risk factors for all patients with atherosclerosis (n=258). In both analyses the most severe stenosis per patient and the most severe plaque surface morphology per patient was used.

a		
	COMPLICATED PLAQUE	
Variable	Odds ratio (95% CI)	p-value
Age (per increasing decade)	1.1 (0.8-1.5)	0.50
Gender	1.1 (0.5-2.3)	0.88
Previous cerebrovascular disease	1.8 (0.9-3.7)	0.12
Previous cardiac disease	0.8 (0.4-1.7)	0.55
Hypertension	0.9 (0.4-2.3)	0.87
Hypercholesterolemia	3.0 (1.0-8.9)	<0.05
Diabetes	0.6 (0.2-1.9)	0.43
Smoking	1.9 (0.9-4.1)	0.09
Degree of stenosis (per 10% increase)	2.3 (1.9-2.9)	<0.001

b		
	ULCERATED PLAQUE	
Variable	Odds ratio (95% CI)	p-value
Age (per increasing decade)	1.0 (0.7-1.4)	0.92
Gender	1.2 (0.6-2.6)	0.61
Previous cerebrovascular disease	1.0 (0.5-2.0)	0.94
Previous cardiac disease	0.8 (0.4-1.6)	0.52
Hypertension	0.9 (0.4-2.2)	0.27
Hypercholesterolemia	0.9 (0.4-2.2)	0.89
Diabetes	0.5 (0.2-1.4)	0.21
Smoking	1.6 (0.8-3.3)	0.23
Degree of stenosis (per 10% increase)	1.5 (1.4-1.8)	<0.001

with at least atherosclerotic disease in one of the carotid arteries (n=258) are shown in Table 2-IV. A significant association was found with hypercholesterolemia (OR 3.0, 95%CI 1.0-8.9), and a trend towards an association with smoking (OR 1.9, 95%CI 0.9-4.1).

The multivariable analysis for the association between cardiovascular risk factors and plaque ulceration in one of the carotid arteries showed no significant association between cardiovascular risk factors and plaque ulceration.

**Table 2-V:** Plaque surface morphology in symptomatic and asymptomatic carotid arteries stratified for cerebrovascular symptoms.

	Total	CEREBROVASCULAR SYMPTOMS	
		Amaurosis fugax	TIA / Minor stroke
<b>Symptomatic carotid artery</b>	350	83	267
Ipsilateral			
Atherosclerotic plaque (%)	193 (55%)	39 (47%)	154 (58%)
Complicated plaque (%)	89 (25%)	14 (17%)	75 (28%)
<b>Asymptomatic carotid artery</b>	458	83	267
Contralateral			
Atherosclerotic plaque (%)	255 (56%)	41 (49%)	155 (58%)
Complicated plaque (%)	83 (18%)	14 (17%)	54 (20%)

For patients with vertebrobasilar symptoms both carotidarteries were considered asymptomatic. Symptomatic vs. asymptomatic complicated plaque for all patients:  $p = 0.01$ ; Symptomatic vs. asymptomatic complicated plaque surface for patients with TIA or minor stroke:  $p = 0.03$ .

Table 2-V shows that atherosclerotic plaques were present in both symptomatic and asymptomatic carotid arteries (55% vs 56%). Symptomatic carotid arteries more often harbored complicated plaques than asymptomatic carotid arteries (25% vs 18%,  $p=0.01$ , respectively). However, multivariable analysis showed that this can be attributed to the significantly higher degree of stenosis present in symptomatic arteries compared to asymptomatic arteries ( $p < 0.01$ ).

Complicated plaques were less often observed among patients with amaurosis fugax (17%) compared to patients with focal cerebral ischemia (28%); moreover, in the patients with amaurosis fugax symptomatic arteries were not more often complicated than asymptomatic arteries (17% vs 17%), as opposed to patients with focal cerebral ischemia (28% vs 20%;  $p=0.03$ ). Nonetheless, also in patients with focal cerebral ischemia the difference in incidence of complicated plaques was attributable to the significantly higher stenosis degree present in symptomatic arteries.

## DISCUSSION

This study demonstrates that MDCTA can assess atherosclerotic carotid plaque surface morphology, with differentiation between smooth, irregular and ulcerated surfaces. It shows that the majority of ulcerations are located proximally to the maximum stenosis, and that ulcerated and irregular plaques are more frequently encountered with a higher degree of stenosis. Of all cardiovascular risk factors, hypercholesterolemia was associated with complicated plaque while smoking showed a trend towards an association with complicated plaque. Finally, it was shown that complicated plaque is more common in the symptomatic artery of patients with cerebrovascular symptomatology than in the asymptomatic artery, however this can be ascribed to the significantly higher stenosis degree present in symptomatic arteries compared to asymptomatic arteries.

The present study found ulceration in 11% of the symptomatic carotid artery, and in 40% of the carotid arteries with a moderate to severe degree of stenosis (30-99%). Although, the proportion of ulcerated plaques in high grade stenosis is not significantly different from the proportion in the group with 50-69% stenosis our results are suggestive for the fact that there might be a real discrepancy, for which we can think of two possible explanations: 1) With severe stenosis calcifications are larger, which hampers identification of ulcerations with MDCTA. 2) The risk of rupture might differ with plaque composition. Plaques with a moderate stenosis degree have a larger proportion of lipid, while plaque with severe stenosis are more calcified.

Based on the DSA data of the ECST study Lovett et al. [9] reported a prevalence of ulceration of 14% in 3007 symptomatic carotid arteries in patients with atrial fibrillation, TIA or minor stroke patients, and a prevalence of 18% for symptomatic carotid arteries with a stenosis >30%. In the NASCET study ulcerations were found in 35% of symptomatic carotid arteries with a stenosis >70% [3]. In the present study, complicated plaque was present in 89% of the carotid arteries with stenosis >30%, which exceeds the reported frequency (63%) of carotid plaque surface abnormality detected with DSA [4]. The discrepancy in the frequencies of ulceration with MDCTA and DSA can be explained by the higher sensitivity of MDCTA in the detection of ulcerations [13]: MDCTA has a reported sensitivity of 60-94% [14,15], whereas DSA has a sensitivity of 46%-69%

[4,11]. The lower sensitivity for DSA might be a result of the limited viewing directions (usually two). Besides MDCTA and DSA, MRA has been used for the assessment of atherosclerotic carotid plaque surface morphology. One study made a comparison between these techniques (n=22, number of carotids studied 44) and concluded that luminal surface irregularities were most frequently seen at CTA, and that with CTA and MRA more ulcerations were detected than with DSA [13]. Saba et al. [15] have recently showed that ultrasound has a high specificity (93%), but a low sensitivity (38%) for the detection of carotid ulceration, which is in concordance with previous studies [20,21]. The low sensitivity can be ascribed, in part, to the fact that acoustic shadowing from calcifications obscures the presence of ulcerations.

A recent histological study [22] of symptomatic carotid endarterectomy specimens from 526 consecutive patients with a stenosis degree of 75-90% found ulceration in 58% of the specimens. The discrepancy in the frequencies of ulceration between MDCTA and histology in patients with a severe degree of stenosis can be explained by the higher resolution of histology which enables the detection of small ulcerations, the higher volume of calcifications in severe stenosis, which hampers accurate detection of small ulcerations by MDCTA. In addition, thrombus formation on the location of a rupture may fill the ruptured site, which will lead to non-visualization with MDCTA.

Lovett et al. [8] characterized ulcerations as type 1 to 4, and determined that type 1 and type 3 are the most frequent type of rupture; the present study confirms these findings. However, the categorization of ulcers is only important when their occurrence can be related to different clinical behavior; this has not yet been demonstrated.

Ulcerations were most frequently seen at the proximal site of the maximum stenosis. The ECST data revealed the same distribution of ulcer location in the carotid artery (71% at the proximal site) as in the present study [9]. An intracoronary ultrasound study found that 69% of the ulcerated ruptured plaques (80%) were proximal to the minimal lumen site [23]. The proximal site as predilection site for ulceration is in concordance with shear stress theories. It is thought that high shear stress on the plaque surface (due to the lumen narrowing) weakens the cap through numerous signaling pathways [10]. Indeed, in a recent case report Groen et al. [24] showed in a serial MRI study that the ulceration was located at the high



shear stress region. Shear stress may therefore play an important role in the rupture of plaques.

The present study showed that plaque ulceration is not only present in high-grade stenosis, but can also occur in hemodynamically insignificant stenosis. A similar observation was made on the ECST data [4]. Most of the patients with an ischemic stroke did not have a severe stenosis, despite the accumulation of a substantial amount of atherosclerotic plaque in the carotid bifurcation. Detection of plaque ulceration thereby provides a clue to the underlying pathophysiology of the previously occurring ischemic stroke: rupture of the plaque may have been accompanied by thrombus formation and embolisation of plaque material or thrombus into the intracranial circulation. In addition, detection of plaque ulceration indicates that a patient has an increased risk of a new ipsilateral ischemic stroke [4]. Whether surgical or endovascular intervention in symptomatic patients without a significant stenosis but with a plaque ulceration is justified remains to be demonstrated in larger prospective studies. Ideally, these studies should use the non-invasive imaging tools that are currently available. In the present study hypercholesterolemia is positively and significantly associated with the presence of complicated plaques, while smoking, had a positive (but not significant) association with the presence of complicated plaques. Previous studies with univariate analysis revealed associations between irregular plaques and gender [3], age [4], carotid stenosis [4], hypercholesterolemia [4] and previous myocardial infarction [4]. Since irregular plaques are related to the severity of stenosis, multivariable analysis with adjustment for the severity of stenosis is necessary to demonstrate whether certain cardiovascular risk factors are independently related to the presence of irregular plaques.

The association with hypercholesterolemia might be explained by the atherogenic effect of lipoprotein(a) in the presence of high plasma LDL-C levels, which increases lipid deposition in atherosclerotic plaque [25,26], making the plaque probably more vulnerable for rupture. Cigarette smoking is considered to influence inflammation and hemostasis in such a way that plaque inflammation and thrombogenicity increases, with cap degradation, plaque rupture and subsequent thrombus formation as a possible result [27].

In the present study, ulcerated and irregular plaques are significantly more common in the ipsilateral symptomatic carotid artery than in the asymp-

omatic carotid artery, which is in line with the findings of Sitzer et al. [28], who concluded that plaque ulceration is more common in carotid endarterectomy specimens from symptomatic arteries, than from asymptomatic arteries. However, multivariate analysis showed that this difference does not remain significant when severity of stenosis was added to the model. This indicates that besides local factors like plaque composition or shear stress, also systemic factors are important in the occurrence of plaque rupture. A reasoning that is supported by the findings of Rothwell et al. [29], who reported that patients with irregular plaque in the symptomatic carotid artery were more likely to have irregular plaques in the contralateral artery, and by a study from Fisher et al. [30] which concluded that plaque ulceration was more common in symptomatic patients than in asymptomatic patients, but that the prevalence of ulceration in the ipsilateral and contralateral carotid artery in symptomatic patients was the same.

Although, the recent paper by Saba et al. [15] showed that MDCTA is an excellent technique to evaluate carotid ulceration, we realize that it is a limitation of our study that we do not have a gold standard (e.g. histologic specimens). Unfortunately, correlation with histological results is troublesome, because only patients with a severe stenosis (NASCET >70% stenosis) are eligible for intervention, which in our hospital includes stenting in approximately 50% of the cases. Therefore, it is not possible to obtain histology from a vast majority of patients.

A second limitation of our study is its cross-sectional design. The evaluation of the causal association between severity of stenosis and complicated plaques, between cardiovascular risk factors and complicated plaques, and between complicated plaques and ischemic cerebrovascular disease requires a prospective design in which the atherosclerotic plaque is evaluated serially to detect changes in plaque surface morphology.

## CONCLUSION

This study shows that MDCTA can classify atherosclerotic carotid plaque surface morphology. Furthermore, it shows that the presence of a complicated plaque surface in an atherosclerotic plaque is strongly related with the severity of stenosis, and that the site of ulceration is mostly proximal to the most stenotic site. In addition, it is shown that hypercholesterol-

emia and probably smoking are related with the presence of complicated plaques.

## REFERENCES

1. Caplan LR, Diagnosis and treatment of ischemic stroke. *Journal of the American College of Cardiology*, 1991. 266(17): p. 2413-8.
2. Warlow C, et al., Stroke. *Lancet*, 2003. 362(9391): p. 1211-24.
3. Eliasziw M, et al., Significance of plaque ulceration in symptomatic patients with high-grade carotid stenosis. *North American Symptomatic Carotid Endarterectomy Trial. Stroke*, 1994. 25(2): p. 304-8.
4. Rothwell PM, Gibson R, and Warlow CP, Interrelation between plaque surface morphology and degree of stenosis on carotid angiograms and the risk of ischemic stroke in patients with symptomatic carotid stenosis. On behalf of the European Carotid Surgery Trialists' Collaborative Group. *Stroke*, 2000. 31(3): p. 615-21.
5. Naghavi M, et al., From vulnerable plaque to vulnerable patient: a call for new definitions and risk assessment strategies: Part I. *Circulation*, 2003. 108(14): p. 1664-72.
6. Polak JF, et al., Hypoechoic plaque at US of the carotid artery: an independent risk factor for incident stroke in adults aged 65 years or older. *Cardiovascular Health Study. Radiology*, 1998. 208(3): p. 649-54.
7. Takaya N, Association Between Carotid Plaque Characteristics and Subsequent Ischemic Cerebrovascular Events: A Prospective Assessment With MRI--Initial Results. *Stroke*, 2006. 37(3): p. 818-23.
8. Lovett J, Histological Correlates of Carotid Plaque Surface Morphology on Lumen Contrast Imaging. *Circulation*, 2004. 110(15): p. 2190-97.
9. Lovett J and Rothwell P, Site of Carotid Plaque Ulceration in Relation to Direction of Blood Flow: An Angiographic and Pathological Study. *Cerebrovascular Diseases*, 2003. 16(4): p. 369-75.
10. Slager C, et al., The role of shear stress in the destabilization of vulnerable plaques and related therapeutic implications. *Nature Clinical Practice Cardiovascular Medicine*, 2005. 2(9): p. 456-64.
11. Streifler JY, et al., Angiographic detection of carotid plaque ulceration. Comparison with surgical observations in a multicenter study. *North American Symptomatic Carotid Endarterectomy Trial. Stroke*, 1994. 25(6): p. 1130-2.

12. Oliver TB, et al., Atherosclerotic plaque at the carotid bifurcation: CT angiographic appearance with histopathologic correlation. *American Journal of Neuroradiology*, 1999. 20(5): p. 897-901.
13. Randoux B, et al., Carotid artery stenosis: prospective comparison of CT, three-dimensional gadolinium-enhanced MR, and conventional angiography. *Radiology*, 2001. 220(1): p. 179-85.
14. Walker LJ, et al., Computed tomography angiography for the evaluation of carotid atherosclerotic plaque: correlation with histopathology of endarterectomy specimens. *Stroke*, 2002. 33(4): p. 977-81.
15. Saba L, et al., Efficacy and sensitivity of axial scans and different reconstruction methods in the study of the ulcerated carotid plaque using multidetector-row CT angiography: comparison with surgical results. *American Journal of Neuroradiology*, 2007. 28(4): p. 716-23.
16. de Monyé C, et al., Sixteen-detector row CT angiography of carotid arteries: comparison of different volumes of contrast material with and without a bolus chaser. *Radiology*, 2005. 237(2): p. 555-62.
17. de Monyé C, et al., Optimization of CT angiography of the carotid artery with a 16-MDCT scanner: craniocaudal scan direction reduces contrast material-related perivenous artifacts. *American Journal of Roentgenology*, 2006. 186(6): p. 1737-45.
18. de Weert TT, et al., In vitro characterization of atherosclerotic carotid plaque with multidetector computed tomography and histopathological correlation. *European Radiology*, 2005. 15(9): p. 1906-14.
19. Rothwell PM, et al., Prognostic value and reproducibility of measurements of carotid stenosis. A comparison of three methods on 1001 angiograms. *European Carotid Surgery Trialists' Collaborative Group. Stroke*, 1994. 25(12): p. 2440-4.
20. Bluth EI, et al., The identification of ulcerative plaque with high resolution duplex carotid scanning. *Journal of Ultrasound in Medicine*, 1988. 7(2): p. 73-6.
21. Lammie GA, et al., What pathological components indicate carotid atheroma activity and can these be identified reliably using ultrasound? *Eur J Ultrasound*, 2000. 11(2): p. 77-86.
22. Redgrave J, Histological Assessment of 526 Symptomatic Carotid Plaques in Relation to the Nature and Timing of Ischemic Symptoms: The Oxford Plaque Study. *Circulation*, 2006. 113(19): p. 2320-28.
23. Fujii K, Intravascular Ultrasound Assessment of Ulcerated Ruptured Plaques: A Comparison of Culprit and Nonculprit Lesions of Patients With Acute Coronary Syndromes and Lesions in Patients Without Acute Coronary Syndromes. *Circulation*, 2003. 108(20): p. 2473-78.
24. Groen HC, et al., Plaque rupture in the carotid artery is localized at the high shear stress region: a case report. *Stroke*, 2007. 38(8): p. 2379-81.

25. Baldassarre D, et al., Plasma lipoprotein(a) is an independent factor associated with carotid wall thickening in severely but not moderately hypercholesterolemic patients. *Stroke*, 1996. 27(6): p. 1044-9.
26. Rath M, et al., Detection and quantification of lipoprotein(a) in the arterial wall of 107 coronary bypass patients. *Arteriosclerosis*, 1989. 9(5): p. 579-92.
27. MacCallum PK, Markers of hemostasis and systemic inflammation in heart disease and atherosclerosis in smokers. *Proceedings of the American Thoracic Society*, 2005. 2(1): p. 34-43.
28. Sitzer M, et al., Plaque ulceration and lumen thrombus are the main sources of cerebral microemboli in high-grade internal carotid artery stenosis. *Stroke*, 1995. 26(7): p. 1231-3.
29. Rothwell PM, et al., Evidence of a chronic systemic cause of instability of atherosclerotic plaques. *Lancet*, 2000. 355(9197): p. 19-24.
30. Fisher M, et al., Carotid plaque pathology: thrombosis, ulceration, and stroke pathogenesis. *Stroke*, 2005. 36(2): p. 253-7.



CHAPTER

# 3

---

## **ATHEROSCLEROTIC PLAQUE RUPTURE IN CAROTID ARTERIES IS ASSOCIATED WITH HIGHER WALL SHEAR STRESS AND PLAQUE THICKNESS**

Harald Groen, Sietske Rozie, Frank Gijssen, Wouter Edeling,  
Thomas de Weert, Johan Reiber, Antonius van der Steen,  
Aad van der Lugt, Jolanda Wentzel

*Submitted*

### ***Background***

Cerebrovascular events are related to atherosclerotic disease in the carotid arteries. Blood flow induced wall shear stress (WSS) influences many processes affecting vascular remodelling, including tissue regression. Fibrous-cap-regression induced by high WSS might enhance plaque vulnerability, eventually leading to plaque rupture. We investigated the relation between WSS and plaque rupture location in symptomatic carotid artery bifurcations.

### ***Methods***

Patients with a ruptured carotid atherosclerotic plaque as determined by multidetector computed tomography angiography were studied. The WSS, calculated based on a 3D- reconstruction of the carotid bifurcation, at the rupture location was compared to the WSS at the non-ruptured atherosclerotic wall.

### ***Results***

The WSS and wall thickness at the location of the rupture tended to be higher compared to the WSS ( $4.6\pm 1.3$  Pa vs  $2.5\pm 0.3$  Pa,  $p=0.11$ ) and wall thickness ( $3.8\pm 0.3$ mm vs  $2.3\pm 0.1$  mm,  $p<0.001$ ) at the non-ruptured plaque regions.

### ***Conclusion***

Plaque rupture at higher WSS suggests that WSS is involved in the (biological) weakening of the thicker region of atherosclerotic plaques.



## INTRODUCTION

Atherosclerosis is a local disease of the arterial vessel wall. It is found at inner curves of vessels and near bifurcations, where endothelial cells sense a low wall shear stress (WSS) [1]. WSS is the frictional force on the vessel wall resulting from the flowing blood. Low WSS patterns make the vessel wall more susceptible to lipid accumulation, initiating the early phase of atherosclerosis [2,3]. Vascular remodelling prevents luminal narrowing [4] which enables the plaque to continue growing [5], usually without any symptoms. At a certain moment, plaque growth cannot be compensated anymore and lumen narrowing will occur. A subset of plaques develops into vulnerable plaques, containing lipids, calcifications, covered by a thin fibrous cap. When mechanical forces in the cap, due to the blood pressure, exceed the maximal strength of the cap, it will rupture leading to thrombus formation, and/or embolisation of thrombus or plaque material into the intracranial circulation. Rupture of the atherosclerotic carotid plaque can therefore result in neurological events like transient ischemic attack (TIA) or ischemic stroke.

It has been observed that plaques more often rupture at the proximal site of the minimal lumen diameter (MLD) than at the distal site [6-8]. The reason for this preferred location is currently unknown. When a plaque starts to encroach into the lumen, the WSS at the proximal plaque region gradually increases during narrowing of the vessel. Evidence is accumulating for a role of high WSS in biological processes involved in plaque destabilization [3,5,9-11]. We demonstrated that plaque rupture developed at the location with high WSS values using a serial MRI dataset in one patient [9]. Unfortunately, serial datasets are quite rare and the chance of imaging a plaque before and after rupture is small.

We studied 25 patients with ischemic cerebrovascular symptoms (amaurosis fugax, TIA and minor ischemic stroke) with a ruptured atherosclerotic plaque in the symptomatic carotid artery, visible as ulceration on multidetector computed tomography angiography (MDCTA) [8,12]. The relationship between plaque rupture location and WSS values was investigated.

## MATERIALS AND METHODS

### *Patients*

We selected from our MDCTA database the first 25 patients with atherosclerotic plaque ulceration in the symptomatic carotid artery [8]. This database included patients with amaurosis fugax, TIA or minor ischemic stroke. The MDCTA images were collected in a study, which was approved by the Institutional Review Board. All patients had given written informed consent.

### *Scanning protocol*

The patients were scanned using a 16-slice MDCT scanner (Siemens Sensation 16, Forchheim, Germany) with a contrast-enhanced protocol (120 kVp, 180 mAs, collimation 16 x 0.75 mm, table feed 12 mm/rotation, pitch 1) [13]. Image reconstructions were made with field of view 100 mm, matrix size 512 x 512 (real in-plane resolution 0.6 x 0.6 mm), slice thickness 1.0 mm, increment 0.6 mm and with an intermediate reconstruction algorithm.

### *Carotid bifurcation analysis*

Firstly, the degree of stenosis in the symptomatic carotid artery was determined according to the North American Symptomatic Carotid Endarterectomy Trial (NASCET) criteria [14]. Measurements were performed on oblique multiplanar-reformatting images, parallel to the central lumen line. Severity of stenosis was defined as the remaining lumen at the site of minimal luminal diameter (MLD) as percentage of the normal lumen distal to the stenosis. The location of the ulceration was classified as proximal, distal to or at the point of the MLD.

### *Vessel segmentation*

To investigate the WSS at the site of plaque rupture we needed to generate a 3D reconstruction of the carotid bifurcation lumen as if there was no ulceration present. Therefore the lumen of the common (CCA), internal (ICA) and external (ECA) carotid artery (Figure 3-1a) was semi-automatically segmented in each MDCTA dataset.

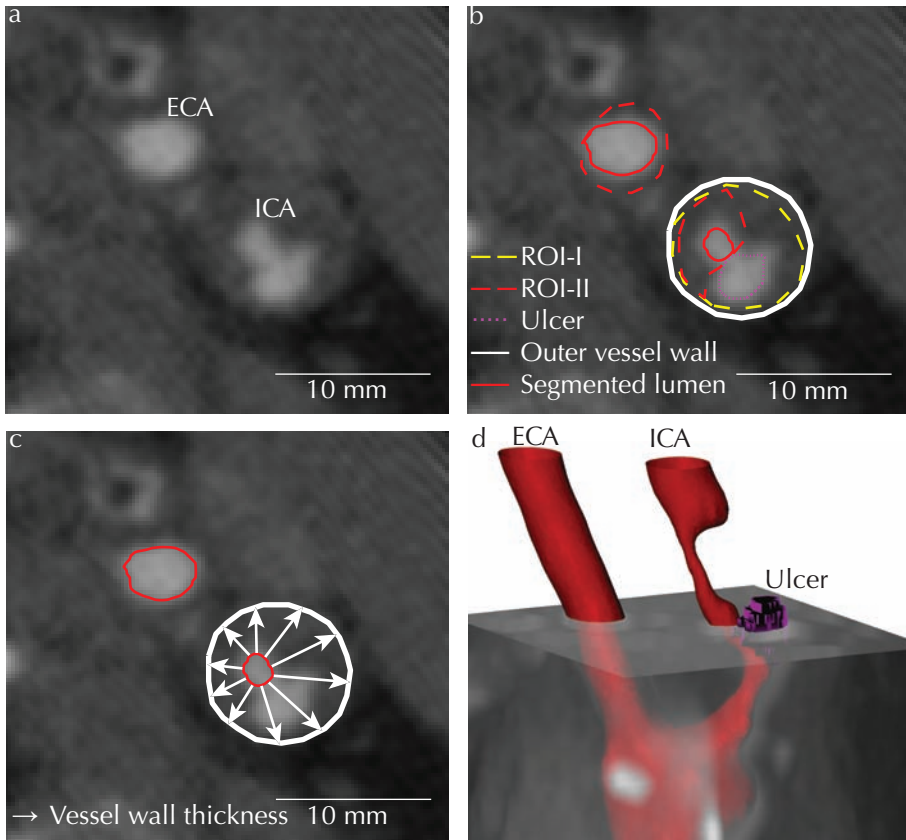


**Figure 3-1:** **a)** Original MDCTA slice, showing internal (ICA) and external (ECA) carotid arteries; **b)** Manual contours of the outer vessel wall (white), ROI-I (lumen including ulceration, dashed yellow) and ROI-II (lumen excluding ulceration, dashed red) together with resulted lumen segmentation (red) and ulceration (dotted magenta); **c)** Illustration of local vessel wall thickness measurement; **d)** Final 3D lumen segmentation together with part of the 3D MDCTA data and segmented ulceration.

As described before [15], a patient-specific Hounsfield unit (HU) threshold-value for the density of the contrast-enhanced lumen was used. In plaques without juxtaluminal calcifications, a region of interest (ROI-I) was drawn on each slice to separate the vessel wall from the lumen and then lumen was automatically differentiated from atherosclerotic plaque based on a patient-specific HU value [15]. In plaques with juxtaluminal calcifications, calcifications were separated completely by manual drawing. Side branches were also separated manually from the lumen. This resulted in a segmentation of the carotid bifurcation including the ulceration. Subsequently, ROI-I was duplicated (ROI-II) and adjusted in order

to exclude the ulceration, visible as contrast outside the lumen and inside the plaque, from the lumen (Figure 3-1b). This procedure was performed by an experienced radiologist (AvdL) with more than 5 years of experience with carotid MDCTA scans.

The area enclosed by ROI-I but not by ROI-II was used to segment the ulceration (Figure 3-1b) based on the patient-specific HU value as well. Subsequently, to measure local vessel wall thickness, the outer-vessel-wall was drawn manually on all slices containing atherosclerosis (Figure 3-1c). In the end, a smooth 3D reconstruction of the lumen border was obtained by Gaussian filtering of the HU-lumen values inside the luminal ROI-II (Figure 3-1d).

### *Wall shear stress*

The smooth 3D lumen reconstruction was exported to VMTK ([www.vmtk.org](http://www.vmtk.org)) for various pre-processing steps necessary for the blood flow simulation. The reconstruction was meshed using Netgen (<http://www.hpfem.jku.at>). The length of the CCA to the bifurcation was at least 3 times the diameter of the vessel to assure a fully developed flow profile [16]. The Navier-Stokes equations were solved by using FIDAP (Fluent Inc Canonsburg, Pennsylvania, USA). The blood-flow was modelled as a time-average stationary, incompressible (density  $1060 \text{ kg/m}^3$ ) flow with a non-Newtonian behaviour of the viscosity described by the Carreau model [17]. Since the absolute inflow for each patient was unknown, a physiological WSS value of 1.2 Pa at the most proximal part of the CCA vessel wall was assumed [18]. The parabolic inflow profile was adjusted such the WSS at the inflow matched the 1.2 Pa. Outflow boundary conditions were assumed to be pressure free. After the simulation, WSS values were calculated using FieldView (Intelligent Light, New Jersey, USA) and exported to Matlab (The MathWorks, Massachusetts, USA) for further analysis.

### *Data analysis*

For the analysis, only the WSS at the lumen covering atherosclerotic plaque was used. Atherosclerotic plaque was defined as those lumen regions with a wall thickness of more than 1 mm [19,20]. The rupture site was defined as luminal surface directly connected to the ulceration (Figure 3-2). The

non-rupture site was defined as the surface of atherosclerotic plaque minus the rupture site. For each patient, we compared both the wall thickness and WSS at the rupture site with the non-rupture site.

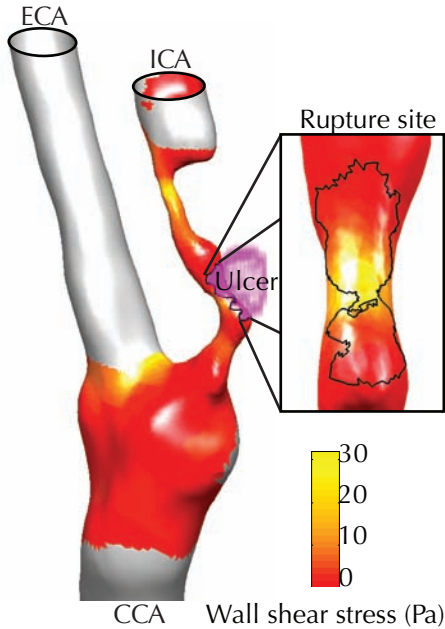


**Figure 3-2:** Illustration of colour-coded wall WSS distribution at the lumen (internal (ICA), external (ECA) and common (CCA) carotid artery) with atherosclerosis (a wall thickness of >1 mm), including ulceration (magenta) and rupture site.

### *Statistical analysis*

Data is presented as mean value  $\pm$  standard error of the mean (SEM). If the data was not distributed normally, the median was used for comparison. A two-tailed paired Student's t-test was used to test whether the WSS and the plaque thickness at the rupture site was different from the non-rupture site. A chi-square test was performed for testing the location of the ulceration. Statistics were performed in SPSS (SPSS, Chicago, IL, USA), where  $p < 0.05$  was considered significant.

## RESULTS

From the 25 patients, 5 were excluded from the analysis due to different reasons (1 ulceration was too large to determine original lumen, 1 incorrect reconstruction filter, 3 due to technical difficulties during blood flow modelling). In total, twenty patients (15 male, mean age  $69 \pm 2$ , range 56 to 84) with an ulceration in the symptomatic artery as seen on MDCTA were analysed. Patient characteristics are summarized in Table 3-I. In this patient group, the full range of stenosis degree was present: 7 vessels had a stenosis of 0-29%; 4 vessels 30-49%; 8 vessels 50-69% and 1 vessel of 70-99%.

**Table 3-I:** Patients' baseline characteristics (n=20).

Age (mean $\pm$ SEM)	69 $\pm$ 2	
Male	70 $\pm$ 2	
Female	65 $\pm$ 3	
Male	15	(75%)
Stenosis <sup>a</sup> 0-29%	7	(35%)
30-49%	4	(20%)
50-69%	8	(40%)
70-99%	1	(5%)
Hypercholesterolemia <sup>b</sup>	15	(75%)
Hypertension <sup>c</sup>	13	(65%)
Diabetes <sup>d</sup>	2	(10%)
Smoking <sup>e</sup>	15	(75%)
Previous cardiac disease	5	(25%)
Previous cerebrovascular disease	7	(35%)

a NASCET criteria.

b Fasting cholesterol >5 mmol/l and/or using cholesterol-lowering drugs.

c Systolic blood pressure > 140 mmHg and/or diastolic blood pressure > 90mmHg and/or using blood pressure-lowering drugs.

d Fasting serum glucose levels > 7.9 mmol/l or nonfasting > 11 mmol/l and/or using antidiabetic drugs.

e Current and former.

The main results are presented in Table 3-II. Plaque ruptures were in 70% (n=14, p=0.002) of the cases located proximally from the MLD, while the others were observed distal (20%, n=4) from or at the MLD (10%, n=2). The surface area of non-rupture site was 350 $\pm$ 46 mm<sup>2</sup> and the rupture site was 6.3 $\pm$ 1.0 mm<sup>2</sup>. The atherosclerotic wall-thickness was 60% thicker (p<0.001) at the rupture site (3.8 $\pm$ 0.4 mm) compared to the non-rupture site (2.3 $\pm$ 0.1 mm, Table 3-II), independent on the degree of stenosis. We found a large variation in WSS values at the non-rupture site in the patient group (Table 3-II), ranging from 0.3 to 6.4 Pa. In 65% of the cases, the WSS at the rupture site was higher than the non-rupture site. In general, the WSS tended to be almost 2 times higher than the non-rupture site (4.6 $\pm$ 1.3 vs 2.5 $\pm$ 0.3 Pa, paired t-test, p=0.11). Interestingly, 3 out of the 4 ulcers located distally from the MLD were exposed to WSS higher than the non-rupture sites.

**Table 3-II:** Geometric and WSS values at rupture and non-rupture sites. Values are mean  $\pm$  SEM.

Stenosis <sup>a</sup>	Age	Sex	Location <sup>b</sup>	Average wall thickness (mm)		Median WSS (Pa)	
				Non-ruptured	Ruptured	Non-ruptured	Ruptured
0-29%	56	F	Proximal	2.4	1.3	2.8	0.9
	60	M	Proximal	2.4	4.1	1.6	1.0
	65	M	Proximal	1.7	2.9	1.2	1.5
	70	M	Proximal	1.9	3.1	0.7	2.2
	74	M	At MLD	1.7	3.7	0.7	2.2
	77	M	Proximal	2.6	6.2	3.4	5.8
	83	M	Proximal	1.8	3.2	1.6	3.4
30-49%	63	F	Proximal	1.6	2.0	6.4	12.0
	69	M	Proximal	2.1	2.2	2.6	0.3
	79	M	Proximal	2.7	6.2	1.9	1.8
	84	M	Proximal	2.4	3.2	2.8	10.1
50-69%	58	M	Distal	3.4	7.1	3.3	5.3
	62	F	Proximal	2.7	2.6	4.5	5.6
	63	M	Distal	2.7	3.8	2.3	0.5
	65	M	Proximal	2.0	2.4	2.2	6.1
	69	M	Proximal	2.6	5.1	5.5	3.6
	71	F	Distal	2.2	2.7	2.7	25.8
	72	M	At MLD	2.7	4.4	2.8	0.7
74	F	Distal	2.8	5.5	0.3	0.9	
70-99%	63	M	Proximal	2.6	3.7	1.2	2.9
Mean $\pm$ SEM				2.3 $\pm$ 0.1	3.8 $\pm$ 0.3	2.5 $\pm$ 0.3	4.6 $\pm$ 1.3
p-value				<0.001 <sup>c</sup>		0.11 <sup>c</sup>	

a NASCET criteria.

b With respect to the minimal lumen diameter (MLD).

c Paired Student's t-test: rupture vs non-rupture site.

## DISCUSSION

We showed that plaque rupture is most often located at the upstream side of the plaque. Moreover, at these locations the plaque was significantly thicker and the WSS tended to be higher than the non-rupture plaque region.

Probably the main reason for not reaching statistical significance for the WSS is the low power of the study ( $n=20$ ), because of the inhomogeneous patient population containing the full range of lumen stenosis with a relative large range of ages. However, the results are in line with the recent studies showing also a higher WSS at the site of rupture [11,21]. Note that the WSS force is too small to fracture the cap directly [22,23], probably high stresses in the cap lead to the actual plaque rupture [21]. This does not exclude that preceding the plaque rupture; WSS can contribute to a biological weakening of the cap. There is growing evidence for a role of high WSS in plaque destabilization [5,9,10]. Gijssen and colleagues [10] showed a strong correlation between WSS and strain in human coronary arteries, suggesting that high WSS decreased the mechanical strength of the plaque by biological processes. Although atherosclerotic plaques are generated at low WSS locations in the arterial system [1,3], lack in compensatory positive remodelling and thus lumen narrowing will result in exposure to high WSS at the endothelium [5]. The involvement of WSS in plaque destabilization is mediated by matrix breakdown by plasmin, MMPs and SMCs apoptosis [5].

Twenty percent of the ruptures were located distally and although the downstream side of the plaque is considered to be exposed to low WSS [10], we observed that three out of these four ruptures were exposed to higher WSS than the non-ruptured plaque regions. Since the WSS is largely influenced by both the local lumen shape and the 3D geometry proximally, apparently the WSS at the distal site of the stenosis is not per se low.

The average WSS values we found at the non-rupture sites were 2 times higher than reported in literature for healthy carotid arteries [18]. With atherosclerotic plaques, the luminal area is compromised which will increase the WSS values. But since we compared the WSS at the rupture site to the non-rupture site, the absolute values are of little influence on the results. Although the severity of stenosis is considered a risk factor for cardiovascular events [14], our data showed an equal distribution in degree of



stenosis among the patients with plaque rupture. Interestingly, the location of rupture occurred at the thicker part of the vessel wall, potentially the more diseased sites of the vessel wall which could be more susceptible to the biological high WSS weakening. This finding could contribute in the current discussion whether carotid-wall-thickness can improve stroke prediction [24,25]. Thereby, knowledge on wall thickness and WSS could serve in final decision making for invasive therapy.

In order to define the region where plaque was located; we choose a threshold of 1 mm for the wall thickness [19,20]. If we increased this threshold to 2 mm, to include only the more severely diseased locations for analysis, we obtained similar results. So our data were not affected by the definition for atherosclerotic plaque.

This study has several limitations. Our study on the influence of WSS on plaque rupture was performed on plaques already ruptured. Therefore, we needed to manually reconstruct the lumen geometry before rupture. Because the ulceration is a small cavity inside the plaque, filled with blood and connected to the lumen, it can easily be separated from the lumen and for that reason we are confident that the lumen without the ulceration, as we reconstructed, represents the lumen before rupture.

Furthermore, based on visual inspection of various ulcerations, we expect that the continuity of the lumen is not compromised by the rupture. For the best possible analysis, serial imaging data is required.

A small group of patients was studied, which did not allow stratifying the patients accordingly to age, gender and risk factors. Nevertheless, the data with respect to the location of rupture were consistent with results in larger patient groups [7,8].

As boundary conditions for our computational fluid dynamics we used time averaged flow and a rigid, non-moving geometry. Previously it has been shown that the WSS locations as calculated in a rigid geometry with time averaged flow resembled the WSS locations as derived from calculations with time dependent flow and flexible tubes [26]. Moreover Lee et al. [27] showed in carotid arteries that the time-averaged WSS was highly correlated to oscillatory WSS. Both observations justify the chosen boundary conditions and therefore it is unlikely that our data are influenced by the assumption of time averaged flow and rigid walls.

## CONCLUSIONS

Our data showed that plaque rupture was located at the thicker part of the plaque, where the WSS tended to be higher than at the non-ruptured plaque regions. This suggests that higher WSS plays a role in the (biological) weakening and subsequent rupture of atherosclerotic plaque.

## REFERENCES

1. VanderLaan PA, Reardon CA, and Getz GS, Site specificity of atherosclerosis: site-selective responses to atherosclerotic modulators. *Arteriosclerosis, Thrombosis, and Vascular Biology*, 2004. 24(1): p. 12-22.
2. Malek AM, Alper SL, and Izumo S, Hemodynamic shear stress and its role in atherosclerosis. *Journal of the American Medical Association*, 1999. 282(21): p. 2035-42.
3. Slager C, et al., The role of shear stress in the generation of rupture-prone vulnerable plaques. *Nature Clinical Practice Cardiovascular Medicine*, 2005. 2(8): p. 401-7.
4. Glagov S, et al., Compensatory enlargement of human atherosclerotic coronary arteries. *the New England Journal of Medicine*, 1987. 316(22): p. 1371-5.
5. Slager C, et al., The role of shear stress in the destabilization of vulnerable plaques and related therapeutic implications. *Nature Clinical Practice Cardiovascular Medicine*, 2005. 2(9): p. 456-64.
6. Dirksen MT, et al., Distribution of inflammatory cells in atherosclerotic plaques relates to the direction of flow. *Circulation*, 1998. 98(19): p. 2000-3.
7. Lovett J and Rothwell P, Site of Carotid Plaque Ulceration in Relation to Direction of Blood Flow: An Angiographic and Pathological Study. *Cerebrovascular Diseases*, 2003. 16(4): p. 369-75.
8. de Weert TT, et al., Atherosclerotic Plaque Surface Morphology in the Carotid Bifurcation Assessed With Multidetector Computed Tomography Angiography. *Stroke*, 2009. 40(4): 1334-40
9. Groen HC, et al., Plaque rupture in the carotid artery is localized at the high shear stress region: a case report. *Stroke*, 2007. 38(8): p. 2379-81.
10. Gijzen FJ, et al., Strain distribution over plaques in human coronary arteries relates to shear stress. *American Journal of Physiology - Heart and Circulatory Physiology*, 2008. 295(4): p. H1608-14.

11. Fukumoto Y, et al., Localized elevation of shear stress is related to coronary plaque rupture: a 3-dimensional intravascular ultrasound study with in-vivo color mapping of shear stress distribution. *Journal of the American College of Cardiology*, 2008. 51(6): p. 645-50.
12. Saba L, et al., Efficacy and sensitivity of axial scans and different reconstruction methods in the study of the ulcerated carotid plaque using multidetector-row CT angiography: comparison with surgical results. *American Journal of Neuroradiology*, 2007. 28(4): p. 716-23.
13. de Monyé C, et al., Sixteen-detector row CT angiography of carotid arteries: comparison of different volumes of contrast material with and without a bolus chaser. *Radiology*, 2005. 237(2): p. 555-62.
14. Rothwell PM, et al., Prognostic value and reproducibility of measurements of carotid stenosis. A comparison of three methods on 1001 angiograms. *European Carotid Surgery Trialists' Collaborative Group. Stroke*, 1994. 25(12): p. 2440-4.
15. de Weert TT, et al., In vivo characterization and quantification of atherosclerotic carotid plaque components with multidetector computed tomography and histopathological correlation. *Arteriosclerosis, Thrombosis, and Vascular Biology*, 2006. 26(10): p. 2366-72.
16. Moyle KR, Antiga L, and Steinman D, Inlet conditions for image-based CFD models of the carotid bifurcation: is it reasonable to assume fully developed flow? *Journal of Biomechanical Engineering*, 2006. 128(3): p. 371-9.
17. Seo T, Schachter L, and Barakat A, Computational Study of Fluid Mechanical Disturbance Induced by Endovascular Stents. *Annals of Biomedical Engineering*, 2005. 33(4): p. 444-56.
18. Cheng C, et al., Large variations in absolute wall shear stress levels within one species and between species. *Atherosclerosis*, 2007. 195(2): p. 225-35.
19. Chambless LE, et al., Carotid wall thickness is predictive of incident clinical stroke: the Atherosclerosis Risk in Communities (ARIC) study. *American Journal of Epidemiology*, 2000. 151(5): p. 478-87.
20. Harloff A, et al., Carotid intima-media thickness and distensibility measured by MRI at 3 T versus high-resolution ultrasound. *European Radiology*, 2009. 19(6): p. 1470-9.
21. Tang D, et al., Sites of rupture in human atherosclerotic carotid plaques are associated with high structural stresses. An in vivo mri-based 3d fluid-structure interaction study. *Stroke*, 2009. 40: p. 3258-63.
22. Li ZY and Gillard JH, Plaque rupture: plaque stress, shear stress, and pressure drop. *Journal of the American College of Cardiology*, 2008. 52(13): p. 1106-7; author reply 1107.

23. Hoeks AP, et al., Local blood pressure rather than shear stress should be blamed for plaque rupture. *Journal of the American College of Cardiology*, 2008. 52(13): p. 1107-8; author reply 1108-9.
24. Finn AV, Kolodgie FD, and Virmani R, Correlation between carotid intimal/medial thickness and atherosclerosis: a point of view from pathology. *Arteriosclerosis, Thrombosis, and Vascular Biology*, 2010. 30(2): p. 177-81.
25. Simon A, Megnien JL, and Chironi G, The value of carotid intima-media thickness for predicting cardiovascular risk. *Arteriosclerosis, Thrombosis, and Vascular Biology*, 2010. 30(2): p. 182-5.
26. Younis HF, et al., Hemodynamics and wall mechanics in human carotid bifurcation and its consequences for atherogenesis: investigation of inter-individual variation. *Biomechanics and Modeling in Mechanobiology*, 2004. 3(1): p. 17-32.
27. Lee SW, Antiga L, and Steinman D, Correlations among indicators of disturbed flow at the normal carotid bifurcation. *Journal of Biomechanical Engineering*, 2009. 131(6): p. 061013.





CHAPTER

# 4

---

## **PLAQUE RUPTURE IN THE CAROTID ARTERY IS LOCALIZED AT THE HIGH SHEAR STRESS REGION: A CASE REPORT**

Harald Groen, Frank Gijssen, Aad van der Lugt, Marina Ferguson,  
Thomas Hatsukami, Antonius van der Steen, Chun Yuan, Jolanda Wentzel

*Published in: Stroke 2007, 38(8):2379-8*

### ***Background***

Cerebrovascular events are related to atherosclerotic disease in the carotid arteries and are frequently caused by rupture of a vulnerable plaque. These ruptures are often observed at the upstream region of the plaque, where the wall shear stress (WSS) is considered to be highest. High WSS is known for its influence on many processes affecting tissue regression. Until now there have been no serial studies showing the relationship between plaque rupture and WSS.

### ***Methods***

We investigated a serial magnetic resonance imaging (MRI) dataset of a 67-year-old woman with a plaque in the carotid artery at baseline and an ulcer at 10 months follow-up. The lumen, plaque components (lipid/necrotic core, intraplaque hemorrhage) and ulcer were segmented and the lumen contours at baseline were used for WSS calculation.

### ***Results***

Correlation of the change in plaque composition with the WSS at baseline showed that the ulcer was generated exclusively at the high WSS location.

### ***Conclusion***

In this serial MRI study we found plaque ulceration at the high WSS location of a protruding plaque in the carotid artery. Our data suggests that high WSS influences plaque vulnerability and therefore may become a potential target for predicting future events.



## INTRODUCTION

Cerebrovascular events are related to atherosclerotic disease in the carotid arteries and are frequently caused by rupture of a vulnerable plaque. These plaques are characterized by the presence of a large lipid pool covered by a thin fibrous cap with infiltration of macrophages and a scarcity of smooth muscle cells. Plaque rupture has been more frequently observed at the proximal, upstream side of the minimal lumen diameter [1] which is supposedly exposed to higher WSS. There is ample evidence that the endothelium responds to high WSS such that it induces an anti-proliferative action [2] which may lead to cap thinning. For that reason, we hypothesized that high WSS at the upstream side of the plaque has a biological effect on the fibrous cap and therefore enhance plaque vulnerability [3]. We present a case study, in which we demonstrate the relation between high WSS and plaque rupture.

## MATERIALS AND METHODS

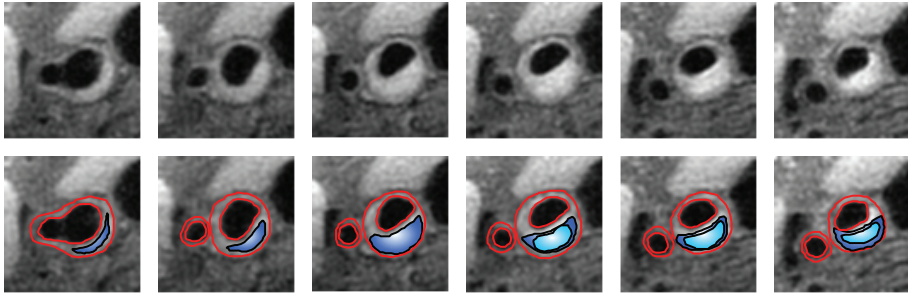
### *Patient*

Serial carotid MRI examinations were performed on a 67-years-old individual, who was found to have moderate carotid stenosis by duplex ultrasonography. The institutional review committee approved the study and the patient gave informed consent. The patient's baseline MRI showed a plaque in the right carotid artery and the 10-month follow-up MRI showed a plaque rupture with an ulcer [4].

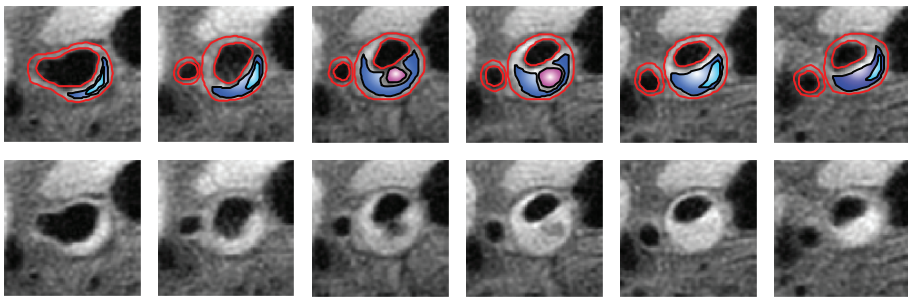
### *MRI*

The high-resolution, multi-sequence MRI protocol at baseline and follow-up included 4 sequences: 3D time of flight (TOF), T1, T2 and Proton Density (PD) weightings. The in-plane resolution was 0.3x0.3 mm with a slice thickness of 2 mm. The image segmentation was based on the signal intensities (SI) relative to the adjacent sternocleidomastoid muscle. A validated scheme [5] of hyper-, iso- and hypo-intense SIs from the TOF-, T1-, T2- and PD-images was used to identify the lumen, plaque components (lipid/necrotic core, intraplaque hemorrhage) and ulcer (Figure 4-1)

Baseline



Follow-up



■ Lipid/necrotic core ■ Intraplaque hemorrhage ■ Ulcer

**Figure 4-1:** Matched MRI images (T1) with and without superimposed vessel wall segmentation at baseline (**top**) and 10-months follow-up (**bottom**).

### *Computational fluid dynamics*

In preparation for the WSS calculation, the baseline lumen contours were imported into GAMBIT (Fluent Inc., Canonsburg, Pennsylvania, USA) from which a 3D meshed volume was created. At the entrance and exit of the carotid bifurcation circular segments were added to minimize the influence of the boundary conditions. A static parabolic inflow profile with a peak velocity of 0.6 m/s was chosen to obtain physiological shear stress values (1.2 Pa) at the common carotid artery. FIDAP (Fluent Inc., Canonsburg, Pennsylvania, USA) was used to compute the flow velocities and WSS distribution by using free outflow for the internal- and external carotid arteries, no slip at the wall and blood was simulated as an incompressible Newtonian fluid (viscosity 3.5 mPa.s, density 1050 kg/m<sup>3</sup>).

## Analysis

The segmentations at baseline and follow-up were matched using the bifurcation as marker to align the slices in the superior direction and the center of the lumen in the transversal direction. The slices containing plaque at baseline and/or follow-up were selected for further analysis. For each slice the wall was divided into 256 parts, such that each baseline lumen contour was divided into 256 equidistant sections. In each part the average baseline WSS and the baseline wall component volumes (i.e. area times slice thickness) were calculated using in-house created software. Subsequently, in each part the volumes of the wall components at follow-up were determined.

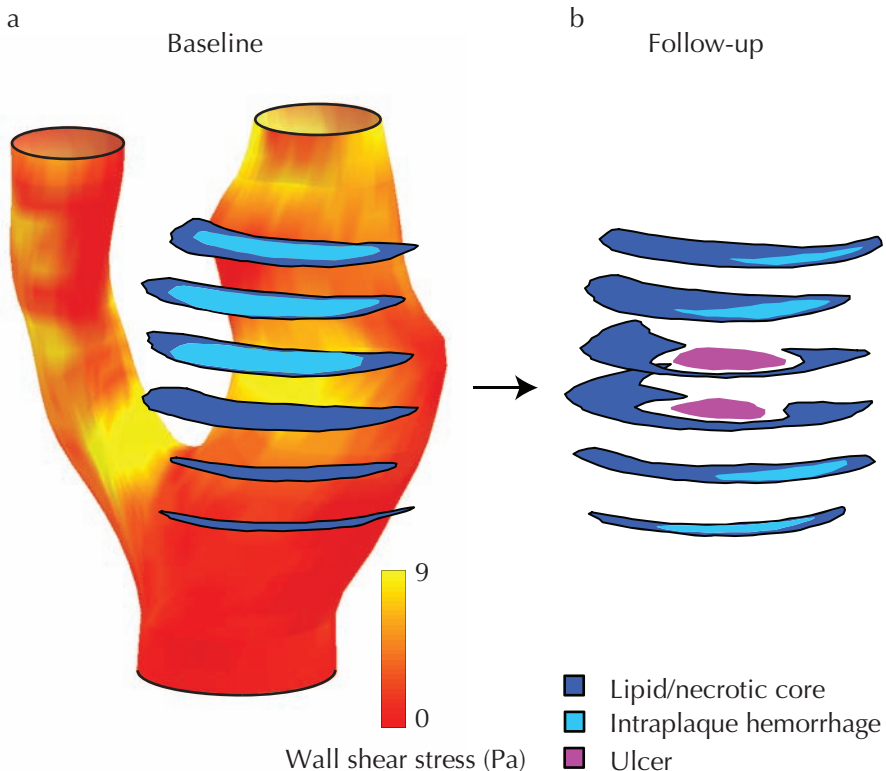


**Figure 4-2:** a) Baseline wall shear stress mapped at baseline 3D lumen geometry of a carotid bifurcation including plaque segmentation; b) Plaque segmentation at 10-months follow-up, including the ulcer.

### Results

Six matched pairs of MRI images were available for analysis (Figure 4-1). At baseline, the lipid/necrotic core volume was 308 mm<sup>3</sup>, from which 34% consisted of intraplaque hemorrhage, and increased to 335 mm<sup>3</sup> with 16% intraplaque hemorrhage during 10-month follow-up period. The average WSS at baseline in the carotid bifurcation was 3.2±2.0 Pa and the site of ulceration was observed at the highest WSS (Figure 4-2).

To quantify this observation, the data, linking plaque composition to WSS, was divided into tertiles with respect to their WSS value (low, middle, and high). For each tertile the average volume of wall component per part at baseline (Figure 4-3a) and follow-up (Figure 4-3b) was computed. The total volume and the lipid/necrotic volume increased both with WSS and time and the ulcer at follow-up was found in the highest WSS tertile (Figure 4-3).

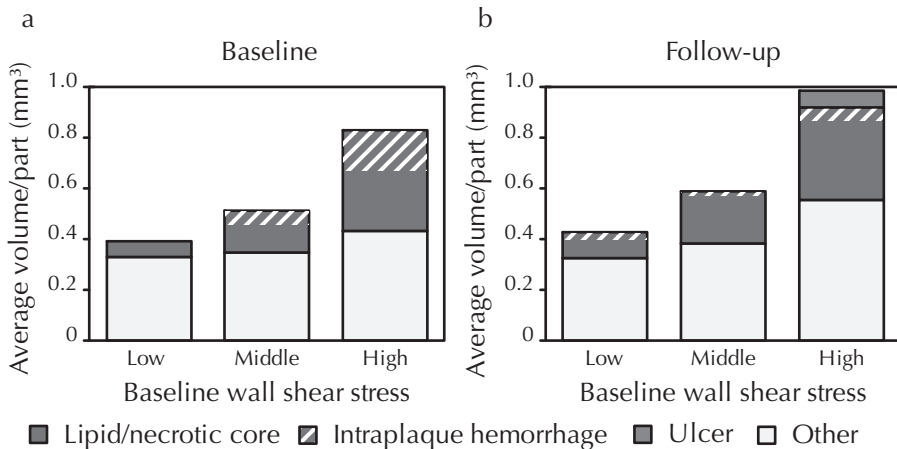


**Figure 4-3:** a) Vessel wall composition at baseline; b) 10-months follow-up as function of baseline wall shear stress (Low: 0.1-2.1; Middle 2.1-3.8; High 3.8-8.8 Pa).

## DISCUSSION

This case report shows the co-localization of high WSS at baseline and a subsequent ulceration 10-months later using serial MRI. Little is known about the mechanisms, which make the vulnerable plaque susceptible to rupture. In a recent review [3] a number of biological pathways were

proposed, which could explain the important role of high WSS in destabilization of the vulnerable plaque. In this case study the weakest location appeared at the upstream highest WSS region of the plaque. This agrees with observations that plaque-destabilizing components, including macrophages and MMP-9 are highest in concentration at the upstream (high WSS) region of the plaque [3].

Assumptions were made for calculating the WSS distribution. Although the assumptions could have influenced the absolute WSS, several studies showed that they are of second order of importance. Moreover, we used the distribution rather than the absolute WSS, so that the assumptions most likely did not influence the final conclusion of the study.

Intraplaque hemorrhage is known to be involved in plaque progression and cerebral events. The observed intraplaque hemorrhage at baseline could have accelerated the destabilisation of the plaque, however, in this case the site of rupture was precisely at the highest WSS region. More patients will be required to confirm this preliminary finding that high WSS is involved in plaque rupture and to prove the value of this technology in risk prediction.

## REFERENCES

1. Lovett J and Rothwell P, Site of Carotid Plaque Ulceration in Relation to Direction of Blood Flow: An Angiographic and Pathological Study. *Cerebrovascular Diseases*, 2003. 16(4): p. 369-75.
2. Malek AM, Alper SL, and Izumo S, Hemodynamic shear stress and its role in atherosclerosis. *Journal of the American Medical Association*, 1999. 282(21): p. 2035-42.
3. Slager C, et al., The role of shear stress in the destabilization of vulnerable plaques and related therapeutic implications. *Nature Clinical Practice Cardiovascular Medicine*, 2005. 2(9): p. 456-64.
4. Chu B, et al., Images in cardiovascular medicine. Serial high-spatial-resolution, multisequence magnetic resonance imaging studies identify fibrous cap rupture and penetrating ulcer into carotid atherosclerotic plaque. *Circulation*, 2006. 113(12): p. e660-1.
5. Saam T, et al., Quantitative evaluation of carotid plaque composition by in vivo MRI. *Arteriosclerosis, Thrombosis, and Vascular Biology*, 2005. 25(1): p. 234-9.



CHAPTER

# 5

---

## THREE-DIMENSIONAL REGISTRATION OF HISTOLOGY OF HUMAN ATHEROSCLEROTIC CAROTID PLAQUES TO *IN VIVO* IMAGING

Harald Groen, Theo van Walsum, Sietske Rozie, Stefan Klein,  
Kim van Gaalen, Frank Gijssen, Piotr Wielopolski, Heleen van Beusekom,  
Rini de Crom, Hence Verhagen, Antonius van der Steen,  
Aad van der Lugt, Jolanda Wentzel, Wiro Niessen

*Published in: Journal of Biomechanics 2010, 43(11):2087-92*

### ***Background***

An accurate spatial relationship between 3D *in vivo* carotid plaque and lumen imaging and histological cross sections is required to study the relationship between biomechanical parameters and atherosclerotic plaque components.

### ***Methods***

We present and evaluate a fully three-dimensional approach for this registration problem which accounts for deformations that occur during the processing of the specimens. By using additional imaging steps during tissue processing and semi-automated non-linear registration techniques a 3D-reconstruction of the histology is obtained. The methodology was evaluated on five specimens obtained from patients, operated for severe atherosclerosis in the carotid bifurcation.

### ***Results***

In more than eighty percent of the histology slices, the quality of the semi-automated registration with computed tomography angiography (CTA) was equal to or better than the manual registration. The inter-observer variability was between one and two *in vivo* CT voxels and was equal to the manual inter-observer variability. Our technique showed that the angles between the normals of the registered histology slices and the *in vivo* CTA scan direction ranged from 6° to 56°, indicating that proper 3D-registration is crucial for establishing a correct spatial relation with *in vivo* imaging modalities.

### ***Conclusion***

This new 3D-reconstruction technique of atherosclerotic plaque tissue opens new avenues in the field of biomechanics as well as in the field of image processing, where it can be used for validation purposes of segmentation algorithms.



## INTRODUCTION

There is ample evidence that wall shear stress (WSS) plays an important role in atherosclerotic plaque formation and progression [1]. Moreover, some recent studies suggest that WSS is also involved in determining plaque composition [2] and plaque destabilization in advanced atherosclerosis [3-5]. More detailed studies on the relationship between WSS and plaque composition are needed to confirm those relationships.

Histology is the gold standard for obtaining plaque composition, while WSS is often assessed applying computational fluid dynamics in a geometrical model representing the *in vivo* geometry. Often non-invasive *in vivo* imaging techniques are used to create a 3D model of the artery for these calculations. As histological features of carotid atherosclerosis differ considerably across plaques [6,7], accurate 3D-registration of histological slices to *in vivo* images is a prerequisite for studying relationships between plaque components and biomechanical parameters.

Usually, histological sections of vessels are registered to *in vivo* images, by manual selecting the 2D image slice that best matches a histological slide [8-11], neglecting out-of-plane angulations, shrinkage and non-rigid deformations that may have occurred during tissue processing. Methods have been developed for *ex vivo* registration for brain tissue [12-14] and vessels [15,16], which include either in-plane rotation, translation, and/or non-rigid registration based on landmarks. However, registration of atherosclerotic tissue with a heterogeneous composition and thus irregular deformations differs significantly from that of large, homogeneous, solid brain tissue. The aim of this work was to develop, implement and validate a new method to optimally register histological sections of human carotid plaques to *in vivo* imaging data. This is the first study which I) combined a fully 3D approach -including out-of-plane rotation- in registering human carotid plaque histology to *in vivo* images; II) used *ex vivo* high-resolution imaging techniques to capture deformations that occur during the tissue processing; III) included semi-automated non-rigid registration techniques to compensate for these deformations and IV) compared the results with manual registration.

## MATERIALS AND METHODS

### *Specimen processing*

Carotid plaques from five patients (male, mean age  $63 \pm 8$  year), who prior to carotid endarterectomy (CEA) underwent computed tomography angiography (CTA) imaging, were used for this study. This study was approved by the Institutional Review Board, and patients gave informed consent for using the CEA material. After careful removal, the plaque was gently washed and snap-frozen using liquid nitrogen and stored at  $-80^{\circ}\text{C}$ . Later, the plaques were thawed and fixed using 3.5-4.0% buffered formalin for 24 h, followed by decalcification with EDTA and embedding in paraffin. Serial  $5 \mu\text{m}$  thick axial slices were obtained at 1 mm intervals and stained with Elastica von Gieson (EvG, Merck, Germany). Figure 5-1a gives an overview of the different specimen-processing steps.

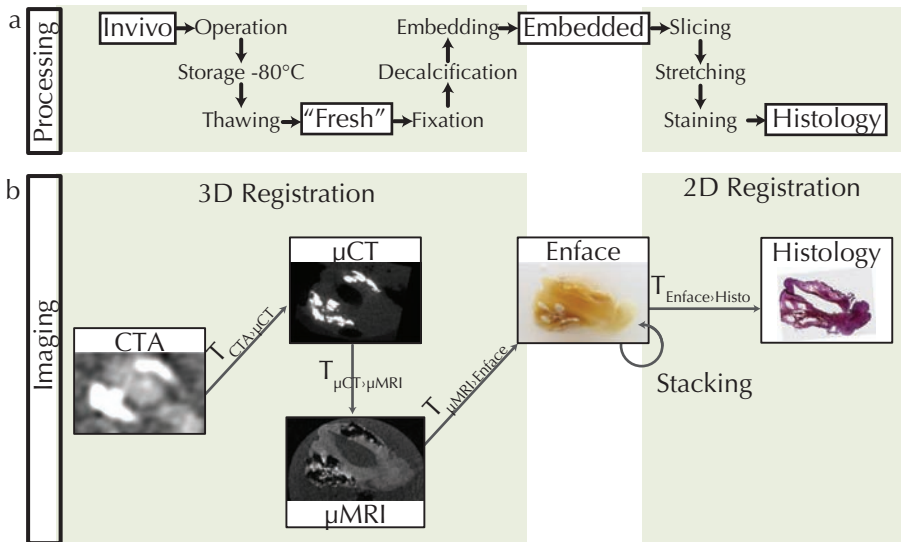


**Figure 5-1:** a) The specimen processing pathway and b) imaging, in combination with the registrations performed. Transformation subscripts denote the domains that are registered.

## *In vivo and ex vivo image acquisition*

**Table 5-1:** Image modalities.

Modality	Voxel/pixel size ( $\mu\text{m}$ )	Information
CTA	255 x 255 x 600	16-slice: 1.0 B46f, 80cc visip 320 4/s
	300 x 300 x 400	64-slice: 0.75 B46f, 80cc visip 320 4/s
$\mu\text{CT}$	18 x 18 x 18	Scanned in air
$\mu\text{MRI}$	100 x 100 x 100	3DT1w, scanned in formalin
Enface	15 x 15	2D enface photo of sample embedded in paraffin
Histology	1.82 x 1.82	Elastica von Gieson

Before CEA ( $39 \pm 42$  days), the patients underwent CTA on a 16-slice or 64-slice multidetector CT scanner (Siemens, Sensation 16 ( $n=1$ ) or Sensation 64 ( $n=4$ ), Erlangen, Germany) with a standardized contrast-enhanced protocol [17]. Additional *ex vivo* imaging was performed during the tissue processing (Figure 5-1b) to capture the specimen deformations (Table 5-1):

**Fresh:** After thawing, the specimen was put in a vial and imaged at high resolution with both MRI and CT. For the MR images a 3.0-T MRI scanner (Signa Excite, GE Healthcare, USA) using a 2 cm single-loop coil (Flick Engineering Solutions B.V., the Netherlands) was applied. A high resolution, i.e.  $0.1 \times 0.1 \times 0.1 \text{ mm}^3$ , 3DT1w scan was used in the registration process because of the clear plaque component discrimination [18]. We refer to the *ex vivo* MRI as  $\mu\text{MRI}$ . Next, for calcium imaging the vial was scanned with a  $\mu\text{CT}$  scanner (Skyscan 1072, Skyscan, Belgium), operating at 80 kV and 100  $\mu\text{A}$  ( $18 \times 18 \times 18 \mu\text{m}^3$ ). These images were used as guides to deform the histological slices to resemble the *in vivo* shape, and to determine the position of the histology slices in the *in vivo* image.

**Embedded:** Slicing the embedded specimen will stretch the thin tissue samples resulting in considerable deformations of both vessel wall tissue and luminal area [15]. To capture those deformations, we imaged the specimen in paraffin during the slicing process. This allowed us to first apply a 2D shape correction of the histological slices and subsequently stack the histology in 3D prior to registration with the  $\mu\text{MRI}$  images. To this end, a digital photo (IXUS 60, Canon, Japan) was taken of the cutting plane (called: *enface*) at each 1 mm interval, once without and once with

a calibration sheet in the field of view (not shown). The stained histological slices were digitized using the NanoZoomer Digital Pathology (C9600, Hamamatsu, Japan) at 40x magnification.

### *Registration*

Our semi-automatic registration approach consists of three distinct stages using rigid and non-rigid registrations (Figure 5-1b) and the manual segmentations of the lumen and outer vessel wall (this is the outer boundary present in histology after CEA, i.e. the media-adventitia interface). Note that the description below is from right to left.

#### *Histology to enface 3D*

In the first stage, the histology slices were correctly stacked in 3D, which is a two-step approach (Figure 5-1b): First, the *enface* images were stacked, and, second, the histological slices are registered to their corresponding *enface* slice to obtain a stack of deformed histology slices.

**Stacking:** Before the *enface* images were stacked into a 3D image, a 2D in-plane rigid registration was applied to each of the 2D *enface* slices. In the registration, first each 2D image was calibrated with the calibration grid, and then registered to its adjacent image by point-based registration using manually annotated landmarks.

**$T_{\text{Enface} \rightarrow \text{Histo}}$ :** Each of the histological slices was registered to its corresponding slice in the 3D *enface* stack, which gave a 3D stack of histological images. This step was the most challenging, since histological processing introduces non-rigid deformations such as tearing and folding (Figure 5-1b). To account for these non-rigid deformations, a high-dimensional deformation model was used. We choose to parameterize the displacement field with a B-spline model [19]. In both imaging modalities, the lumen and the outer vessel wall were manually segmented. The registration was initialized with a rigid registration, based on manually annotated landmarks in the *enface* and histology images. We then proceeded with an automatic registration, in which the B-spline control point displacements were found by maximizing the sum of three terms: mutual information (MI) between the original images, MI between the lumen segmentations, and MI between the outer vessel wall segmentations. This similarity measure was maximized with an iterative stochastic gradient-descent algorithm

[20]. By including manual segmentations in the similarity measure, prior knowledge is incorporated in the registration process.

### *Enface 3D to $\mu$ MRI and $\mu$ CT*

The purpose of this step is twofold: I) we determine the 3D orientation of the 3D stack of histological slices with respect to the  $\mu$ MRI, as the slicing direction does not necessarily coincide with the axial plane of the  $\mu$ MRI images; II) we correct for deformations of the sample prior to embedding.

$T_{\mu\text{MRI} \rightarrow \text{Enface}}$ : The registration was initialized with a rigid registration based on manually annotated landmarks in the *enface* and  $\mu$ MRI images. Subsequently, an automated rigid registration was performed, using the histological image data and a similarity measure identical to the one used for the  $T_{\text{Enface} \rightarrow \text{Histo}}$  registration. Therefore, lumen and outer vessel wall were segmented at each 0.5 mm of the  $\mu$ MRI images, and interpolated between those contours on the intermediate slices. This registration was refined with a 3D B-spline-based non-rigid registration using the same similarity measure. The non-rigid deformations were limited to in-plane 2D deformation of the histological slices, maintaining continuity of these deformations along the longitudinal axis.

$T_{\mu\text{CT} \rightarrow \text{Enface}}$ : This registration was based on manually annotated landmarks in the  $\mu$ CT and *enface* images using a rigid transformation and isotropic scaling. This registration is not used in the current registration chain; the main purpose of it was to assess the overall scaling that occurs during the processing of the specimen. In addition, it is used to compare the rigid registration parts of  $T_{\mu\text{MRI} \rightarrow \text{Enface}}$  and  $T_{\mu\text{CT} \rightarrow \text{Enface}}$ .

### *$\mu$ MRI to *in vivo* CTA*

In the final stage the deformed histology in the  $\mu$ MRI domain was related to the *in vivo* CTA data. We first registered high-resolution images from different modalities ( $\mu$ MRI to the  $\mu$ CT), followed by monomodal registering of images acquired at different resolutions ( $\mu$ CT and CT).

$T_{\mu\text{CT} \rightarrow \mu\text{MRI}}$ : We assumed a rigid registration, as the specimen was kept inside the vial and scanned successively. Registration was point-based, using manually annotated landmarks in the  $\mu$ CT and the  $\mu$ MRI image.

$T_{\text{CTA} \rightarrow \mu\text{CT}}$ : The final step was relating the  $\mu$ CT to the *in vivo* CTA images. In this step, we assumed a similarity transform (rigid transformation and isotropic scaling). Although the CEA operation will always lead to some

deformation of the specimen, we expected the relatively stiff plaque tissue to maintain its approximate shape using our surgical technique. The registration was again based on manual annotation of landmarks, such as calcium spots, lumen and bifurcation position, which are clearly visible in both image modalities.

## ANALYSIS

### *Statistics of method*

One observer (HG) manually placed landmarks and segmented lumen and outer vessel wall in the histology, *enface* and  $\mu$ MRI of the five patients. We report statistics on the root mean squared distances (RMS) in the point-based manual registrations, and scaling factors found in the different registration steps. Additionally, we determined the angulation, i.e. the angle between the normal of the registered histological slice and the normal of the axial CTA slices for each of the specimens.

### *Registration evaluation*

The evaluation of the semi-automatic method was done by comparing the final result of histology and CTA registrations obtained by the semi-automatic registration with the results obtained by manual registration performed by an expert radiologist. For this purpose pairs of histological cross sections and CTA slices were created based on the semi-automatic registration and a manual selection by an experienced researcher (SR). These pairs of histological cross sections and best match of CTA cross-sections were blindly presented to the expert radiologist (AvdL) and he selected the pair that matched best, or stated that the registrations were equally good. Furthermore, an inter-observer study was carried out for both methods. A second observer (TvW) repeated the manual annotations, i.e. lumen and outer vessel wall segmentations and landmarks, for two randomly chosen datasets. The registrations were also performed using these annotations. The overlap of the final deformed segmentations in the CTA domain provides a measure of inter-observer variability [21]. For reference, we also calculated the overlap of the segmentation with itself after translation of the lumen and outer vessel wall segmentations with one voxel, i.e.  $0.3 \times$

0.3 x 0.4 mm<sup>3</sup>, and two CTA voxels. To obtain the inter-observer statistics for the manual registration method, two independent experienced researchers (SR, TdW), blinded for previous registrations and without access to the *ex vivo* imaging modalities, registered the same two datasets using the manual registration method. As measure for the spatial correspondence between the two observers, the overlap was calculated but now 2D slices were translated and rotated according to the average difference between the two observers of in-slice-position and in-plane rotation. We call this measure a surrogate-reference-overlap.

## RESULTS

### *Registration*

Figure 5-2 shows the final result of the registration process for one patient (the others are available in the supplementary Figure S5-1): the  $\mu$ MRI,  $\mu$ CT and *in vivo* CTA images are aligned with the corresponding deformed histology slices. A large plaque is located proximal to the bifurcation (0 mm) with multiple necrotic cores aligning well with the  $\mu$ MRI. At position -4 mm, a small side branch proximal to the bifurcation is clearly visible in all modalities. In this case, no calcifications are present in either CTA or  $\mu$ CT.

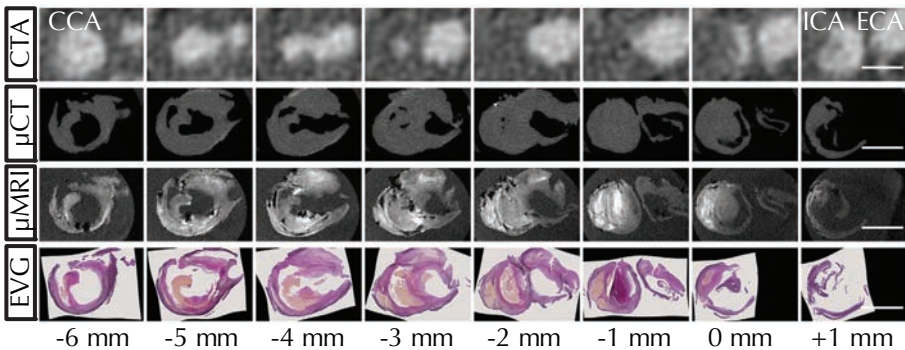


**Figure 5-2:** Slice by slice comparison of a registered atherosclerotic carotid plaque. From left to right: common carotid artery (CCA), through the bifurcation (0 mm) into the internal (ICA) and the external carotid arteries (ECA) in steps of 1 mm. Top to bottom: Registered CTA,  $\mu$ CT,  $\mu$ MRI (3DT1w), and EVG (histology, Elastica von Gieson staining) slices showing a large atherosclerotic plaque at the bifurcation with multiple necrotic cores. Scale bar is 5 mm.

**Table 5-II:** Patients (N=5) average values of affine transformations.

From	To	Scale	RMS	N
CTA	μCT	0.97 ± 0.11	0.85 ± 0.23	8 ± 2
μCT	μMRI	1*	0.21 ± 0.04	8 ± 1
μCT	Enface	0.89 ± 0.06	0.83 ± 0.18	10 ± 2
μMRI	Enface	0.88 ± 0.03	0.81 ± 0.23	9 ± 2
Enface	Histology	1.13 ± 0.15	0.35 ± 0.25	5 ± 2
μCT	Histology	1.06 ± 0.19		
CTA	Histology	1.02 ± 0.11		

The average ± standard deviation scaling factor (-) for the registration of the different modalities. RMS (mm) and number of points (N) used for registration based on manually placed landmarks. \*Scaling is not allowed.

Table 5-II shows the average scaling factors for the landmark-based registrations. On average the histological slices expanded 13±15% after being cut from the paraffin block. The entire tissue processing seems to have a small effect (1.02±0.11) on the final histology size relative to the situation *in vivo* although the large standard deviation indicates large variation among the samples. Figure 5-3 shows the out-of-plane angulation found per patient after registration. Two were smaller than 10°, two between 20° and 30° and one was even 56°, indicating that large differences between the *in vivo* scan direction and tissue slicing are present.

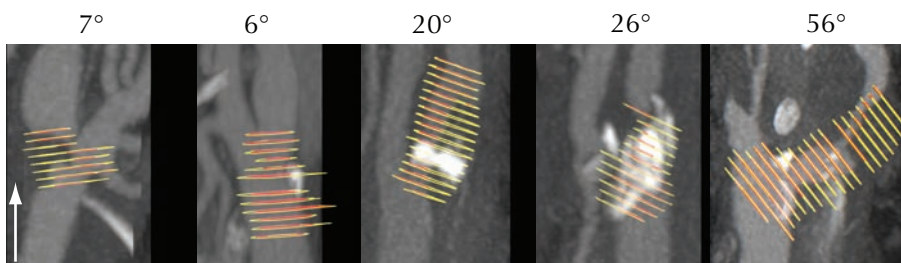


**Figure 5-3:** Out-of-plane angle between histology and CTA scan direction (arrow) for all patients. Yellow lines are the outer vessel wall contours, red lines are the lumen contours of the histological slices. CTA is visualized using volume rendering, with bright white structures calcifications.



## Registration evaluation

For the comparison of the manual with the semi-automatic registration, 70 histology-CTA combinations were available from the five patients. Due to poor quality of the histology slices, 7 (10%) could not be judged. Of the remaining 63 combinations, 11 (18%) combinations were in favor of the manual registration, in 19 (30%) of the cases there was no difference between the two methods and in 33 (52%) combinations the semi-automatic registration was considered better (Figure 5-4).

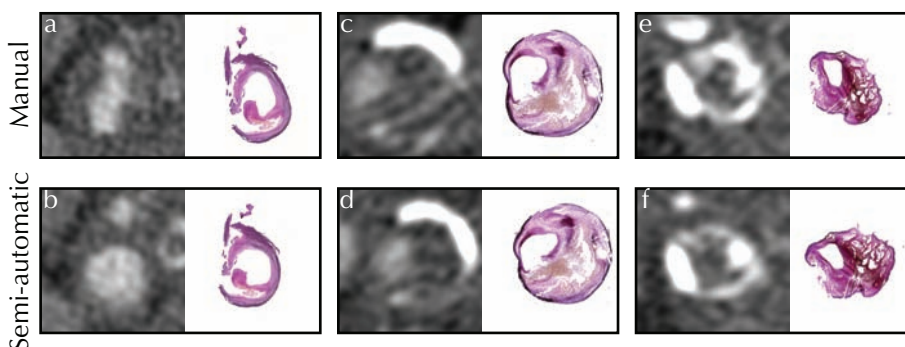


**Figure 5-4:** Slice-based comparison of manual (a, c, e) and semi-automatic registration (b, d, f). For these examples, the radiologist scored the registration of b better than a, c and d equal and e better than f.

Table 5-III shows the result of the inter-observer variability. It shows the overlap for the lumen (0.71 and 0.67) and the outer vessel wall area (0.87 and 0.84) for two of the five patients. The table also shows the overlap for the lumen and outer vessel wall when shifted one or two voxels in the CTA data, and the average difference in translation (0.6 and 1.2 mm) and rotation ( $5^\circ$  and  $16^\circ$ ) of the manual registration. Based on comparison of the overlap (Table 5-III, column 3 vs column 4 and column 5) we concluded that the inter-observer variability of the new registration technique was between one and two *in vivo* voxel, and is comparable to the overlap of manual registration as expressed in the surrogate-reference-overlap (column 6).

**Table 5-III:** Inter-observer for two patients.

Patient	Segmentation	Overlap	Reference overlap		
			1 CTA voxel <sup>†</sup>	2 CTA voxels	Surrogate <sup>#</sup>
1	Lumen	0.71	0.77	0.61	0.73
2	Lumen	0.67	0.74	0.57	0.66
1	Outer vessel wall	0.87	0.92	0.85	0.92
2	Outer vessel wall	0.84	0.89	0.81	0.81

\* Overlap with itself after translation of one CTA voxel (0.3 x 0.3 x 0.4 mm<sup>3</sup>). Overlap=1 means perfect overlap; overlap=0 means no overlap.

# Based on the mean difference in in-plane translation and rotation between manual registrations (patient 1: 0.6 mm and 5°; patient 2: 1.2 mm and 16°).

### Example of 3D histology

Figure 5-5 shows a volume rendering of the CTA dataset together with a number of 3D-registered histology slices. In this case, an old plaque rupture (ulcer) was confirmed by histology (top slice). The remaining slices are positioned in the narrowed part of the artery, where a thin cap covering the necrotic core was present.

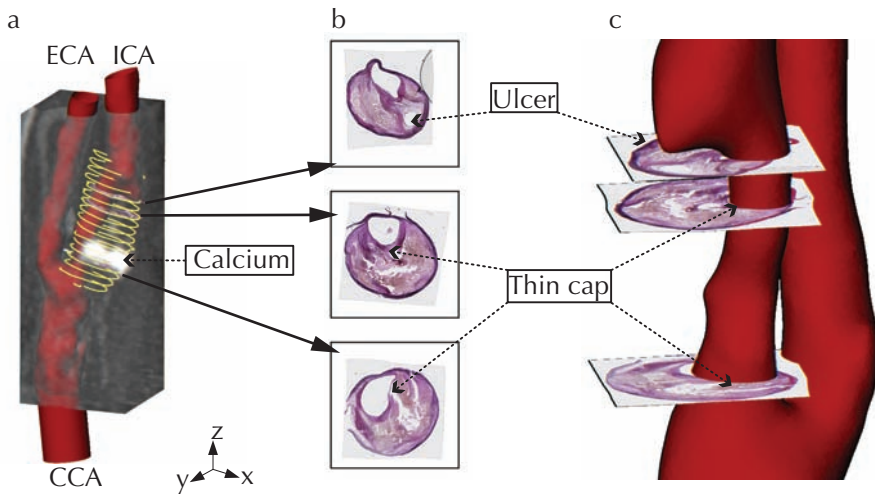


**Figure 5-5:** **a)** The carotid bifurcation region (CCA=common, ICA=internal and ECA=external carotid artery) with a volume rendering of the original CTA image (showing also calcification) combined with the lumen segmentation and deformed histology (yellow contours are the outer wall of the histology); **b)** Selected histological slices showing an old plaque rupture (ulcer) and two slices showing a thin cap covering a necrotic core in regions; **c)** Detailed plaque region showing severe lumen narrowing together with the histology.

## DISCUSSION

This article presents a framework for advanced 3D-registration of plaque histology to *in vivo* CTA data, accounting for large deformations, translations and angulations. The results show that a 3D-registration approach, including out-of-plane rotation, is essential to correctly register histology to *in vivo* CTA images. A small angulation error of  $7^\circ$  already gives a longitudinal displacement error of 0.6 mm (1.5 voxel) at a distance of 5 mm (approximately half the outer diameter). Of the five cases, three samples had an angulation much larger than  $7^\circ$ . Ignoring this angulation, which results from *in vivo* vessel orientation during acquisition and the final specimen processing, would negatively affect the spatial registration of the vessel wall. Because this angulation is hard to constrain during tissue processing, it should be corrected using registration techniques.

The stretching of the samples after slicing resulted in a tissue enlarging by a factor of  $1.13 \pm 0.15$ . The large variation can be explained by the individual processing of the slices and the variations in composition and dimensions. The overall scaling from fresh *ex vivo* ( $\mu$ CT) to histology ( $1.06 \pm 0.19$ ) is consistent with literature [11,22-25].

Since no ground-truth exists for our registration technique, we can not report the final accuracy of our method. Therefore a qualitative evaluation was performed showing that in more than eighty percent of the registrations, the quality of the semi-automatic 3D-registration was equal or better than the manual registration. Moreover, the inter-observer variability study showed that the similarity indices are between one and two *in vivo* voxel, comparable to the manual registration, which was expected given the intrinsic resolution of *in vivo* CTA imaging.

Although processing of plaque specimens is slightly more complicated because of the additional intermediate imaging steps, the additional workload is not substantial. In our experience, each of the images acquired in our current setup plays its own indispensable role in the registration process. Without the stack of *enface* images, the registration of each of the 2D histological slices to 3D  $\mu$ MRI would not have been feasible. The high resolution *ex vivo* images is also essential for the alignment in 3D and the further deformation-correction of the histological slices, as the resolution of the *in vivo* images does not seem to be sufficient for this purpose.

Our work shows that spatially relating 3D histology of carotid plaques to *in vivo* measurements is feasible. We aim to establish a large database of *in vivo* plaque images registered with multiple immuno-histological stains for detailed plaque analysis. The applications of such a database are many. As explained before, this method can be used to study the relationship between fluid dynamics and plaque composition. Although studies were performed relating histology to WSS either using generalized WSS patterns [26], or manual registered cross sections to imaging, to our knowledge, this is the first time that 3D-registered histology can be related to local WSS calculated on the *in vivo* geometry. Moreover this technique can serve as the gold standard for validation of automatic plaque segmentation and characterization algorithms.

## CONCLUSION

This study presents the successful development and thorough evaluation of a methodology for relating histological sections of atherosclerotic plaque to *in vivo* imaging. By imaging the plaque specimen at different time points during the histological processing, we were able to establish the spatial relationship between histological sections and *in vivo* images. This work is of crucial importance for establishing the relationship between biomechanical parameters and histology.

## REFERENCES

1. Malek AM, Alper SL, and Izumo S, Hemodynamic shear stress and its role in atherosclerosis. *Journal of the American Medical Association*, 1999. 282(21): p. 2035-42.
2. Cheng C, et al., Atherosclerotic lesion size and vulnerability are determined by patterns of fluid shear stress. *Circulation*, 2006. 113(23): p. 2744-53.
3. Groen HC, et al., Plaque rupture in the carotid artery is localized at the high shear stress region: a case report. *Stroke*, 2007. 38(8): p. 2379-81.
4. Gijzen FJ, et al., Strain distribution over plaques in human coronary arteries relates to shear stress. *American Journal of Physiology - Heart and Circulatory Physiology*, 2008. 295(4): p. H1608-14.

5. Tang D, et al., Sites of Rupture in Human Atherosclerotic Carotid Plaques Are Associated With High Structural Stresses. An In Vivo MRI-Based 3D Fluid-Structure Interaction Study. *Stroke*, 2009. 40: p. 3258-63.
6. Lovett J, Gallagher P, and Rothwell P, Reproducibility of Histological Assessment of Carotid Plaque: Implications for Studies of Carotid Imaging. *Cerebrovascular Diseases*, 2004. 18(2): p. 117-23.
7. Lovett JK, Redgrave JN, and Rothwell PM, A critical appraisal of the performance, reporting, and interpretation of studies comparing carotid plaque imaging with histology. *Stroke*, 2005. 36(5): p. 1091-7.
8. Liu F, et al., Automated in vivo segmentation of carotid plaque MRI with Morphology-Enhanced probability maps. *Magnetic Resonance in Medicine*, 2006. 55(3): p. 659-68.
9. de Weert TT, et al., In vivo characterization and quantification of atherosclerotic carotid plaque components with multidetector computed tomography and histopathological correlation. *Arteriosclerosis, Thrombosis, and Vascular Biology*, 2006. 26(10): p. 2366-72.
10. Kaazempur-Mofrad MR, et al., Characterization of the atherosclerotic carotid bifurcation using MRI, finite element modeling, and histology. *Annals of Biomedical Engineering*, 2004. 32(7): p. 932-46.
11. Wintermark M, et al., High-resolution CT imaging of carotid artery atherosclerotic plaques. *American Journal of Neuroradiology*, 2008. 29(5): p. 875-82.
12. Dauguet J, et al., Three-dimensional reconstruction of stained histological slices and 3D non-linear registration with in-vivo MRI for whole baboon brain. *Journal of Neuroscience Methods*, 2007. 164(1): p. 191-204.
13. Yelnik J, et al., A three-dimensional, histological and deformable atlas of the human basal ganglia. I. Atlas construction based on immunohistochemical and MRI data. *Neuroimage*, 2007. 34(2): p. 618-38.
14. Meyer CR, et al., A methodology for registration of a histological slide and in vivo MRI volume based on optimizing mutual information. *Molecular Imaging*, 2006. 5(1): p. 16-23.
15. Lowder LM, et al., Correction of distortion of histologic sections of arteries. *Journal of Biomechanics*, 2007. 40(2): p. 445-50.
16. Clarke S, Validation of Automatically Classified Magnetic Resonance Images for Carotid Plaque Compositional Analysis. *Stroke*, 2005. 37(1): p. 93-97.
17. de Monyé C, et al., Sixteen-detector row CT angiography of carotid arteries: comparison of different volumes of contrast material with and without a bolus chaser. *Radiology*, 2005. 237(2): p. 555-62.

18. Adame I, et al., Automatic segmentation and plaque characterization in atherosclerotic carotid artery MR images. *Magnetic Resonance Materials in Physics, Biology and Medicine*, 2004. 16(5): p. 227-34.
19. Rueckert D, et al., Nonrigid registration using free-form deformations: application to breast MR images. *IEEE Transactions on Medical Imaging*, 1999. 18(8): p. 712-21.
20. Klein S, Staring M, and Pluim JP, Evaluation of optimization methods for nonrigid medical image registration using mutual information and B-splines. *IEEE Transactions on Image Processing*, 2007. 16(12): p. 2879-90.
21. Dice LR, Measures of the Amount of Ecologic Association Between Species. *Ecology*, 1945.
22. Choy JS, Mathieu-Costello O, and Kassab GS, The effect of fixation and histological preparation on coronary artery dimensions. *Annals of Biomedical Engineering*, 2005. 33(8): p. 1027-33.
23. Dobrin PB, Effect of histologic preparation on the cross-sectional area of arterial rings. *The Journal of Surgical Research*, 1996. 61(2): p. 413-5.
24. Siegel RJ, et al., Limitations of postmortem assessment of human coronary artery size and luminal narrowing: differential effects of tissue fixation and processing on vessels with different degrees of atherosclerosis. *Journal of the American College of Cardiology*, 1985. 5(2 Pt 1): p. 342-6.
25. Wong M, et al., Ultrasonic-pathological comparison of the human arterial wall. Verification of intima-media thickness. *Arteriosclerosis and Thrombosis*, 1993. 13(4): p. 482-6.
26. Friedman MH, Himburg HA, and LaMack JA, Statistical hemodynamics: a tool for evaluating the effect of fluid dynamic forces on vascular biology in vivo. *Journal of Biomechanical Engineering*, 2006. 128(6): p. 965-8.

## SUPPLEMENT

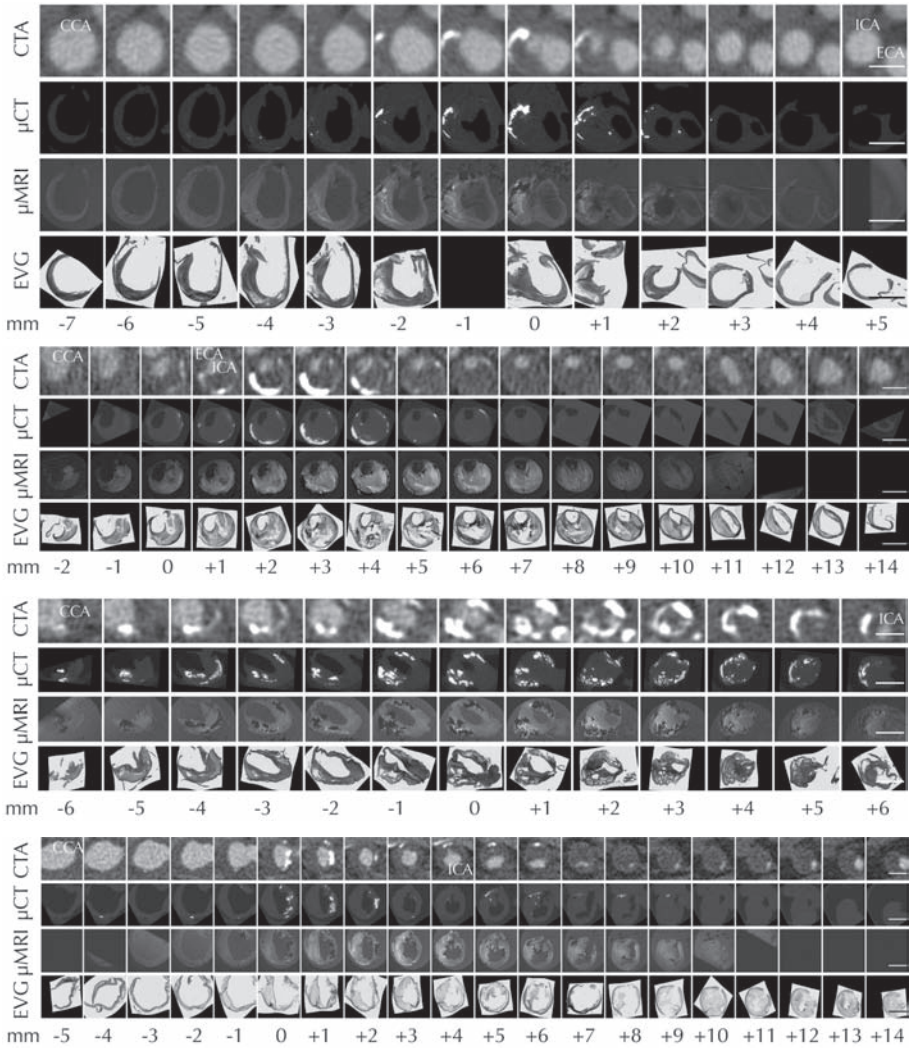


**Figure S5-1:** Slice by slice comparison of four different registered atherosclerotic carotid plaques. From left to right: common carotid artery (CCA), through the bifurcation (0 mm) into the internal (ICA) and the external carotid arteries (ECA) in steps of 1 mm. Top to bottom: Registered CTA,  $\mu$ CT,  $\mu$ MRI (3DT1w), and EVG (histology Elastica von Gieson staining). Scale bar is 5 mm.





CHAPTER

# 6

**CALCIFICATION LOCATES TO  
TRANSGLUTAMINASES IN ADVANCED  
HUMAN ATHEROSCLEROTIC LESIONS**

Hanke Matlung, Harald Groen, Judith de Vos, Theo van Walsum,  
Aad van der Lugt, Wiro Niessen, Jolanda Wentzel,  
Ed vanBavel, Erik Bakker

*Published in: American Journal of Pathology 2009, 175(4):1374-9*

### ***Background***

Transglutaminases play an important role in vascular smooth muscle cell-induced calcification *in vitro*. We determined whether these enzymes are also involved in human atherosclerotic calcification.

### ***Methods***

Sections of 9 different carotid artery specimens were registered to  $\mu$ CT images and stained for tissue-type transglutaminase (TG2), plasma transglutaminase Factor XIIIa (FXIIIa), the N $\epsilon$  ( $\gamma$ -L-glutamyl)-L-lysine cross-link, and the macrophage marker CD68.

### ***Results***

*Ex vivo* mCT revealed extensive calcification, which significantly correlated with the cross-link. FXIIIa was found to be the dominant transglutaminase, rather than TG2, albeit staining of both transglutaminases correlated with the cross-link. Staining for FXIIIa co-localized with CD68 at both cellular and tissue level.

### ***Conclusion***

Areas of calcification locate to the presence and activity of transglutaminases in human atherosclerotic arteries. FXIIIa appears to be the dominant transglutaminase and may be derived from local macrophages. These results are consistent with the hypothesis that transglutaminases participate in the calcification process of human atherosclerotic arteries.

## INTRODUCTION

Vascular calcification is considered a tightly regulated process of matrix deposition by osteoblast-like cells [1]. These cells may be derived from stem cells or differentiate from smooth muscle cells or pericytes. Recent work from Johnson et al. [2] suggests a role for transglutaminases in the process of arterial calcification. Based on *in vitro* experiments on cultured healthy arterial segments and smooth muscle cells, these authors proposed a novel mechanism of arterial calcification, where tissue-type transglutaminase (TG2) is central in the chondro-osseous differentiation and calcification of smooth muscle cells. Transglutaminases form a class of enzymes with pleiotropic function [3] and consists of 9 known members. Among these, TG2 is expressed in endothelial cells, smooth muscle cells and monocytes/macrophages. The plasma transglutaminase, Factor XIIIa (FXIIIa) is expressed in monocytes/macrophages [4]. TG2 has been implicated in an animal model for atherosclerotic lesion formation [5], while both TG2 and FXIIIa are involved in vascular remodeling [6,7]. TG2 and FXIIIa are also involved in normal bone formation, where they act in concert to promote chondrocyte maturation [8]. While these data suggest an important role of transglutaminases in the development of atherosclerotic calcification, evidence of their role in human atherosclerotic lesion development is lacking. Therefore, we investigated the presence of transglutaminases, i.e. TG2 and FXIIIa, the transglutaminase-induced cross-link and macrophages in human atherosclerotic carotid arteries. These markers were correlated to calcified areas that were detected *ex vivo* with  $\mu$ CT imaging.

## MATERIALS AND METHODS

### *Tissue specimens*

Atherosclerotic plaque tissue was collected from patients undergoing carotid endarterectomy (8 males and 1 female, aged 51 to 80 years). All patients displayed cerebrovascular symptoms, for detailed patients characteristics see Table 6-I. From the 9 symptomatic patients, 8 of the atherosclerotic plaques were collected from the symptomatic artery and 1 from the asymptomatic carotid artery in a patient with an occlusion of the

symptomatic artery. Specimens were kept in a tissue bank at  $-80^{\circ}\text{C}$  until further processing. The study was approved by the medical ethic committee and all patients gave written informed consent.

**Table 6-I:** Patient characteristics.

Patient	Gender	Age	Medication		Risk factors		
			Statins	Hypercholesterolemia	Diabetes mellitus	Hypertension	Smoking
1	Female	76	Yes	No	No	Yes	0
2	Male	59	Yes	Yes	No	Yes	1
3	Male	51	No	No	No	Yes	2
4	Male	70	Yes	No	Yes	Yes	1
5	Male	68	Yes	Yes	Yes	Yes	2
6	Male	67	Yes	Yes	No	No	2
7	Male	57	Yes	Yes	No	Yes	2
8	Male	78	Yes	Yes	No	Yes	1
9	Male	80	Yes	No	No	Yes	1

Smoking: Never (0), Ever (1); Current (2)

### *Ex vivo $\mu\text{CT}$*

After storage specimens were defrosted before scanning with  $\mu\text{CT}$  (Skyscan 1072, Skyscan, Kontich, Belgium) operating at 80 kV and 100  $\mu\text{A}$  to image calcifications inside the plaques. The samples were scanned in air as a whole during 15-30 minutes, depending on their length, varying from 8-25 mm. After reconstruction the image resolution of the sample was  $18 \times 18 \times 18 \mu\text{m}^3$ .

### *Immuno-histochemical staining*

After scanning with  $\mu\text{CT}$  the carotid arteries were fixed in formalin for 24-48 hours and decalcified with EDTA for an additional 24-48 hours before routine processing and embedding in paraffin. Adjacent sections (5  $\mu\text{m}$ ) were de-paraffinized and antigen retrieval was performed by boiling in 0.01M citrate buffer. Thereafter slides were blocked with 5% goat serum and primary antibodies were incubated either for 60 minutes at

room temperature (TG2) or overnight at 4°C (FXIII A and cross-link); overnight incubation with the antibody against TG2 yielded similar results (data not shown). Secondary antibodies were applied for 30 minutes at room temperature. Bound antibodies were visualized using AEC chromogen (Sigma). Sections were counterstained with hematoxylin. Negative controls were obtained by omission of the primary antibody. For detection of TG2 a rabbit polyclonal antibody was used (concentration 1:10, Labvision, Runcorn, United Kingdom) in combination with a HRP conjugated polyclonal goat anti-rabbit antibody (concentration 1:100, Dakocytomation, Glostrup, Denmark). FXIII A was detected by a rabbit polyclonal antibody against FXIII A (prediluted, Labvision, Runcorn, United Kingdom) in combination with a HRP conjugated polyclonal goat anti-rabbit and mouse secondary antibody (prediluted, Abcam, Cambridge, United Kingdom). The product of transglutaminase activity was detected by a mouse monoclonal antibody against the N $\epsilon$  ( $\gamma$ -L-glutamyl)-L-lysine isopeptide cross-link (concentration 1:100, Covalab, Villeurbanne, France) together with a HRP conjugated goat anti-mouse secondary antibody (concentration 1:100, Southern Biotech). Macrophages were detected by a mouse monoclonal antibody against human CD68 (concentration 1:1600, Dakocytomation, Glostrup, Denmark) in combination with the Dako REAL En-Vision Detection System, Peroxidase/DAB $^{+}$ . Digitized images were made with a NanoZoomer Digital Pathology (C9600, Hamamatsu, Hamamatsu City, Japan) setup at 40x magnification.

Double immunofluorescent staining was performed by overnight incubation of slides with a rabbit polyclonal antibody against FXIII A (prediluted, Labvision, Runcorn, United Kingdom) and a mouse anti-human monoclonal antibody against CD68 (concentration 1:100, Abcam, Cambridge, United Kingdom). Slides were then incubated for 1 hour at room temperature with secondary antibodies: goat anti-rabbit-Cy3 (concentration 1:100, Jackson, West Grove, USA) and goat anti-mouse-FITC (concentration 1:100, Abcam, Cambridge, United Kingdom). Nuclei were stained with DAPI (VectorLabs, Burlingame, USA). Images were made with a confocal microscope (Leica), using sequential scanning to avoid cross-talk of the dyes.

For localization of the stainings and  $\mu$ CT images, every image was subdivided in sections of 1.6 x 1.6 mm. These subsections were presented in a random manner and orientation to two blinded observers. Hereby,

subsections were selected randomly from the complete dataset including all patients and stainings and analyzed for the percentage of positive staining and the presence of calcium per area of tissue present in that section. Only sections with minimal folding and distortion of tissue were used for analysis (n=2-3 locations per patient, 76 cross sections in total stained for either TG2, FXIIIa, the cross-link or CD68, and subdivided into 304 subsections). Averaged scores were converted to binary measurements (negative staining, positive staining) with a cut-off value of 4%.

### ***Matching of $\mu$ CT and immunohistochemical images***

In order to correlate the immunostainings with  $\mu$ CT data, a matching (registration) of the images between both modalities is needed. This matching requires the localization of the histological sections in the three-dimensional  $\mu$ CT data. We included seven degrees of freedom for the registration of these image modalities. Thus, with respect to the volumetric  $\mu$ CT data, the sections were translated in three dimensions, rotated in three dimensions and isotropically scaled. These registrations were done manually, using landmarks such as the internal and external contours of the vessel. Applying these procedures directly to the histological sections is not so straightforward because of the many degrees of freedom. Therefore, as an intermediate step, during the microtome slicing process, *enface* images of the remaining embedded tissue were made at 1 mm intervals. From these *enface* images a 3D stack was created which was first registered with the  $\mu$ CT data as described above. This provided estimates for position along the length axis, for tilting and overall shrinkage of the tissue during embedding. Subsequently, each individual histological section was registered to the corresponding *enface* image, using translation, rotation and isotropic scaling. The full registration is the combination of the registration of the *enface* images to the  $\mu$ CT data, and the registration of histology images to the *enface* images. Finally, small errors in this two-stage registration procedure, such as slice dependent deformations resulting from microtome sectioning, were corrected by minor manual adjustments in the positioning of the histological section within the 3D  $\mu$ CT data.

Additionally, an inter-observer study was used to validate the registration process. Hereby, two patients were randomly selected and registered by a second observer, blinded for the previous results. The 3D orientation of

the histological slices in the  $\mu$ CT domain was compared between the two observers, and differences were found to be well within the grid size used for the data analysis (1.6 x 1.6 mm).

### *Statistics*

The associations between calcium and the cross-link and between the TG2, FXIIIa, CD68 and cross-link staining were analyzed using cross tabulation and chi-square tests. Associations were considered statistically significant at  $p < 0.05$ .

## RESULTS

A volume rendering of a carotid artery including atherosclerotic plaque and calcifications, visible as bright spots in the  $\mu$ CT images, is shown in Figure 6-1. The lumen was segmented manually from the  $\mu$ CT for visualization. There was a diverse appearance of calcification, ranging from isolated spots to large, complex dense structures. On the basis of the  $\mu$ CT images, we found that calcification was present in 24% of the total analyzed plaque area. Histological cross sections were registered to corresponding reformatted slices from the  $\mu$ CT to co-localize calcifications and cross-link staining. This revealed that calcified areas stain heavily for the cross-link, as shown in a typical example in Figure 6-2a-c.

Staining for the cross-link was abundant, but not restricted to calcified areas. In total, the cross-link was present in 62% of the analyzed areas. Staining for FXIIIa was found in 38% of the areas, and co-localized with calcifications (Figure 6-2d). Macrophages, as identified by CD68 staining (Figure 6-2e) also co-localized with calcification and with FXIIIa, which was also shown by the double immuno-fluorescent staining for FXIIIa and CD68 (Figure 6-2g-h;  $n=3$ ). In contrast, minimal positive staining for TG2 was seen throughout the plaques (Figure 6-2f). In total, only 7% of the scored areas stained positively. Positive control staining for TG2 as well as negative controls for the cross-link, FXIIIa and CD68 (immunohistochemical and double immunofluorescent staining) can be found in supplementary Figure S6-1.

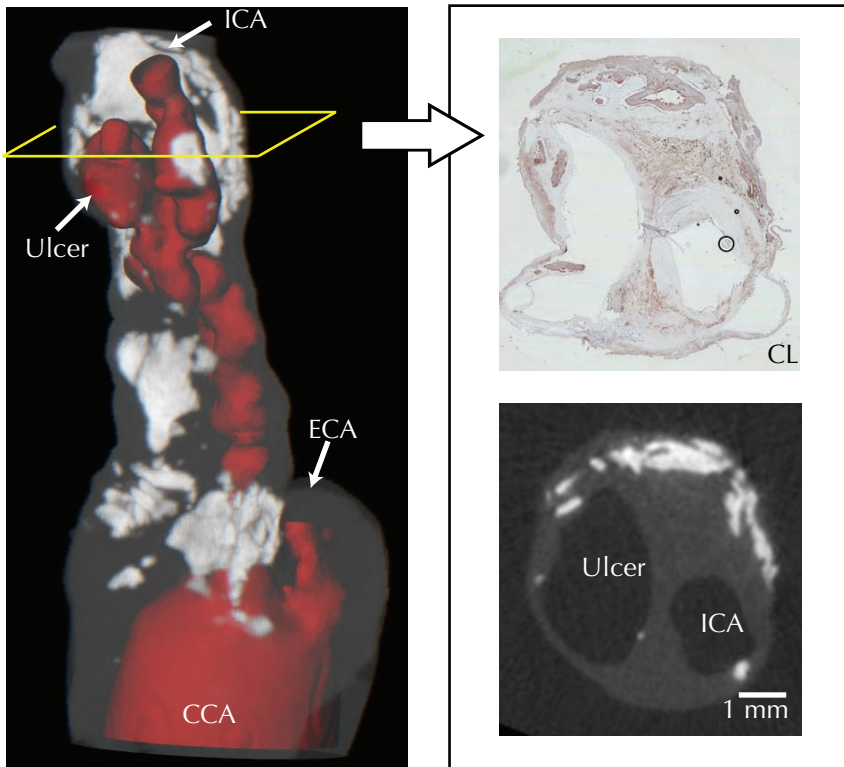


**Figure 6-1:** Appearance of calcifications throughout the length of a plaque. A 2D representation of the  $\mu$ CT data is shown here; red indicates the lumen of the vessel; the outer wall of the vessel is shown in grey. CCA: common carotid artery; ECA: external carotid artery; ICA: internal carotid artery. White areas indicate calcifications. Cross sections were used to correlate  $\mu$ CT images to accompanying histological sections, in this case stained for the cross-link. Scale bar represents 1 mm.

Cross-tabulation (Table 6-II) showed that calcifications are strongly associated with the cross-link (Pearson chi-square  $p < 0.001$ ). Thus, of the calcified areas 88% showed positive staining for the cross-link. Both transglutaminases, TG2 and FXIIIa, are associated with the cross-link (Pearson chi-square,  $p = 0.002$  and  $p < 0.001$ ). However, in only 10% of the cross-link positive areas TG2 was present, while 50% of the cross-link positive areas showed positive staining for FXIIIa. Macrophages, a possible source of FXIIIa, are strongly correlated with FXIIIa in the plaques (Pearson chi-square,  $p < 0.001$ ). Staining for the cross-link and FXIIIa outside calcified areas was located mainly in the necrotic core, rather than in fibrous cap or shoulder regions of the plaque (supplementary Figure S6-2).



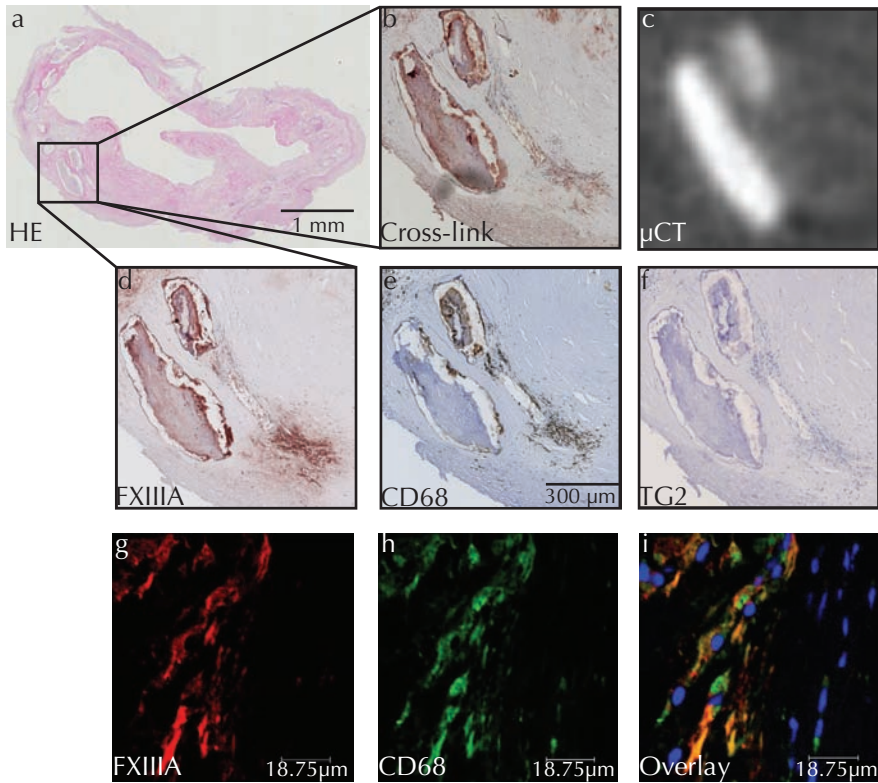


**Figure 6-2:** Example of immunohistochemical and double immunofluorescent staining of a carotid atherosclerotic plaque section. **a)** HE staining, 5x magnification; **b)** Cross-link staining; **c)** Corresponding  $\mu$ CT image, bright spots indicating calcium; **d)** FXIIIa staining; **e)** CD68 staining, scale bar represents 300  $\mu$ m; **f)** TG2 staining; **g-i)** Confocal images of double immunofluorescent staining of FXIIIa (red) and CD68 (green). Nuclei are stained with DAPI (blue).

## DISCUSSION

In this study we tested the hypothesis that transglutaminases are associated with calcification in human atherosclerosis. The main findings of the current study are that I) calcified areas in human atherosclerotic plaque stain positively for the transglutaminase-induced cross-link; II) this  $N\epsilon(\gamma$ -glutamyl)lysine cross-link correlates significantly with staining for TG2 and FXIIIa, both members of the transglutaminase family; III) FXIIIa staining is dominant over TG2, which is only marginally present and IV) FXIIIa staining correlates with CD68 staining and also co-localizes with CD68

**Table 6-II:** Crosstabulation tables between **a)** calcium and cross-link; **b)** FXIIIa and CL; **c)** TG2 and CL and **d)** FXIIIa and CD68. Indicated are observed numbers and their expected numbers on the basis of absence of correlation.

a		CL			b		CL				
		neg	pos	Total			neg	pos	Total		
Calcium	neg	observed	106	124	230	FXIIIa	neg	observed	94	94	188
		expected	87	143	230			expected	71	117	188
	pos	observed	9	65	74		pos	observed	21	95	116
		expected	28	46	74			expected	44	72	116
	Total	observed	115	189	304		Total	observed	115	189	304
		expected	115	189	304			expected	115	189	304
Pearson chi-square p<0.001					Pearson chi-square p<0.001						
c		CL			d		CD68				
		neg	pos	Total			neg	pos	Total		
TG2	neg	observed	114	170	284	FXIIIa	neg	observed	104	84	188
		expected	107	177	284			expected	81	107	188
	pos	observed	1	19	20		pos	observed	27	89	116
		expected	8	12	20			expected	50	66	116
	Total	observed	115	189	304		Total	observed	131	173	304
		expected	115	189	304			expected	131	173	304
Pearson chi-square p=0.002					Pearson chi-square p<0.001						

positive cells as shown by double immunofluorescent staining, suggesting that macrophages represent the major source of FXIIIa.

### *Role of transglutaminases in atherosclerosis*

Previous work from others addressed the expression of TG2 and the cross-link in human atherosclerotic specimens [9-11]. These publications showed that transglutaminases, through cross-linking of extra-cellular matrix proteins, could contribute to increased plaque stability. However, in the current study we found transglutaminases and the cross-link to be absent from cap and shoulder regions and mainly associated with calcified areas. While the present study reveals a strong correlation of transglutaminases with calcification in human atherosclerotic specimens, detailed mechanistic insight is provided by the recent *in vitro* experimental work performed by Johnson et al. [2]. These authors found transglutaminases

to be crucial for the switch of smooth muscle cells towards a chondro-osseous phenotype and subsequent mineralization. Work on osteoblast differentiation also supports the role of transglutaminases in tissue mineralization. Thus, cross-linking activity of transglutaminases affects cell differentiation and ultimately mineralization of osteoblast cultures by the formation and stabilization of a fibronectin-collagen network [12]. Also, osteoblasts differentiate faster on a TG2-crosslinked type I collagen matrix than on native collagen [13]. It is however not clear whether transglutaminases contribute to calcification through cross-linking activity only. Transglutaminases also accelerate the maturation of chondrocytes, which relates to the engagement of transglutaminases with integrins [8], a process that does not require TGase-catalyzed transamidation.

### ***FXIIIa in atherosclerosis***

Previous work by the group of vanBavel showed that in vascular remodeling, FXIIIa can substitute for the lack of TG2. This was also shown to be the case for *in vitro* calcification of smooth muscle cells and arteries [2], where exogenous FXIIIa could rescue the phenotypic switch of TG2<sup>-/-</sup> smooth muscle cells towards the chondro-osseous phenotype by phosphate donor treatment. This may also explain why the TG2 knockout mouse does not display an overt skeletal phenotype. FXIIIa may originate from plasma, platelets, and monocytes/macrophages. In the current study we found a significant correlation between FXIIIa and CD68 staining, suggesting that within the plaque, macrophages are a major source of FXIIIa. An alternative possibility is that osteochondrogenic trans-differentiated smooth muscle cells produce FXIIIa, as in endochondral ossification FXIIIa is released by chondrocytes [14]. However, the double fluorescent immunostaining for CD68 and FXIIIa clearly show that macrophages are the main source of local FXIIIa synthesis. We found FXIIIa and CD68 staining also outside calcified areas. It is not clear whether these sites reflect early stages in calcification.

The currently found colocalization of transglutaminase activity and calcification adds to a variety of transglutaminase effects that may aggravate atherosclerosis. Thus, FXIIIa is considered to be a marker of alternatively activated (Th2) macrophages and plays a role in the phagocytosis of erythrocytes and other particles [15]. In addition, FXIIIa may act in an autocrine

manner on angiotensin receptors. Thus, FXIIIa is able to induce dimerization of AT1 receptors on monocytes. These AT1 receptor dimers show increased activation, resulting in increased attachment to endothelial cells. This process could ultimately affect atherosclerosis, since blocking receptor dimerization resulted in decreased atherosclerotic lesion development in ApoE-deficient mice [16].

Transglutaminases have also been found to mediate inward remodeling in small arteries under a variety of conditions [6,7]. In those vessels, transglutaminases mainly affect remodeling through cross-linking the media and adventitia. It remains to be established whether transglutaminases are also involved in large vessel media remodeling during atherosclerosis. Yet, it is conceivable that media cross-linking would counteract the Glagov phenomenon [17].

In summary, transglutaminase activity may determine the outcome of atherosclerotic lesion development through an array of mechanisms, including calcification. The challenge for future work will be to further unravel these mechanisms, and to explore possibilities for beneficially affecting local transglutaminase activity.

## REFERENCES

1. Johnson RC, Leopold JA, and Loscalzo J, Vascular calcification: pathobiological mechanisms and clinical implications. *Circulation Research*, 2006. 99(10): p. 1044-59.
2. Johnson KA, Polewski M, and Terkeltaub RA, Transglutaminase 2 is central to induction of the arterial calcification program by smooth muscle cells. *Circulation Research*, 2008A. 102(5): p. 529-37.
3. Lorand L and Graham RM, Transglutaminases: crosslinking enzymes with pleiotropic functions. *Nature Reviews - Molecular Cell Biology*, 2003. 4(2): p. 140-56.
4. Bakker EN, Pistea A, and VanBavel E, Transglutaminases in vascular biology: relevance for vascular remodeling and atherosclerosis. *Journal of Vascular Research*, 2008. 45(4): p. 271-78.
5. Boisvert WA, et al., Leukocyte transglutaminase 2 expression limits atherosclerotic lesion size. *Arteriosclerosis, Thrombosis, and Vascular Biology*, 2006. 26(3): p. 563-69.
6. Bakker EN, et al., Small artery remodeling depends on tissue-type transglutaminase. *Circulation Research*, 2005. 96(1): p. 119-26.

7. Bakker EN, et al., Flow-dependent remodeling of small arteries in mice deficient for tissue-type transglutaminase: possible compensation by macrophage-derived factor XIII. *Circulation Research*, 2006. 99(1): p. 86-92.
8. Johnson KA, Rose DM, and Terkeltaub RA, Factor XIIIa mobilizes transglutaminase 2 to induce chondrocyte hypertrophic differentiation. *Journal of Cell Science*, 2008B. 121(Pt 13): p. 2256-64.
9. Auld GC, et al., Thrombin upregulates tissue transglutaminase in endothelial cells: a potential role for tissue transglutaminase in stability of atherosclerotic plaque. *Arteriosclerosis, Thrombosis, and Vascular Biology*, 2001. 21(10): p. 1689-94.
10. Haroon ZA, et al., Localization of tissue transglutaminase in human carotid and coronary artery atherosclerosis: implications for plaque stability and progression. *Laboratory Investigation*, 2001. 81(1): p. 83-93.
11. Sumi Y, et al., Expression of tissue transglutaminase and elafin in human coronary artery: implication for plaque instability. *Atherosclerosis*, 2002. 160(1): p. 31-39.
12. Al Jallad HF, et al., Transglutaminase activity regulates osteoblast differentiation and matrix mineralization in MC3T3-E1 osteoblast cultures. *Matrix Biology*, 2006. 25(3): p. 135-48.
13. Chau DY, et al., The cellular response to transglutaminase-cross-linked collagen. *Biomaterials*, 2005. 26(33): p. 6518-29.
14. Nurminskaya M, et al., Plasma transglutaminase in hypertrophic chondrocytes: expression and cell-specific intracellular activation produce cell death and externalization. *the Journal of Cell Biology*, 1998. 142(4): p. 1135-44.
15. Torocsik D, et al., Identification of factor XIII-A as a marker of alternative macrophage activation. *Cellular and Molecular Life Sciences*, 2005. 62(18): p. 2132-39.
16. AbdAlla S, et al., Factor XIIIa transglutaminase crosslinks AT1 receptor dimers of monocytes at the onset of atherosclerosis. *Cell*, 2004. 119(3): p. 343-54.
17. Glagov S, et al., Compensatory enlargement of human atherosclerotic coronary arteries. *the New England Journal of Medicine*, 1987. 316(22): p. 1371-5.

## SUPPLEMENT

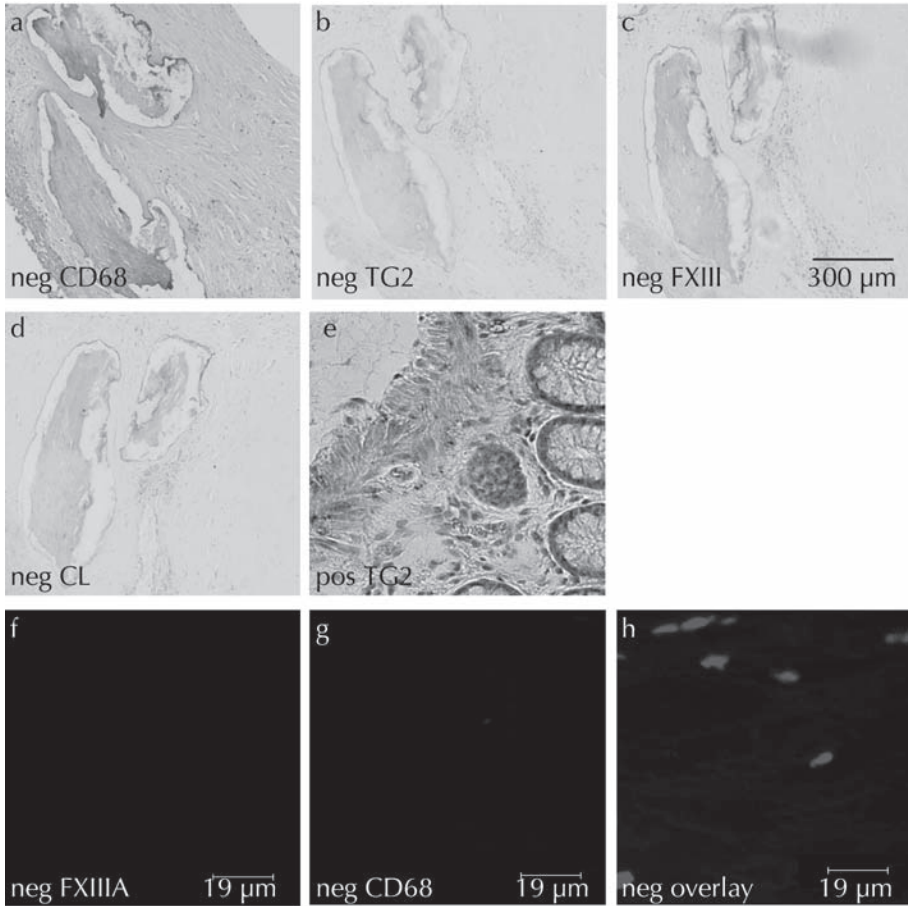


**Figure S6-1:** Negative controls for **a)** CD68; **b)** TG2; **c)** FXIII, scale bar represents 300  $\mu\text{m}$ ; **d)** The cross-link; **e)** Human colon tissue as positive control for TG2. Negative controls for double immunofluorescent staining of **f)** FXIII and **g)** CD68. **h)** Overlay with DAPI stained nuclei.

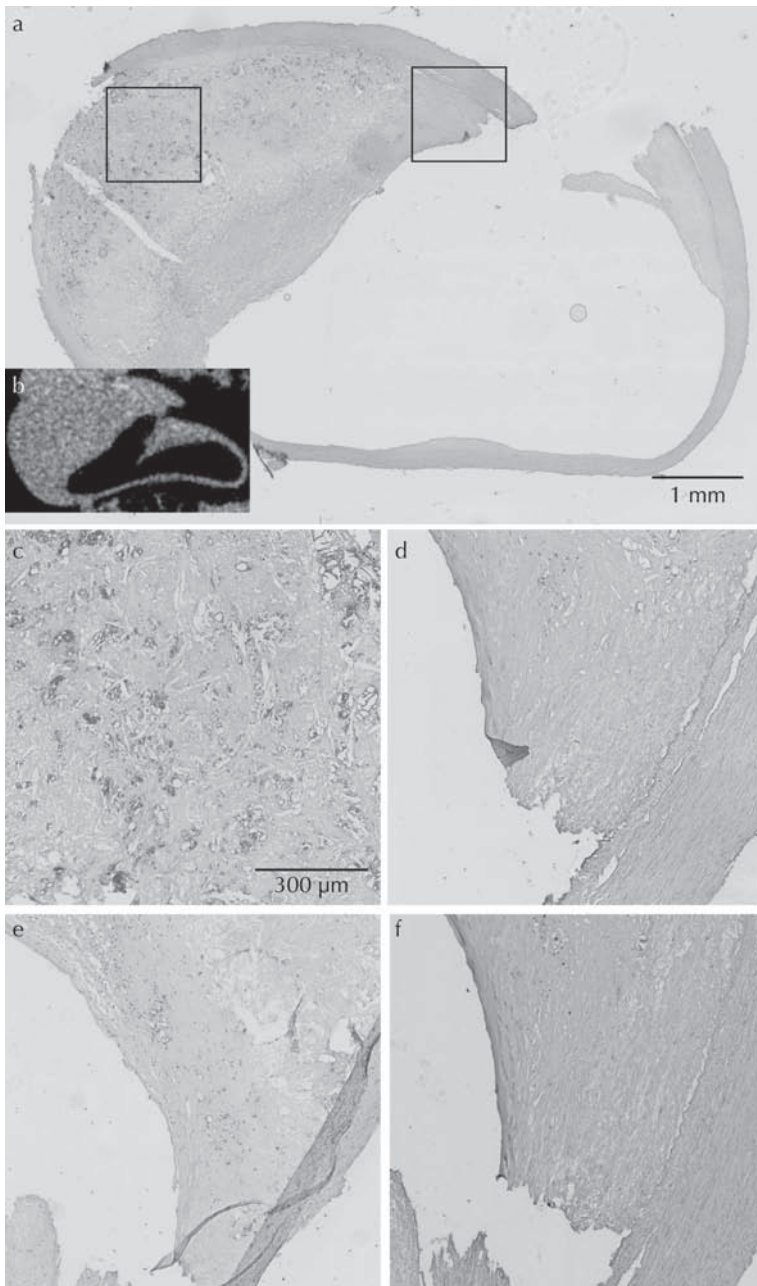


**Figure S6-2:** a) Cross-link and transglutaminase staining outside calcified regions, scale bar represents 1 mm; b)  $\mu$ CT image shows absence of calcification in this particular section. Insets show: c) Positive staining for cross-link in necrotic core; d) Absence of cross-link staining; e) Absence of FXIII staining; f) Absence of TG2 staining in shoulder regions of the plaque, scale bars represent 300  $\mu$ m.





CHAPTER

# 7

---

## MRI-BASED QUANTIFICATION OF OUTFLOW BOUNDARY CONDITIONS FOR COMPUTATIONAL FLUID DYNAMICS OF STENOSED HUMAN CAROTID ARTERIES

Harald Groen, Lenette Simons, Quirijn van den Bouwhuijsen,  
Marielle Bosboom, Frank Gijzen, Alina van der Giessen,  
Frans van de Vosse, Antonius van der Steen, Jacqueline Witteman,  
Albert Hofman, Aad van der Lugt, Jolanda Wentzel

*Published in: Journal of Biomechanics 2010, 43(12), 2332-8*

### ***Background***

Accurate assessment of wall shear stress (WSS) is vital for studies on the pathogenesis of atherosclerosis. WSS distributions can be obtained by computational fluid dynamics (CFD) using patient-specific geometries and flow measurements. If patient-specific flow measurements are unavailable, in- and outflow have to be estimated, for instance by using Murray's Law. It is currently unknown to what extent this law holds for carotid bifurcations, especially in cases where stenoses are involved.

### ***Methods***

We performed flow measurements in the carotid bifurcation using phase-contrast MRI in patients with varying degree of stenosis. An empirical relation between outflow and degree of area stenosis was determined and the outflow measurements were compared to estimations based on Murray's Law. Furthermore, the influence of outflow conditions on the WSS distribution was studied.

### ***Results***

For bifurcations with an area stenosis smaller than 65%, the outflow-ratio of the internal carotid artery (ICA) to the common carotid artery (CCA) was  $0.62 \pm 0.12$  while the outflow-ratio of the external carotid artery (ECA) was  $0.35 \pm 0.13$ . If the area stenosis was larger than 65%, the flow to the ICA decreased linearly to zero at 100% area stenosis. The empirical relation fitted the flow data well ( $R^2=0.69$ ), whereas Murray's Law overestimated the flow to the ICA substantially for larger stenosis, resulting in an overestimation of the WSS.

### ***Conclusion***

If patient-specific flow measurements of the carotid bifurcation are unavailable, estimation of the outflow-ratio by the presented empirical relation will result in a good approximation of calculated WSS using CFD.

## INTRODUCTION

Atherosclerosis is one of the main causes of cerebrovascular and cardiovascular events. Blood-flow-induced wall shear stress (WSS) is considered to play an important role in atherosclerotic plaque initiation [1], as well as in the progression of the disease [2]. Many studies have been performed to investigate the contribution of WSS to pathophysiological processes related to atherosclerosis [3-5]. To investigate these relationships in human carotid arteries, accurate assessment of WSS is required. WSS can be calculated *in vivo* by coupling medical imaging and computational fluid dynamics (CFD). It has been shown that for time-averaged WSS calculations, the time-dependent flow and flexible vessel wall can be simplified using steady flow and rigid walls [6,7]. The stationary 3D geometry can be obtained from e.g. CT or MRI, but for appropriate in- and outflow boundary conditions, additional flow measurements have to be performed. When these patient-specific flow measurements are unavailable, flow through the common (CCA), internal (ICA) and external (ECA) carotid artery needs to be estimated. Murray's Law has been used to approximate outflow-ratio of daughter vessels [8-10]. However, this law might not hold for outflow estimation in stenotic carotid bifurcations.

The goal of this study was to determine outflow boundary conditions for WSS calculations in stenosed carotid bifurcations. Therefore, we first quantified the flow in the carotid arteries for different degrees of area stenosis using phase-contrast MRI and determined an empirical relation between outflow-ratio and degree of area stenosis. Secondly, we compared the outflow-ratios estimated by Murray's Law and by the empirical relation to the measured outflow-ratios. Finally we analyzed the influence of the outflow conditions on the calculated WSS using CFD.

## METHODS

### *Subject population*

Subjects included in this study were recruited from 2 groups. Twelve patients with a high degree of stenosis, scheduled for carotid endarterectomy (CEA) in the Erasmus MC were included, and 21 subjects were enrolled from the Rotterdam Study. The Rotterdam Study is a prospective population-based study among subjects aged 45 years and older in a municipality of Rotterdam [11]. For this study, participants with uni- or bilateral maximum intima-media thickness of more than 2.5 mm in the carotid artery [12] are imaged using MRI. We selected subjects that had a good quality of flow scan and were aged 70 years or older.

### *MRI protocol*

In each subject, a non-triggered 3D phase-contrast MRI sequence was performed using a 1.5T MR system (Signa Excite, GE Healthcare, Milwaukee, USA) to measure time-averaged blood-flow velocities [13] in the right and left carotid bifurcations with bilateral 4-channel phased array surface coil system (Machnet, The Netherlands). For flow measurements, a gradient echo spin sequence was used with velocity encoding (VENC) in all three directions. The scan parameters were TR/TE=13/4.26 ms, 256x256 matrix, coronal FOV=180x180 mm<sup>2</sup> and NEX=1. For the participants from the Rotterdam Study, the voxel size was 0.7x1.0x0.7 mm<sup>3</sup> with VENC=60 cm/s and for the patients scheduled for CEA the voxel size was 0.7x1.2x0.7 mm<sup>3</sup> with VENC=90 cm/s.

### *Flow assessment*

The flow ( $Q$ ) through the CCA ( $Q_{CCA}$ ), ICA ( $Q_{ICA}$ ) and the ECA ( $Q_{ECA}$ ) was determined in MRI slices perpendicular to the centerline of the vessel. Axial slices of the magnitude image were used to draw luminal contours (Figure 7-1a) with ImageJ (<http://rsbweb.nih.gov/ij/>) and their centers were connected to obtain the centerline (Figure 7-1b). Subsequently, in the plane perpendicular to the vessel centerline velocities were calculated from the phase images (Figure 7-1c). The average signal intensity of the adjacent sternocleidomastoid muscle was subtracted from the measurement data

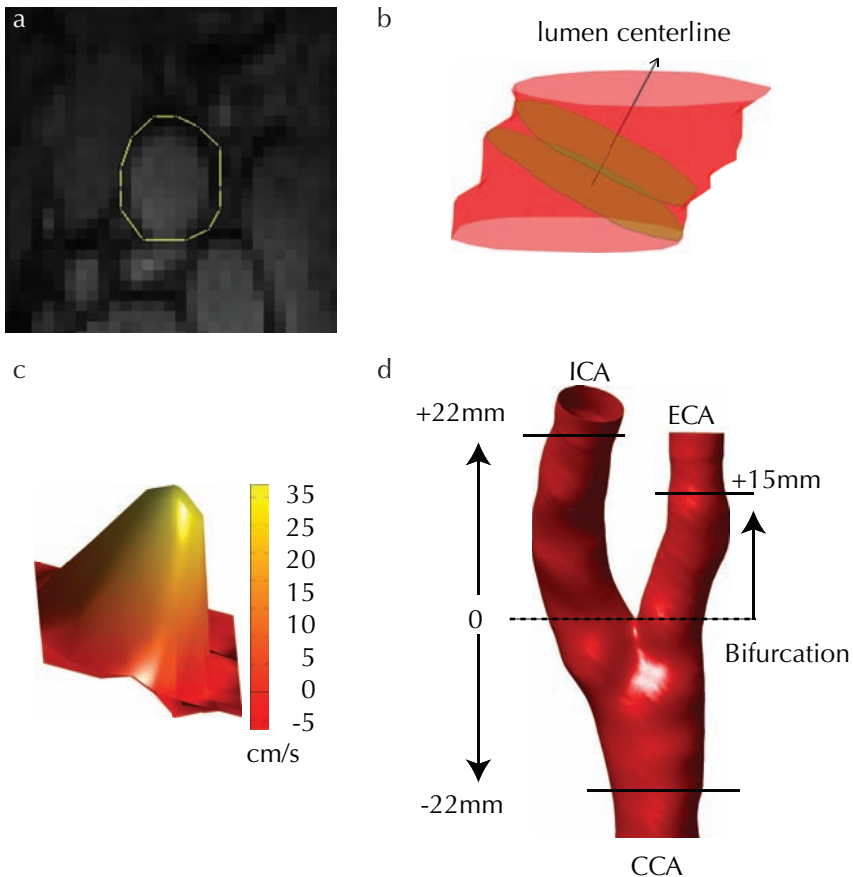


**Figure 7-1:** **a)** Lumen contours were drawn on the axial magnitude images; **b)** Slices perpendicular to the centerline of the artery were determined; **c)** Velocity profile in a perpendicular slice was derived from the phase images using linear interpolation and **d)** Location of flow measurements in the common (CCA), internal (ICA) and external (ECA) carotid arteries.

to correct for possible phase offset [14]. The flow was determined at pre-defined locations (Figure 7-1d): In the CCA 22 mm proximal to the bifurcation, in the ICA 22 mm distal to the bifurcation and in the ECA 15 mm distal to the bifurcation. If side branches in the ECA closer to the bifurcation were present, flow was determined proximally to the first side branch. Finally, the outflow-ratios were calculated for ICA:  $Q_{ICA}/Q_{CCA}$  and ECA:  $Q_{ECA}/Q_{CCA}$ .

### *Degree of area stenosis assessment*

The degree of area stenosis was defined as one minus the ratio of the minimal lumen area and the reference lumen area times 100%, both measured perpendicular to the lumen centerline using the magnitude images. The reference lumen area was determined as the average lumen area of three most distal disease free cross-sections [15].

### *Outflow-ratio estimation*

Two different models were used to describe the outflow-ratios. The first model is Murray's Law [16], a well-known relationship between flow and radius to the third power (Equation 7.1):

$$\frac{Q_1}{Q_0} = \frac{r_1^3}{r_0^3} \quad 7.1$$

Here,  $Q_1$  is the flow through the ICA or the ECA,  $Q_0$  is the flow through the CCA,  $r_1$  is the radius of the ICA or ECA and  $r_0$  is the radius of the CCA. The second model is an empirical relation, which was determined based on the flow measurements using parameter estimation. As the relationship would potentially change above a certain degree of area stenosis (cut-off-point), a model was fitted that consisted of 2 linear equations (Equation 7.2), connecting at a cut-off-point:

$$\begin{aligned} \frac{Q_1}{Q_0} &= a_1x + b_1 \quad \text{when } x \leq \frac{b_2 - b_1}{a_1 - a_2} \\ \frac{Q_1}{Q_0} &= a_2x + b_2 \quad \text{when } x > \frac{b_2 - b_1}{a_1 - a_2} \end{aligned} \quad 7.2$$

Where  $x$  is the degree of area stenosis,  $Q_1$  is the flow through the ICA or the ECA,  $Q_0$  is the flow through the CCA and  $a_1$ ,  $a_2$ ,  $b_1$ ,  $b_2$  are the parameters that define the linear relationship.

## *Computational fluid dynamics*

The influence of the prescribed outflow-ratio on the WSS distribution in the carotid artery was investigated in five patient-specific geometries with different area stenosis. The 3D surface reconstruction of the carotid bifurcation was obtained by manual contours of the vessel in the magnitude images. The Vascular Modeling ToolKit (VMTK, [www.vmtk.org](http://www.vmtk.org)) was used to add flow-extensions to the in- and outflow boundaries and to smooth the surface of the bifurcation [17]. A volume mesh was created by linear tetrahedral elements (with an average edge-size  $<0.17$  mm at the wall) using the mesh generator Netgen (RWTH Aachen University/Johannes Kepler University Linz), resulting in approximately 1 million elements. Performing mesh refinement studies we found that 0.17 mm was sufficient to obtain accurate WSS values. Blood was modeled as an incompressible non-Newtonian fluid, using the Carreau model ( $\eta_0=0.25$  Pa.s;  $\eta_\infty=0.0035$  Pa.s;  $\gamma=25$ ;  $n=0.25$ ; [18]) with a density of  $1060$  kg/m<sup>3</sup>. The arterial wall was assumed to be rigid with no-slip condition at the wall. At the inlet, a parabolic velocity profile was prescribed with a flow equal to the measured  $Q_{CCA}$  flow. On the ECA outflow boundary, a traction-free condition was applied. To investigate the outflow influence on the WSS calculation, 3 different outflow boundary conditions were applied at the ICA: I) based on the measurements (reference); II) estimated by Murray's Law (Equation 7.1); and III) estimated by the empirical relation (Equation 7.2). Approximate solutions of the Navier-Stokes equations were obtained using FIDAP (Fluent Inc Canonsburg, Pennsylvania, USA), the solution was considered converged if the relative error was smaller than  $10^{-3}$ .

For the CFD calculations, the WSS obtained using the outflow-ratio based on Murray's Law ( $WSS_{Murray}$ ) and WSS with outflow based on the empirical relationship ( $WSS_{ER}$ ), were compared to the WSS with measured outflow ( $WSS_{ref}$ ). Both the difference (error) and percent error (%error) in WSS were calculated and presented in 2D-maps [19] of angle by abscissa, i.e. the length along the lumen centerline, using VMTK and Matlab (The Math-Works, Massachusetts, United States).

Finally, we investigated whether these errors were equal for different levels of WSS. Therefore, each carotid bifurcation was divided into three regions based on  $WSS_{ref}$ : low ( $<0.5$  Pa), normal (0.5-1.5 Pa) and high ( $>1.5$  Pa).

### Statistical analysis

Using non-linear regression analysis, parameters  $a_1$ ,  $a_2$ ,  $b_1$ ,  $b_2$  of Equation 7.2 were fitted. These parameters also determine the cut-off-point. For further analysis, carotid bifurcations were grouped into 4 groups according to this cut-off-point: no stenosis, 0-cut-off-point%, cut-off-point-80% and 80-100%. Paired t-test was used to compare the estimated outflow-ratios with the measured flows. Data is presented as mean  $\pm$  standard deviation. Statistical analyses were performed using SPSS 15 (SPSS, Chicago, United States) where  $p < 0.05$  was considered significant.

## RESULTS

In total 33 subjects (19 males, 14 females) were included with a mean age of  $76 \pm 8$  years and mean blood pressure of  $113 \pm 17$  mmHg. In one subject, only one carotid bifurcation was included in the image volume, resulting in a total of 65 bifurcations. Lumen narrowing was observed only in the ICA, with a mean area stenosis of  $48 \pm 30\%$ .

### Outflow-ratio versus area stenosis

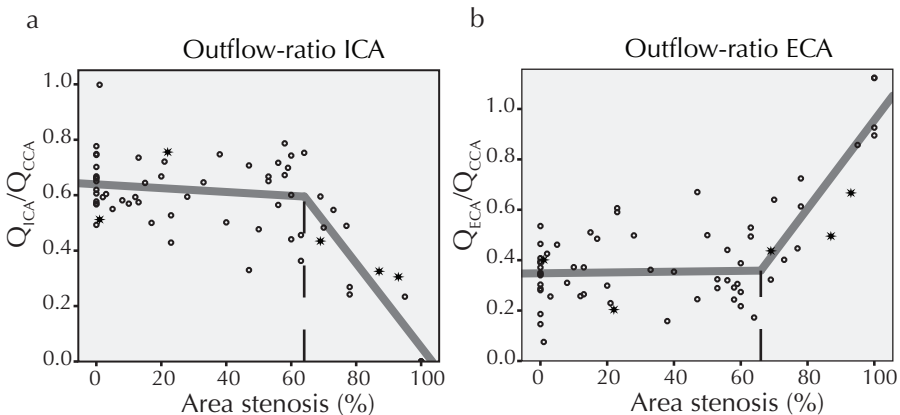


**Figure 7-2:** Measurements of outflow-ratio of **a)**  $Q_{ICA}/Q_{CCA}$  and **b)**  $Q_{ECA}/Q_{CCA}$  as function of area stenosis together with the empirical relation (Equation 7.3). \*indicate the patients used for WSS calculations.



The flow in the CCA was  $5.1 \pm 2.0$  ml/s, in the ICA  $2.8 \pm 1.6$  ml/s and in the ECA  $2.1 \pm 0.9$  ml/s. Combined for all subjects, the  $Q_{ICA}/Q_{CCA}$  outflow-ratio was  $0.55 \pm 0.20$  and the  $Q_{ECA}/Q_{CCA}$  outflow-ratio was  $0.42 \pm 0.20$ . Figure 7-2 shows the relationship between the outflow-ratios and area stenosis in the ICA and ECA. The outflow-ratios as function of the area stenosis was described by the empirical relationship (Equation 7.3) for the  $Q_{ICA}/Q_{CCA}$  ( $R^2=0.69$ ) and  $Q_{ECA}/Q_{CCA}$  ( $R^2=0.65$ ) outflow-ratio.

$$\text{Outflow-ratio} \left\{ \begin{array}{l} \text{ICA} \left\{ \begin{array}{l} \frac{Q_{ICA}}{Q_{CCA}} = -0.001x + 0.64 \quad \text{when} \quad 0 \leq x \leq 64\% \\ \frac{Q_{ICA}}{Q_{CCA}} = -0.015x + 1.57 \quad \text{when} \quad x > 64\% \end{array} \right. \left. \vphantom{\frac{Q_{ICA}}{Q_{CCA}}} \right\} R^2 = 0.69 \\ \text{ECA} \left\{ \begin{array}{l} \frac{Q_{ECA}}{Q_{CCA}} = 0.0001x + 0.35 \quad \text{when} \quad 0 \leq x \leq 66\% \\ \frac{Q_{ECA}}{Q_{CCA}} = 0.018x - 0.80 \quad \text{when} \quad x > 66\% \end{array} \right. \left. \vphantom{\frac{Q_{ECA}}{Q_{CCA}}} \right\} R^2 = 0.65 \end{array} \right. \quad \mathbf{7.3}$$

Where  $x$  is the degree of area stenosis (%).

Both the  $Q_{ICA}/Q_{CCA}$  and  $Q_{ECA}/Q_{CCA}$  outflow-ratio were approximately constant (0.64 and 0.35) when the area stenosis was lower than 64% (measured outflow-ratios were  $0.62 \pm 0.12$  and  $0.35 \pm 0.13$  respectively), while for area stenosis higher than 66% the  $Q_{ICA}/Q_{CCA}$  outflow-ratio decreased linearly to 0 and the  $Q_{ECA}/Q_{CCA}$  increased linearly to 1 with increasing area stenosis. For further analysis, we used a cut-off-point of 65% area stenosis for which the outflow-ratio changed.

The following four groups were thus defined for further analysis: no stenosis ( $n=14$ ), 1-65% ( $n=37$ ), 66-80% ( $n=7$ ) and 81-100% ( $n=7$ ) stenosis. The total flow in both the CCA and ICA decreased with increasing area stenosis ( $p < 0.05$ ), while the flow through the ECA remained constant ( $p=0.95$ , Figure 7-3). The sum of the  $Q_{ICA}$  and  $Q_{ECA}$  did not differ from the measured flow in the CCA.

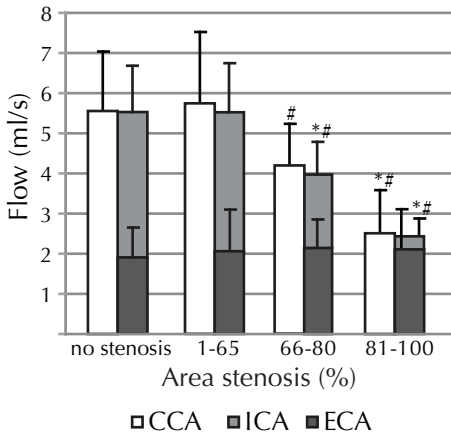


**Figure 7-3:** Flow in the CCA, and stacked flow of the ICA and ECA related to the degree of area stenosis. Significant differences between \*no stenosis and #1-65% degree of stenosis.

### Estimation of outflow-ratio

Figure 7-4 shows for each group the outflow-ratios ( $Q_{ICA}/Q_{CCA}$  and  $Q_{ECA}/Q_{CCA}$ ) measured with MRI, estimated by Murray's Law and estimated with the empirical relationship. The  $Q_{ICA}/Q_{CCA}$  outflow-ratios estimated with Murray's Law were equal among all groups ( $p=0.27$ ), resulting in an underestimation of the outflow-ratio for bifurcations with 1-65% area stenosis ( $p<0.05$ ) and an overestimation of the outflow-ratio for bifurcations with an area stenosis  $\geq 81\%$  ( $p<0.05$ ). For the estimation of the  $Q_{ECA}/Q_{CCA}$ , Mur-

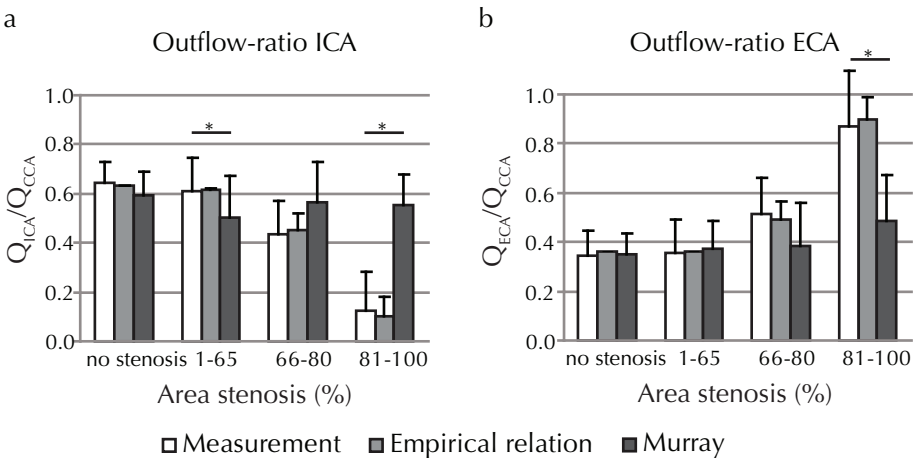


**Figure 7-4:** Outflow-ratios measured by MRI and estimated with the empirical relation and Murray's Law as a function of area stenosis for the a) ICA and b) ECA. \*Significant differences between the measured and the estimated outflow-ratio.

ray's Law underestimated the outflow-ratio for bifurcations with an area stenosis  $\geq 81\%$  ( $p < 0.05$ ). As expected, the outflow-ratio estimated based on the empirical relation did not significantly differ from the measured outflow-ratios ( $p > 0.5$ ) (Figure 7-4).

### *Wall shear stress*

In total 5 different carotid bifurcations were analyzed with regard to the influence of the outflow boundary conditions on the WSS. Table 7-I presents geometrical parameters, measured and estimated outflow-ratios and the  $WSS_{ref}$ , obtained from using the measured outflow-ratios, for these 5 arteries. The  $WSS_{ref}$  in the CCA, ICA and ECA were not related to area stenosis. Moreover, the  $WSS_{ref}$  in the ICA and ECA were almost twice as high compared to the CCA ( $p < 0.05$ ) (Table 7-I).

**Table 7-I:** Inflow and outflow boundary conditions for computational fluid dynamics and mean WSS in the CCA, ICA and ECA for artery 1-5.

Artery	Stenosis (%)	$D_{CCA}$ (mm)	Inflow		ICA outflow-ratio			Mean $WSS_{ref}$ [Pa]		
			CCA (ml/s)	Measured	Murray's Law	Empirical Relation	CCA	ICA	ECA	
1	1	8.8	7.0	0.56	0.54	0.64	$0.4 \pm 0.1$	$0.6 \pm 0.3$	$0.7 \pm 0.4$	
2	22	9.6	5.0	0.77	0.57	0.62	$0.2 \pm 0.1$	$0.5 \pm 0.4$	$0.2 \pm 0.1$	
3	69	7.0	5.3	0.51	0.71	0.52	$0.6 \pm 0.2$	$1.5 \pm 0.8$	$1.3 \pm 0.6$	
4	87	8.6	3.3	0.40	0.57	0.25	$0.3 \pm 0.1$	$0.6 \pm 0.4$	$0.6 \pm 0.3$	
5	93	6.8	1.8	0.37	0.66	0.16	$0.3 \pm 0.1$	$0.6 \pm 0.8$	$0.6 \pm 0.2$	
Mean $\pm$ SD							$0.4 \pm 0.2$	$0.8 \pm 0.4^*$	$0.7 \pm 0.4^*$	

$D_{CCA}$  = CCA lumen diameter;  $WSS_{ref}$ : WSS as obtained with measured outflow-ratios. \* $p < 0.05$ , paired comparison with CCA.

### *The influence of the outflow-ratio on the WSS*

Since the largest influence of the outflow boundary conditions on the WSS are expected distally to the bifurcation, we will discuss the results for the ICA only. The error and %error in WSS, as obtained by each model compared to  $WSS_{ref}$ , are displayed as 2D maps. The %errors are discussed in detail for two bifurcations (artery-2 and artery-4), as these two represent the results for the bifurcations with either area stenosis  $\leq 65\%$  or area stenosis  $\geq 66\%$ . The errors in WSS for these 2 arteries, as well as the complete

set of 2D maps for the other 3 bifurcations, can be found in the supplementary Figure S7-1

The  $WSS_{ref}$  in the ICA of artery-2 with area stenosis of 22% was on average 0.5 Pa, ranging from 0.06 to 2.4 Pa. The highest  $WSS_{ref}$  were found near the

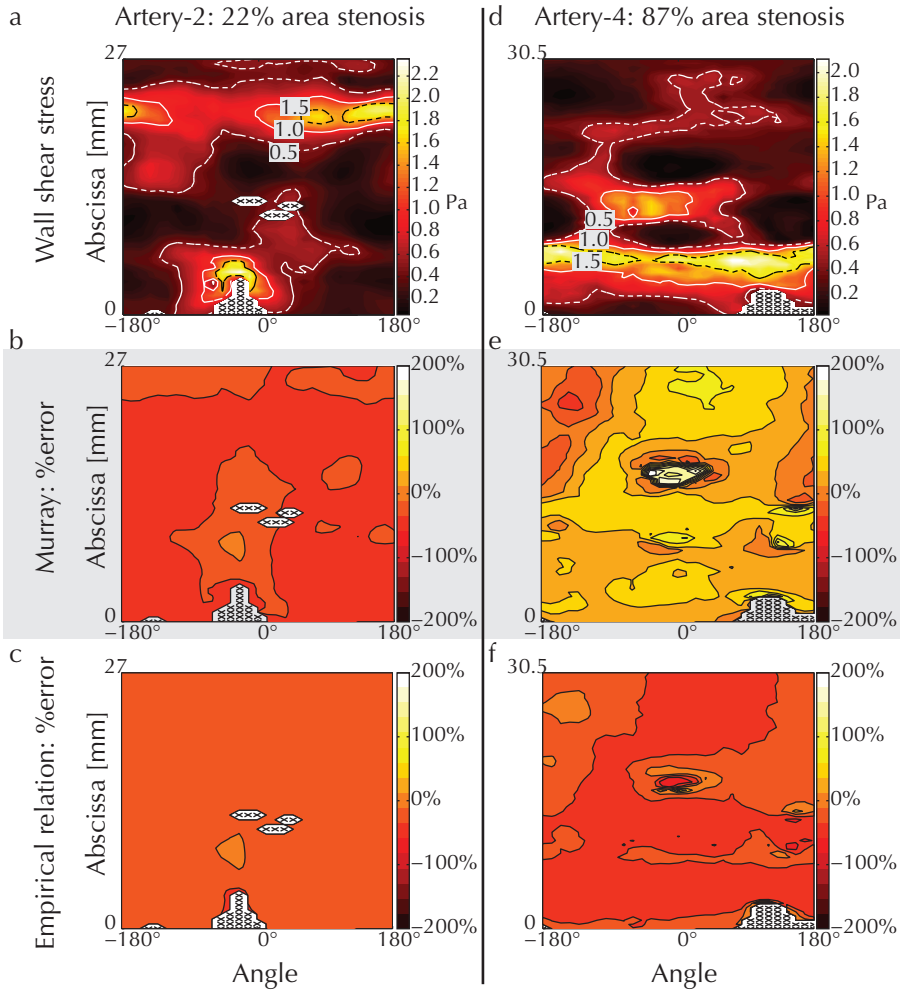


**Figure 7-5:** Wall shear stress ( $WSS_{ref}$ ) regions of two arteries with **a-c**) 22% area stenosis and **d-f**) 87% area stenosis. Dashed white line  $WSS_{ref} = 0.5$  Pa, solid white line  $WSS_{ref} = 1.0$  Pa, dashed black line  $WSS_{ref} = 1.5$  Pa. The percent error (%error) in WSS as obtained with outflow estimation by Murray's Law (**b, e**) and empirical relation (**c, f**) with respect to  $WSS_{ref}$ . The carina is located at abscissa = 0, with abscissa the length along the lumen centerline, X indicates that there is no data at that grid point.

apex of the bifurcation and at the site of the area stenosis (Figure 7-5a). On average, the %error of using the empirical relation was slightly less than using Murray's Law (-16% vs -27%, Table 7-II), which holds also for the maximal %error (-38% vs -49%). For this artery, both models resulted in an underestimation of the WSS in the ICA (Figure 7-5b-c).

For artery-4, with an area stenosis of 87%, the mean  $WSS_{ref}$  in the ICA was 0.6 Pa ranging from 0.04 to 2.1 Pa and was only high at the site of the stenosis (Figure 7-5d). Behind the stenosis, multiple areas of low  $WSS_{ref}$  (<0.5 Pa) were present, including an area of very low WSS. Large %errors were observed at all locations of low (<0.5 Pa), normal (0.5-1.5 Pa) and high (>1.5 Pa) WSS, but the largest differences were observed at the site of very low WSS. Here, the maximal percent error for Murray's Law outflow-ratio estimation was much higher than the empirical relation (257% vs 95%). On average (Table 7-II), the WSS were overestimated applying Murray's Law (44%) and underestimated using the empirical relation (-23%, Figure 7-5e-f).

**Table 7-II:** Difference (error) and percent error (%error) in mean WSS in the ICA of both Murray's Law and the Empirical relation compared to WSS calculated using measured outflow-ratio.

Artery	Stenosis (%)	Murray's Law		Empirical Relation	
		error (Pa)	%error	error (Pa)	%error
1	1	-0.04 ± 0.03	-6 ± 3%	0.07 ± 0.03	13 ± 4%
2	22	-0.15 ± 0.11	-27 ± 7%	-0.09 ± 0.07	-16 ± 5%
3	69	0.67 ± 0.38	45 ± 15%	0.02 ± 0.02	1 ± 2%
4	87	0.26 ± 0.23	44 ± 27%	-0.15 ± 0.14	-23 ± 13%
5	93	0.62 ± 0.74	97 ± 51%	-0.24 ± 0.30	-32 ± 16%
Absolute mean ± SD		0.35 ± 0.28	44 ± 34%	0.11 ± 0.07	17 ± 12%

In general (Table 7-II and supplementary Figure S7-1), in the arteries with an area stenosis  $\leq 66\%$  (arteries 1-2), the differences between  $WSS_{ref}$ ,  $WSS_{Murray}$  and  $WSS_{ER}$  were small, but still locally up to 50%. In the arteries with an area stenosis  $\geq 66\%$  (arteries 3-5), the percent errors of Murray's Law were greater than the empirical relation, which was anticipated as Murray's Law largely overestimated the outflow-ratio in the ICA for those arteries (Table 7-I, Figure 7-4a). Figure 7-6 shows the relationship between %errors and the difference in estimated versus measured ICA outflow-ratio. As expected, the larger the error in outflow-ratio estimation, the

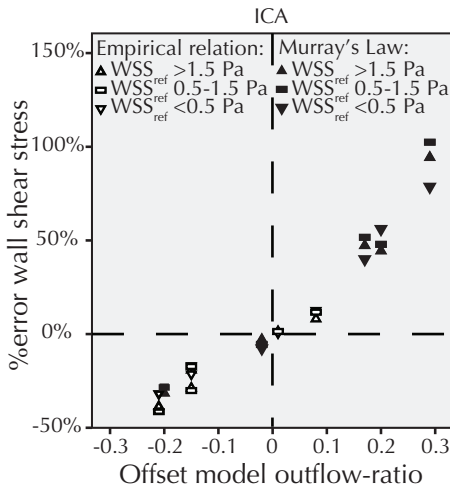


**Figure 7-6:** Percent error (%error) in mean WSS in the low (▽), normal (□) and high (△) WSSref regions as function of the offset in outflow. The offset in outflow is the difference in outflow-ratio as estimated by Murray's Law or the Empirical Relation compared to the measured outflow-ratio. %error as obtained with empirical relationship in open symbols, with Murray's Law in closed symbols.

larger differences in WSS. This effect was equal for low, normal or high WSS regions.

## DISCUSSION

We showed that the outflow-ratios in the carotid bifurcation from the CCA to the ICA and ECA change when the area stenosis exceeds 65%. Although Murray's Law gives a reasonable approximation of outflow-ratios for bifurcations with area stenosis  $\leq 65\%$ , for stenosis  $\geq 66\%$  the outflow-ratios are largely overestimated. The empirical relation, as derived from the measured flow, gives better results regarding estimation of the outflow-ratio and results in WSS values closer to the ones obtained with the measured outflow-ratios.

Flow measurements of the CCA ( $5.1 \pm 2.0$  ml/s) were in the range of previously reported studies (4.6, 6.0 and 6.2 ml/s) of young healthy volunteers [20-22]. This in contrast with the lower flow in the ICA ( $2.8 \pm 1.6$  ml/s vs 4.1 ml/s) [20]. Most likely this difference can be explained by the difference in study population. We studied older persons with lumen narrowing due to atherosclerosis, whereas previous studies used young healthy volunteers. On the other hand, the measured flow in the ECA was somewhat higher ( $2.1 \pm 0.9$  vs. 1.6 ml/s) [20]. Because the flow in the ECA was not related to

the degree of area stenosis, the low scan resolution for these small vessels and partial volume effects might be the reason for this difference [23].

On average, for arteries with an area stenosis  $\leq 65\%$ , the outflow-ratio remained constant for  $Q_{ICA}/Q_{CCA}$  (0.64) and  $Q_{ECA}/Q_{CCA}$  (0.35), which was similar to the outflow-ratios for  $Q_{ICA}/Q_{CCA}$  (0.70) and  $Q_{ECA}/Q_{CCA}$  (0.39) as measured in young healthy volunteers [20]. That even in the presence of a small area stenosis ( $\leq 65\%$ ) the outflow-ratio is maintained is probably due to distal adaptation of the vascular resistance. With increasing area stenosis, the plaque in the ICA becomes flow-limiting which can not be compensated by distal adaptation any more, thus reducing flow through the ICA and CCA.

The calculated mean WSS in the CCA was lower ( $0.4 \pm 0.2$  Pa vs 1.15 Pa), while the mean WSS in the ICA was slightly higher than reported in literature ( $0.7 \pm 0.4$  Pa vs 0.56 Pa) [8,24]. This difference can be partly explained by the combination of a slightly lower flow combined with a larger diameter of the CCA compared to literature ( $8.2 \pm 1.2$  mm vs 6.3 mm) [25], resulting in a lower WSS. This suggests that for patient-specific WSS calculations, correct in- and outflow boundary conditions are a prerequisite. When no flow measurements are available, both flow and outflow-ratio as function of areas stenosis should be used for WSS calculations using CFD. In this paper we addressed the importance of correct outflow boundary conditions for stationary flow. For time-dependent flow simulations including wall deformations, more advanced models describing the distal vascular resistance are required.

Ideally patient-specific flow measurements should be used when performing CFD studies. However, in clinical practice, MR imaging procedures are considered to be lengthy and especially in larger patient studies there is a strong urge to minimize imaging time. Therefore, phase contrast protocols are not always performed, even though MR imaging is carried out. Estimation of outflow-ratio for the CFD calculations using Murray's Law gave in general reasonable results for the area stenosis  $< 65\%$ , but also for those area stenosis a significant underestimation was observed with a large range (Figure 7-4). To find a better solution for the outflow-ratio estimation we fitted an empirical relation using our measurements. Although the empirical relation performed better than Murray's Law, still 35% of the variation in the outflow-ratio measurements was not explained by this relationship.

## *Limitations*

We selected participants from the Rotterdam Study with an age of  $\geq 70$  years. This criterion was applied to avoid uncorrectable phase-wrap in time-averaged flow scans, since the peak systolic velocity in people older than 70 is expected to be lower than 60 cm/s [26], which was used as velocity encoding in the protocol of the MRI phase-contrast study. In general, asymptomatic subjects, as measured in the Rotterdam Study, have a lower degree of stenosis. Therefore, to be able to analyze the flow in the presence of the full range of area stenosis in this study we added symptomatic subjects, often having a higher degree of stenosis, to the study group. If we analyzed the groups separately, we obtained a similar empirical relation for both groups with the same cut-off-point.

In this study, only a limited number of bifurcations ( $n=14$ ) had a degree of area stenosis higher than 65%. Based on this number of bifurcations, the empirical relation between the  $Q_{ICA}/Q_{CCA}$  and  $Q_{ECA}/Q_{CCA}$  outflow-ratio was established. Since the relation had a small confidence interval, we are confident that this relationship can be used in further studies.

## **CONCLUSION**

We determined the outflow-ratio of carotid bifurcations with various degrees of area stenosis using phase-contrast MRI and we derived an empirical relation between the outflow-ratio and area stenosis in the ICA. Ideally patient-specific flow measurements should be used when performing CFD studies. If patient-specific flow measurements are not available for CFD in the carotid bifurcation, estimation of the outflow-ratio based on the presented empirical relation would result in a better approximation of WSS compared to WSS that result from outflow-ratio estimations based on Murray's Law.



## REFERENCES

1. VanderLaan PA, Reardon CA, and Getz GS, Site specificity of atherosclerosis: site-selective responses to atherosclerotic modulators. *Arteriosclerosis, Thrombosis, and Vascular Biology*, 2004. 24(1): p. 12-22.
2. Malek AM, Alper SL, and Izumo S, Hemodynamic shear stress and its role in atherosclerosis. *Journal of the American Medical Association*, 1999. 282(21): p. 2035-42.
3. Kaazempur-Mofrad MR, et al., Characterization of the atherosclerotic carotid bifurcation using MRI, finite element modeling, and histology. *Annals of Biomedical Engineering*, 2004. 32(7): p. 932-46.
4. Ku DN, et al., Pulsatile flow and atherosclerosis in the human carotid bifurcation. Positive correlation between plaque location and low oscillating shear stress. *Arteriosclerosis*, 1985. 5(3): p. 293-302.
5. Groen HC, et al., Plaque rupture in the carotid artery is localized at the high shear stress region: a case report. *Stroke*, 2007. 38(8): p. 2379-81.
6. Perktold K and Rappitsch G, Computer simulation of local blood flow and vessel mechanics in a compliant carotid artery bifurcation model. *Journal of Biomechanics*, 1995. 28(7): p. 845-56.
7. Younis HF, et al., Hemodynamics and wall mechanics in human carotid bifurcation and its consequences for atherogenesis: investigation of inter-individual variation. *Biomechanics and Modeling in Mechanobiology*, 2004. 3(1): p. 17-32.
8. Cheng C, et al., Large variations in absolute wall shear stress levels within one species and between species. *Atherosclerosis*, 2007. 195(2): p. 225-35.
9. Sharefkin JB, et al., Fluid flow decreases preproendothelin mRNA levels and suppresses endothelin-1 peptide release in cultured human endothelial cells. *Journal of Vascular Surgery*, 1991. 14(1): p. 1-9.
10. Sherman TF, On connecting large vessels to small. The meaning of Murray's law. *The Journal of General Physiology*, 1981. 78(4): p. 431-53.
11. Hofman A, et al., The Rotterdam Study: 2010 objectives and design update. *European Journal of Epidemiology*, 2009. 24(9): p. 553-72.
12. Bots ML, et al., Common carotid intima-media thickness and risk of acute myocardial infarction: the role of lumen diameter. *Stroke*, 2005. 36(4): p. 762-7.
13. Tarnawski M, et al., The measurement of time-averaged flow by magnetic resonance imaging using continuous acquisition in the carotid arteries and its comparison with Doppler ultrasound. *Clinical Physics and Physiological Measurement*, 1990(1): p. 27.

14. Bakker CJ, et al., Accuracy and precision of time-averaged flow as measured by nontriggered 2D phase-contrast MR angiography, a phantom evaluation. *Magnetic Resonance Imaging*, 1995. 13(7): p. 959-65.
15. Rothwell PM, et al., Prognostic value and reproducibility of measurements of carotid stenosis. A comparison of three methods on 1001 angiograms. *European Carotid Surgery Trialists' Collaborative Group. Stroke*, 1994. 25(12): p. 2440-4.
16. Murray CD, The Physiological Principle of Minimum Work: I. The Vascular System and the Cost of Blood Volume. *Proceedings of the National Academy of Sciences of the United States of America*, 1926. 12(3): p. 207-14.
17. Taubin G, Zhang T, and Golub G, Optimal Surface Smoothing as Filter Design, in *Fourth European Conference on Computer Vision (ECCV'96)*, and IBM Research Technical Report RC-20404. 1996.
18. Seo T, Schachter L, and Barakat A, Computational Study of Fluid Mechanical Disturbance Induced by Endovascular Stents. *Annals of Biomedical Engineering*, 2005. 33(4): p. 444-56.
19. Antiga L and Steinman D, Robust and objective decomposition and mapping of bifurcating vessels. *IEEE Transactions on Medical Imaging*, 2004. 23(6): p. 704-13.
20. Marshall I, Papathanasopoulou P, and Wartolowska K, Carotid flow rates and flow division at the bifurcation in healthy volunteers. *Physiological Measurement*, 2004. 25(3): p. 691-7.
21. Ford M, et al., Characterization of volumetric flow rate waveforms in the normal internal carotid and vertebral arteries. *Physiological Measurement*, 2005. 26(4): p. 477-88.
22. Holdsworth DW, et al., Characterization of common carotid artery blood-flow waveforms in normal human subjects. *Physiological Measurement*, 1999. 20(3): p. 219-40.
23. Lotz J, et al., Cardiovascular flow measurement with phase-contrast MR imaging: basic facts and implementation. *Radiographics*, 2002. 22(3): p. 651-71.
24. Sui B, et al., Blood flow pattern and wall shear stress in the internal carotid arteries of healthy subjects. *Acta Radiologica*, 2008. 49(7): p. 806-14.
25. Riley WA, et al., Reproducibility of noninvasive ultrasonic measurement of carotid atherosclerosis. The Asymptomatic Carotid Artery Plaque Study. *Stroke*, 1992. 23(8): p. 1062-8.
26. Samijo SK, et al., Wall shear stress in the human common carotid artery as function of age and gender. *Cardiovascular Research*, 1998. 39(2): p. 515-22.

# SUPPLEMENT

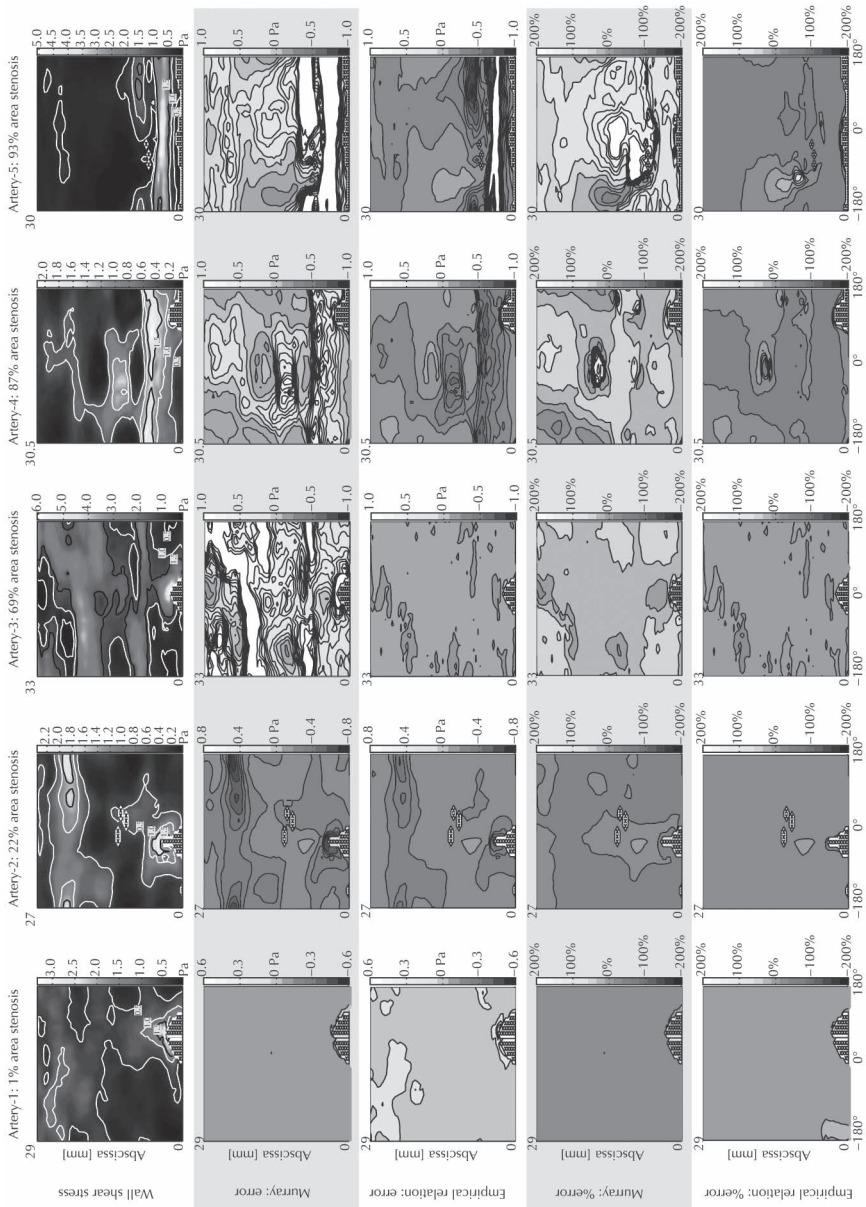


**Figure S7-1:** Wall shear stress ( $WSS_{ref}$ ) in the internal carotid arteries (ICA) of five arteries with increasing degree of area stenosis (left to right) presented as 2D-maps (angle and abscissa, i.e. the length along the lumen centerline). The difference (error and %error) in WSS as obtain with outflow estimation by Murray's Law and empirical with respect to  $WSS_{ref}$  relation presented vertically. Dashed white line  $WSS_{ref} = 0.5$  Pa, solid white line  $WSS_{ref} = 1.0$  Pa, dashed black line  $WSS_{ref} = 1.5$  Pa. The carina is located at abscissa = 0, with abscissa the length along the lumen centerline, X indicates that there is no data at that grid point.



CHAPTER

# 8

---

## SHORT-TERM FLOW INCREASE DESTABILIZES ADVANCED PLAQUES IN APOE<sup>-/-</sup> MICE BY INCREASING LIPID CONTENT

Harald Groen, Kim van Gaalen, Annemiek van Wamel,  
Kim van der Heiden, Frank Gijsen, Rini de Crom,  
Antonius van der Steen, Heleen van Beusekom,  
Jolanda Wentzel

*Manuscript in preparation*

### ***Background***

Evidence is accumulating that in the advanced state of atherosclerosis, higher wall shear stress (WSS) could negatively affect the stability of the plaque. However detailed information is lacking on the influence of high shear stress on plaque composition/stability.

### ***Methods***

Using a flow modifier model, advanced plaques with characteristics of vulnerable plaques were induced in ApoE<sup>-/-</sup> mice. In this model, we doubled the flow at advanced plaques in the carotid arteries. After one week of flow increase the cuffed carotid arteries were analyzed by immuno-histochemistry and compared to the vulnerable plaques without a flow increase.

### ***Results***

The plaques that experienced a short duration of flow increase of more than 200%, five weeks after initiation of the plaque, had a much higher lipid content than the plaques in control mice or mice in which no flow increase was established. This higher lipid content was accompanied with a lower expression of PECAM-1 at the proximal side of the plaque and at the maximum plaque location.

### ***Conclusion***

After exposure to a short duration of flow increase, advanced plaques of ApoE<sup>-/-</sup> contained significant more lipids but the plaque size remained unchanged compared to advanced plaques without flow increase. This finding suggests an increased destabilization of advanced plaques by higher WSS.

## INTRODUCTION

Atherosclerosis is a lipid and inflammation driven disease of the larger arteries [1,2] and is found at specific locations in the vessel wall, i.e. at low and oscillatory wall shear stress regions (WSS) [3]. Low WSS and disturbed flow induce pro-inflammatory transcription factors like NF- $\kappa$ B and AP-1 but reduce expression and/or activity of anti-inflammatory transcription factors such as KLF2 and Nrf2 [4], rendering the vascular wall vulnerable for atherosclerotic lesion development [5,6].

Plaque growth often leads to lumen narrowing, which results in a change in the WSS distribution over the plaque. Downstream, the WSS will be lower than normal and can become oscillatory, while at the upstream and shoulder regions of the plaque the WSS is elevated. Evidence is accumulating that in the advanced state of the disease; this higher WSS could negatively affect the stability of the plaque [7-10]. However detailed information is lacking on the influence of high WSS on plaque composition/stability.

To study the influence of high WSS on advanced plaques *in vivo*, we increased the flow at advanced plaques in the carotid artery of ApoE<sup>-/-</sup> mice. The plaques were induced using the flow-modifier model by Cheng et al. [11]. These advanced vulnerable plaques are characterized by high levels of lipids and high levels of matrix metalloproteinase activity, low levels of vascular smooth muscle cells and collagen and the presence of macrophages [11]. The increase in flow was accomplished by partial ligation of the contra-lateral carotid artery and confirmed by ultrasound-Doppler measurements. After one week of flow increase the cuffed carotid arteries were analyzed by immuno-histochemistry and compared to the vulnerable plaques without a flow increase.

## MATERIALS AND METHODS

### *Mice and diet*

Female apolipoprotein E-deficient (ApoE<sup>-/-</sup>) mice (n=20), were fed a standard chow diet until the age of 13 weeks (Figure 8-1). From week 13, mice were fed a Western-diet (4021.06, Arie Blok BV, Woerden, The Netherlands).

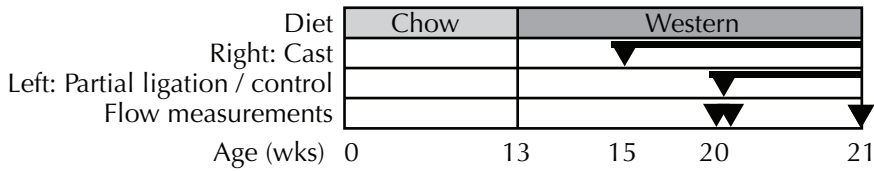


**Figure 8-1:** Experiment protocol.

**Experimental procedures**

At 15 weeks of age, the mice were anesthetized using isoflurane (2%). The right carotid artery was dissected from the surrounding tissue and a tapering polymethylpentene flow modifier [12] was placed around the right common carotid artery (400-200 μm inner diameter: proximal-distal; length=1.5 mm) to create a vulnerable plaque phenotype proximal to the flow modifier (Figure 8-2a) [11].

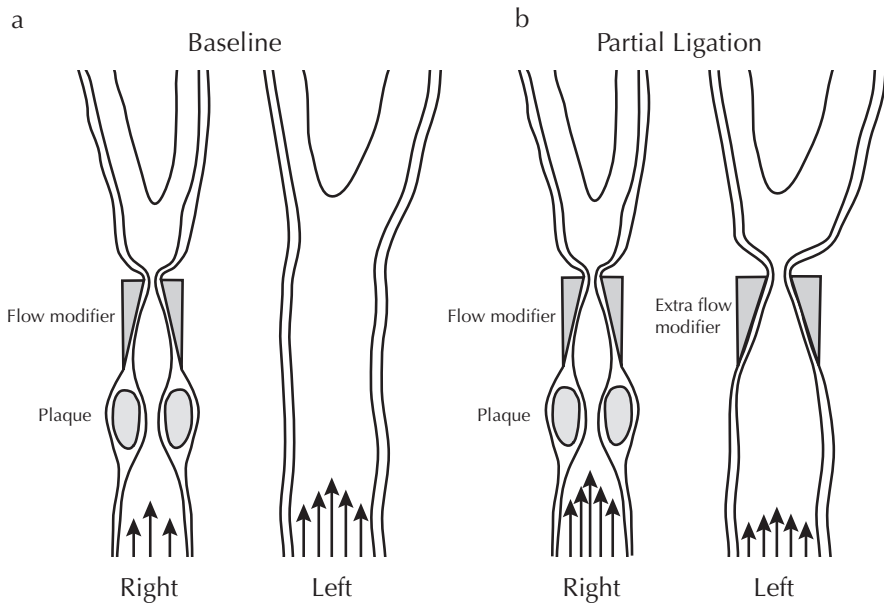


**Figure 8-2:** Location of the plaque with respect to the flow modifier at a) baseline and b) after partial ligation of the left carotid artery.



Five weeks after the flow modifier placement (at 20 weeks of age), a partial ligation inducing a stenosis in the left common carotid artery (n=10) was performed to double the flow in the right carotid (Figure 8-2b). This was done by placing a similar tapering polyethylene flow modifier around the left carotid artery (500- 250  $\mu\text{m}$  inner diameter). For the control group (n=10), a sham operation was performed on the left carotid artery instead of the partial ligation. One week after partial ligation (at 21 weeks of age), the mice were euthanatized, perfused with DPBS and the carotids were collected. The experiment was approved by the Dutch National Animal Experimental Committee and performed in agreement with The Netherlands Experiments on Animals Act (1977) and the European Convention for protection of Vertebrate Animals used for Experimental Purposes (Strasbourg, 18 March 1986).

### *Flow measurements*

Measurements of the blood flow were performed in both common carotid arteries at four different time-points: I) just before partial ligation or sham operation in the control group; II) direct after partial ligation or sham operation for the control animals; III) 3 days after partial ligation or sham operation for the control animals and IV) just before euthanization (Figure 8-1). For all these measurements the mice were anesthetized using isoflurane (2%). Velocity measurements and diameter measurements were performed in both common carotid arteries, proximal to the flow modifier if present, using the Vevo 770 (Visualsonics, Toronto, Canada) and a 40 MHz probe (RMV-704). Heart rate, respiration rate and body temperature were monitored and recorded during the measurements. The time-averaged flow was calculated based on the time-averaged maximum velocity and the time-averaged diameter assuming a parabolic velocity profile ( $Q = \frac{1}{8} \pi D^2 V_{\text{max}}$ ; with  $V_{\text{max}}$  the maximal velocity in the center of the vessel with diameter D). Based on the flow measurements just before and after partial ligation, the procedure was considered successful only if the flow was at least twice as high in the right carotid artery (artery with advanced plaque) after the partial ligation.

### ***Plasma cholesterol levels***

Total plasma cholesterol concentrations were measured enzymatically using a commercially available kit (kit 61218, Biomerieux). Blood samples were collected at 2 time points during the experiment: I) before flow modifier implantation (at week 15, Figure 8-1) using blood from the tail vein and II) at 21 weeks just before euthanization under general anesthesia by hart puncture.

### ***Immunohistochemical analysis of lesions***

After euthanization, blood samples were collected by cardiac puncture and flushing was performed with PBS (DPBS, Biowhittaker). Subsequently, right and left common carotid arteries were isolated and embedded in Tissue-Tec (OCT compound, Electron Microscopy Sciences) together with a part of the liver for support and positive control. Tissues were stored at -80°C for later histological and immunohistochemical processing. Equally spaced (200 µm) serial transverse cryo-sections (5 µm, 7-14 locations per vessel) were obtained from the tissue proximal to the flow-modifier. Adjacent sections were stained for haematoxylin/eosin and for the appearance of fat (Oil-Red-O, Sigma-Aldrich), macrophages (Rat anti-mouse CD68, 1:200, AbDSeroTec) and endothelial cells (Rat anti-mouse PECAM-1, 1:200, AbDSeroTec). For all immunohistochemical stainings, a second HRP-labeled antibody was used (Goat anti-rat HRP, 1:50, AbDSeroTec) with DAB (3,3'-Diaminobenzidine tetrahydrochloride, Sigma-Aldrich) as a chromogen.

Eight consecutive sections at 200 µm intervals immediately proximal to the flow-modifier were analysed. The histological sections were digitized at 20x using the NanoZoomer (Hamamatsu, Japan). Quantification was performed semi-automatically using BioPix (BioPix AB, Göteborg, Sweden). Lesion area was defined as newly formed intima. The quantification of different morphological parameters of the plaque was based on the average of these 8 consecutive sections. In addition, the section with the maximal plaque size was used to define the upstream and downstream side of the plaque. Subsequently, the average morphological parameters were also calculated for both the upstream and downstream side of the plaque.

### ***Statistical analysis***

In order to establish a flow increase in the right carotid artery 5 weeks after plaque initiation by the flow modifier, the left carotid artery was partial ligated. This results in large inter-animal variations of flow change in the right carotid artery. To study the effect of flow increase on the plaque composition, we subdivided the partial ligation group into 2 sub-groups based on the accomplished flow increase in the right carotid artery. Mice that presented a doubling in shear stress levels in the right carotid artery were considered *high flow* group, whereas mice with a flow increase below double were considered *partial ligation non-responding* group. Both groups were compared with the sham-operated control group.

Both the physiological measurements and the areas of stained sections of the groups were compared. One-way ANOVAs with the Tukey post-hoc test were performed and a  $p \leq 0.05$  was considered statistically significant. Statistical analysis was performed using SPSS v15 (SPSS, Chicago, IL, USA) and data is expressed as mean with standard deviation.

## **RESULTS**

### ***Flow measurements***

In four of the ten mice of the partial ligation group, a doubling of the flow was measured (*high flow*), while in 3 mice no flow increase (*partial ligation non-responder*) was observed. In three cases the flow measurement directly after partial ligation was unsuccessful, therefore these mice were excluded from the study. One mouse of the control group was also excluded since the flow was more than doubled after the sham operation (Table 8-I). For the control and non-responders from the partial ligation group, the normalized flows were not statistically different directly after the operation at 3 days and 7 days ( $p = \text{NS}$ , Table 8-I). Since the *high flow* group was selected based on the flow direct after partial ligation, this group had a higher flow direct after ligation ( $p < 0.001$ ) compared to the control group and non-responder group. Although the flow increase seemed to be diminished after 3 days ( $p = 0.11$  compared to control group and  $p = 0.14$  compared to baseline), at day 7 a 100% increase compared to baseline was still recorded ( $p = 0.007$ ) with a strong trend of higher flow compared to the control group ( $p = 0.06$ ), suggesting that the flow was indeed higher in the *high flow* group for up to 7 days.

**Table 8-I:** Normalized flow in right carotid artery in the control and partial ligation group

	Sham	Partial ligation	
	Control N=9	Non-responders N=3	High flow N=4
<b>Normalized flow</b>			
day of flow change	1.1 ± 0.5	1.1 ± 0.1	3.0 ± 1.0
3 days after flow change	0.9 ± 0.5	1.1 ± 0.1	1.6 ± 0.7
7 days after flow change	1.2 ± 0.6	1.3 ± 1.0	2.2 ± 0.5*

Normalized flow: Flow with reference to flow before partial ligation or sham operation.

High flow group: normalized flow at day of flow change > 2 and non-responders: normalized flow at day of flow change < 2. \*Significant different from 1.

### *Plaque composition control versus partial ligation*

**Table 8-II:** General characteristics of mice.

	Sham	Partial ligation	
	Control N=9	Non-responders N=3	High flow N=4
<b>Weight (g)</b>			
Before flow-modifier acement	19.6 ± ± 2.0	19.0 ± 0.6	20.0 ± 0.8
Before flow change	21.0 ± 1.4	20.6 ± 1.2	21.7 ± 1.5
3 days after flow change	21.0 ± 1.9	20.9 ± 1.0	22.2 ± 1.1
7 days after flow change	21.2 ± 1.5	21.4 ± 1.0	22.3 ± 1.4
<b>Heart rate (beats/min)</b>			
Before flow-modifier placement	494 ± 35	423 ± 56	489 ± 30
Before flow change	487 ± 27	460 ± 28	486 ± 20
3 days after flow change	470 ± 30	473 ± 52	484 ± 31
7 days after flow change	485 ± 17	470 ± 35	497 ± 39
<b>Cholesterol level (mM)</b>			
Before flow change	34.2 ± 3.0	31.1 ± 2.8	30.4 ± 4.1
7 days after flow change	34.8 ± 5.0	32.9 ± 4.4	32.8 ± 1.8

High flow group: normalized flow at day of flow change > 2 and non-responders: normalized flow at day of flow change < 2.

During the experiment there was no differences in either heart rate, cholesterol levels ( $p > 0.18$ ) or weight ( $p > 0.4$ ) among the mice in the control

group or the partial ligation groups (Table 8-II). By comparing the general morphology of the control and the partial ligation groups, there was no difference in media, lumen or plaque area (Table 8-III).

**Table 8-III:** Morphology and composition of plaques.

	Sham	Partial Ligation	
	Control	Non-responders	High flow
	N=9	N=3	N=4
Media $\mu\text{m}^2 \times 1000$	36.8 $\pm$ 3.9	40.7 $\pm$ 0.8	40.7 $\pm$ 5.7
Lumen $\mu\text{m}^2 \times 1000$	21.2 $\pm$ 12.2	27.2 $\pm$ 5.4	11.8 $\pm$ 10.9
Plaque $\mu\text{m}^2 \times 1000$	59.9 $\pm$ 15.2	61.5 $\pm$ 3.0	52.4 $\pm$ 24.0
Lipids $\mu\text{m}^2 \times 1000$	7.3 $\pm$ 5.4	7.2 $\pm$ 5.0	16.2 $\pm$ 4.0 <sup>*</sup>
Lipids/Plaque %	10 $\pm$ 6	8 $\pm$ 4	29 $\pm$ 13 <sup>#</sup>
CD68 $\mu\text{m}^2 \times 1000$	12.1 $\pm$ 5.9	9.5 $\pm$ 7.2	9.5 $\pm$ 4.1
CD68/Plaque %	22 $\pm$ 7	15 $\pm$ 10	23 $\pm$ 7
PECAM-1 $\mu\text{m}^2 \times 1000$	2.7 $\pm$ 0.6	2.4 $\pm$ 0.3	1.6 $\pm$ 0.6 <sup>\$</sup>

High flow group: normalized flow at day of flow change > 2 and non-responders: normalized flow at day of flow change < 2; CD68 stain for presence of macrophages. PECAM-1: stain for PECAM-1,\*p<0.01 compared to control, #p<0.02 compared to non-responders, \$p=0.068 compared to non-responders.

Although the plaque area was not different, the plaques contained a larger area of lipid (16.2 $\pm$ 4.0 vs 7.3 $\pm$ 5.4, 7.2 $\pm$ 5.0) resulting in a higher percentage (29 $\pm$ 13% vs 10 $\pm$ 6%, 8 $\pm$ 4%) for the *high flow* group compared to control group and the *partial ligation non-responder* group. Moreover, less PECAM-1 staining was observed for the *high flow* group, whereas no difference in the area of CD68 positive cells was found (Figure 8-3, Table 8-III). Interestingly, no difference was found in either morphology or composition comparing the control group and the *partial ligation non-responders* group. This implied that without short duration of flow increase, but in the presence of partial ligation, similar effects in the plaque size and composition were found as in the control group.

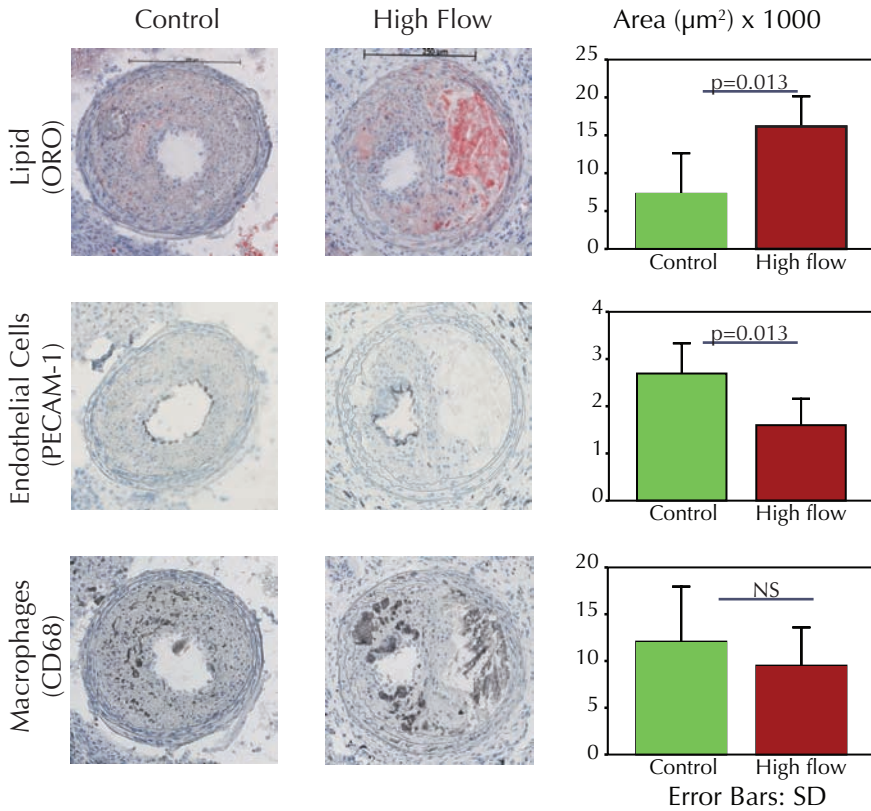


**Figure 8-3:** Typical histological slices and histological quantification of the lipids, endothelial cells and macrophages of the control and the high flow group.

### *Upstream versus downstream*

To check whether there is a difference in spatial distribution within plaque, the plaque was divided into three sections with respect to the section with the maximal plaque area: upstream or downstream from the maximum plaque section and the cross section with the maximum plaque (Figure 8-4a). Again, if stratified according to the 3 locations, the plaque morphology and composition were not different for the plaques from the mice of the non-responder group compared to the plaques of the control mice. Figure 8-4 shows the plaque morphology and composition with respect to cross section with the maximal plaque area for the control and *high flow* group. Per definition, the plaque area (Figure 8-4b) at the cross section with the maximal plaque area differed from the plaque at the upstream

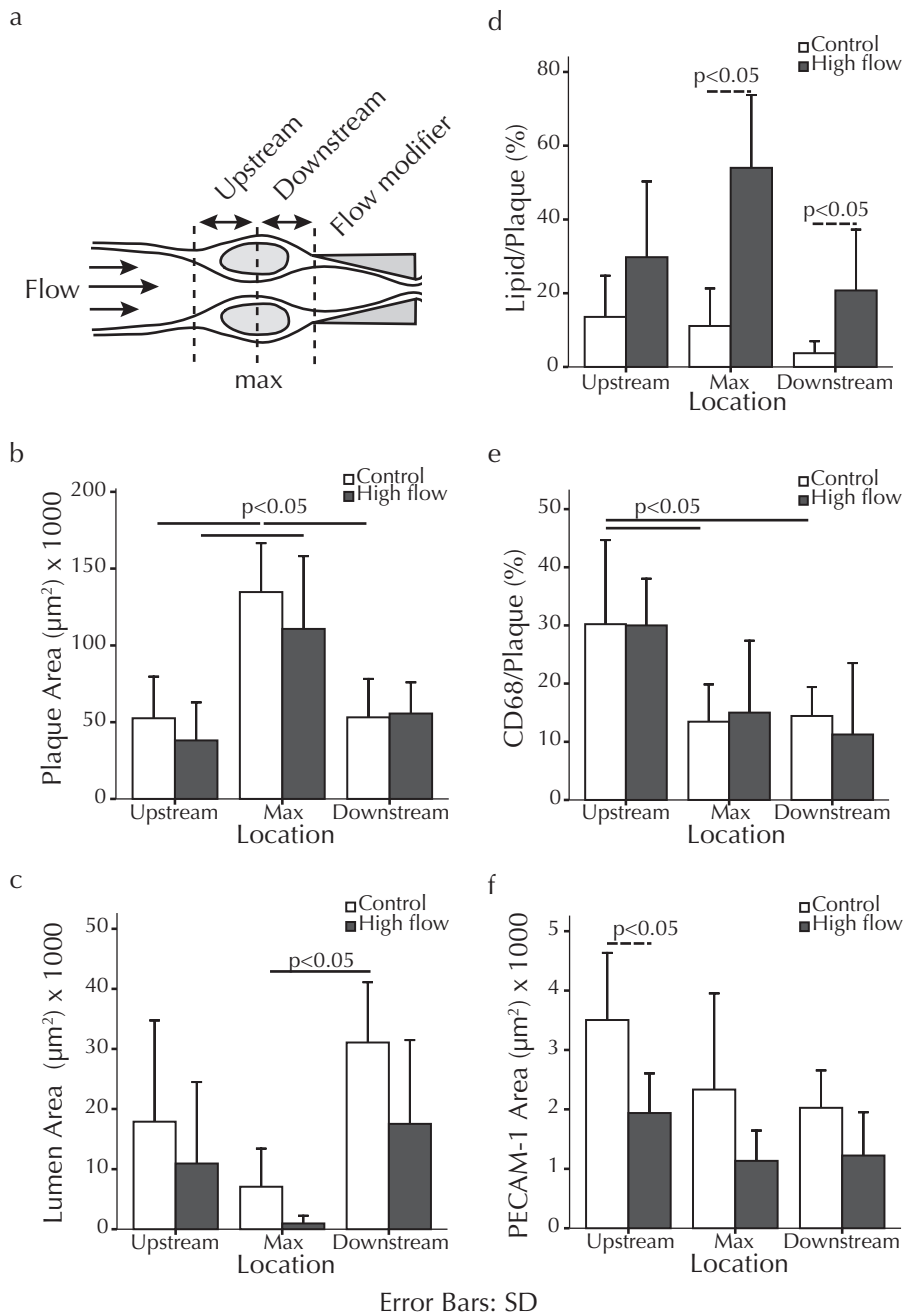


**Figure 8-4:** a) Schematic drawing of the plaque, with the upstream and downstream side defined by the cross-section with the maximal plaque area; b) Plaque area; c) Lumen area; d) Relative lipid area; e) Relative CD68 positive area and f) PECAM-1 positive area of the plaque at the upstream, maximal plaque and downstream location. Solid lines: differences inside group and location; dashed lines: difference between groups and location.

and down stream plaque area for both the control group and the *high flow* group ( $p < 0.05$ ). However the maximal plaque area was not different for both groups.

Presence of the plaque influenced the local lumen dimensions, such that the minimal lumen area was found at the location of the maximal plaque area (Figure 8-4c), however only for the control group statistical significance was reached. In the *high flow* group, both at the maximal plaque and downstream location, the plaque area occupied by lipids was larger compared to the control (Figure 8-4c).

Figure 8-4e shows that for both, the *high flow* group and the control mice, more macrophages were present at the upstream side compared to the two other sides of the plaque. Expression of PECAM-1 (Figure 8-4f) followed that same pattern. For the *high flow* group overall PECAM-1 is reduced (Figure 8-3) with a significant reduction in PECAM-1 at the upstream side of the plaque compared to the control (Figure 8-4f).

## DISCUSSION

We demonstrated that plaques, generated using a flow modifier in high cholesterol diet-fed ApoE<sup>-/-</sup> mice, that experienced a short duration of flow increase of more than 200% had a much higher lipid content than plaques that were not exposed to a flow increase. This higher lipid content was accompanied by a lower expression of PECAM-1, mainly at the proximal side of the plaque. Although more macrophages were present at the upstream side of the plaque, no differences were observed upon the short-term flow increase.

### *Protocol*

Control mice and mice that underwent partial ligation had the same weight, heart rate and cholesterol levels, indicating that the surgical procedures had no effect on their general health status. Not all mice with a partially ligated left carotid artery developed an increased flow in the right carotid artery. The partial ligation technique that was used to induce a flow increase in the contralateral carotid artery is therefore not flawless and should be optimized. As our intention was to study the effects of a



flow increase on plaque composition we selected the mice in which this flow increase was successfully established. We considered an increase in flow by two times to be high and thus used that as selection criterion. After 3 days, the increased flow was less pronounced but recovered at 7 days post partial ligation. Whether this phenomenon is due to distal adaptation of the vasculature and/or decreased lumen area at the plaque is currently unknown and should be further investigated.

### ***Plaques in control mice***

All mice showed plaque formation at the upstream side of the flow-modifier with a high lipid content and macrophage infiltration, as was observed in earlier studies [11,12]. Low WSS flow patterns are associated with extra cellular matrix (ECM) degradation in the vessel wall, increased endothelial permeability, enhanced uptake of low-density lipoprotein cholesterol (LDL), resulting in a subendothelial accumulation of LDL [13], and increased leukocyte recruitment.

We found significant differences between the plaque regions in CD68 positive area. The upstream region had the largest CD68 positive areas, which nicely correlates with data from human carotid endarterectomy specimens in which CD68 positive cells were found at the upstream side of the plaque as well [14,15].

PECAM-1 staining revealed that the endothelium was present in all regions. However, compared to the upstream region, the downstream region showed less PECAM-1 staining. At the downstream region you may expect lower WSS than at the upstream side of the plaque. Low WSS induced reduction in expression may occur as a result of a down-regulation of PECAM-1 expression [16,17].

### ***Plaques in high flow mice***

Maximum plaque size with the largest lipid pool correlates to maximum occlusion, which is in agreement with morphology of a vulnerable plaque [18]. In our experiments, there was no evidence for plaque rupture as a result of the increased flow. Previous experiments established that placement of the flow-modifier did not result in increased blood pressure or alterations in the heart rate [11]. Since it has been shown in mice that

chronic physical stress increases blood pressure and heart rate resulting in plaque rupture [19], it can be argued that increased flow alone is not sufficient to induce plaque rupture in these plaque models.

We found no plaque size reduction, for instance through the activation of NF- $\kappa$ B signaling in endothelial cells [20], probably due to the lower and shorter flow increase of 7 days. Other studies on high flow induced neointima regression or plaque regression [21,22], applied much longer (4-8 weeks) or higher extent of flow increase (6x higher than baseline flow). Moreover, activation of NF- $\kappa$ B largely depends on the underlying matrix. It has been shown that shear stress-induced activation of NF- $\kappa$ B occurs only on fibronectin or fibrinogen matrix, but not in cells plated on collagen or laminin [23]. It is plausible that the lack in plaque regression is attributed to those differences with our setup, but future studies are needed to investigate the role of NF- $\kappa$ B in this model. Furthermore, since in the *high flow* group PECAM-1 staining is lower, mainly at the upstream site, a reduced NF- $\kappa$ B activity could also be responsible for the lack of plaque size reduction [24,25].

PECAM-1 staining revealed that the endothelium was intact in all regions of the *high flow* stimulated plaque. However, compared to the control plaque PECAM-1 expression was reduced, especially at the upstream side of the plaque. This observation coincides with higher percentage of lipids in the plaques exposed to high flow compared to the control plaques. Although PECAM-1 is an important factor as a proatherogenic mechano-responsive molecule at the onset of lesion development [26,27] its role in later plaque development towards a stable or unstable plaque is unknown. PECAM-1 is involved in endothelial cell (EC) EC-EC interaction, contributing to vessel integrity [28], mechanotransduction, regulating WSS[29], and in EC-leukocyte interaction, regulating leukocyte diapedesis into tissues [30]. The contribution of altered PECAM-1 expression to the elevated lipid accumulation at high WSS needs further investigation.

Although we did find more lipids in the *high flow* group compared to the control mice, we did not find any significant difference in the area of CD68 positive cells between the two groups. This does not exclude an increase in macrophages turnover, leaving the lipids behind inside the plaque during apoptosis of the macrophages. Extending the experiment by analyzing the plaque composition two weeks after flow increase could provide information about the change in inflammatory response.

## CONCLUSION

Advanced plaques, induced in genetically modified mice, exposed to a short duration of flow increase gave a significant elevation in lipid content without changing the plaque size. Underlying mechanisms need to be unraveled.

## REFERENCES

1. Libby P, Inflammation and Atherosclerosis. *Circulation*, 2002. 105(9): p. 1135-43.
2. Ross R, Atherosclerosis is an inflammatory disease. *American Heart Journal*, 1999. 138(5 Pt 2): p. S419-20.
3. Malek AM, Alper SL, and Izumo S, Hemodynamic shear stress and its role in atherosclerosis. *Journal of the American Medical Association*, 1999. 282(21): p. 2035-42.
4. Boon RA and Horrevoets AJ, Key transcriptional regulators of the vasoprotective effects of shear stress. *Hamostaseologie*, 2009. 29(1): p. 39-40, 41-3.
5. Chien S, Effects of disturbed flow on endothelial cells. *Annals of Biomedical Engineering*, 2008. 36(4): p. 554-62.
6. Collins T and Cybulsky MI, NF-kappaB: pivotal mediator or innocent bystander in atherogenesis? *Journal of Clinical Investigation*, 2001. 107(3): p. 255-64.
7. Slager C, et al., The role of shear stress in the destabilization of vulnerable plaques and related therapeutic implications. *Nature Clinical Practice Cardiovascular Medicine*, 2005. 2(9): p. 456-464.
8. Groen HC, et al., Plaque rupture in the carotid artery is localized at the high shear stress region: a case report. *Stroke*, 2007. 38(8): p. 2379-81.
9. Gijssen F, et al. Shear stress modulates plaque composition in human coronary arteries in vivo. in *ASME Summer Bioengineering Conference*. 2008. Marco Isl, FL: Amer Soc Mechanical Engineers.
10. Tang D, et al., Sites of Rupture in Human Atherosclerotic Carotid Plaques Are Associated With High Structural Stresses. An In Vivo MRI-Based 3D Fluid-Structure Interaction Study. *Stroke*, 2009. 40: p. 3258-63.
11. Cheng C, et al., Atherosclerotic lesion size and vulnerability are determined by patterns of fluid shear stress. *Circulation*, 2006. 113(23): p. 2744-53.
12. Cheng C, et al., Shear stress affects the intracellular distribution of eNOS: direct demonstration by a novel in vivo technique. *Blood*, 2005. 106(12): p. 3691-8.

13. Chien S, Molecular and mechanical bases of focal lipid accumulation in arterial wall. *Progress in Biophysics and Molecular Biology*, 2003. 83(2): p. 131-51.
14. Yilmaz A, et al., Accumulation of immune cells and high expression of chemokines/chemokine receptors in the upstream shoulder of atherosclerotic carotid plaques. *Experimental and Molecular Pathology*, 2007. 82(3): p. 245-55.
15. Dirksen MT, et al., Distribution of inflammatory cells in atherosclerotic plaques relates to the direction of flow. *Circulation*, 1998. 98(19): p. 2000-3.
16. Rival Y, et al., Inhibition of platelet endothelial cell adhesion molecule-1 synthesis and leukocyte transmigration in endothelial cells by the combined action of TNF-alpha and IFN-gamma. *Journal of Immunology*, 1996. 157(3): p. 1233-41.
17. Stewart RJ, Kashour TS, and Marsden PA, Vascular endothelial platelet endothelial adhesion molecule-1 (PECAM-1) expression is decreased by TNF-alpha and IFN-gamma. Evidence for cytokine-induced destabilization of messenger ribonucleic acid transcripts in bovine endothelial cells. *Journal of Immunology*, 1996. 156(3): p. 1221-8.
18. Schaar JA, et al., Terminology for high-risk and vulnerable coronary artery plaques. Report of a meeting on the vulnerable plaque, June 17 and 18, 2003, Santorini, Greece. *European Heart Journal*, 2004. 25(12): p. 1077-82.
19. Ni M, et al., Atherosclerotic plaque disruption induced by stress and lipopolysaccharide in apolipoprotein E knockout mice. *American Journal of Physiology - Heart and Circulatory Physiology*, 2009. 296(5): p. H1598-606.
20. Castier Y, et al., Role of NF-kappaB in flow-induced vascular remodeling. *Antioxidants & Redox Signaling*, 2009. 11(7): p. 1641-9.
21. Mattsson EJ, et al., Increased blood flow induces regression of intimal hyperplasia. *Arteriosclerosis, Thrombosis, and Vascular Biology*, 1997. 17(10): p. 2245-9.
22. Castier Y, et al., High flow induces plaque regression in LDLR mice. *Vascular Pharmacology*, 2006. 45(3): p. e101.
23. Orr AW, et al., The subendothelial extracellular matrix modulates NF-kappaB activation by flow: a potential role in atherosclerosis. *Journal of Cell Biology*, 2005. 169(1): p. 191-202.
24. Fleming I, et al., Role of PECAM-1 in the shear-stress-induced activation of Akt and the endothelial nitric oxide synthase (eNOS) in endothelial cells. *Journal of Cell Science*, 2005. 118(Pt 18): p. 4103-11.
25. Tzima E, et al., A mechanosensory complex that mediates the endothelial cell response to fluid shear stress. *Nature*, 2005. 437(7057): p. 426-31.
26. Stevens HY, et al., PECAM-1 is a critical mediator of atherosclerosis. *Disease Models & Mechanisms*, 2008. 1(2-3): p. 175-81; discussion 179.

27. Harry BL, et al., Endothelial cell PECAM-1 promotes atherosclerotic lesions in areas of disturbed flow in ApoE-deficient mice. *Arteriosclerosis, Thrombosis, and Vascular Biology*, 2008. 28(11): p. 2003-8.
28. Albelda SM, et al., EndoCAM: a novel endothelial cell-cell adhesion molecule. *Journal of Cell Biology*, 1990. 110(4): p. 1227-37.
29. Fujiwara K, Platelet endothelial cell adhesion molecule-1 and mechanotransduction in vascular endothelial cells. *Journal of Internal Medicine*, 2006. 259(4): p. 373-80.
30. Woodfin A, Voisin MB, and Nourshargh S, PECAM-1: a multi-functional molecule in inflammation and vascular biology. *Arteriosclerosis, Thrombosis, and Vascular Biology*, 2007. 27(12): p. 2514-23.



CHAPTER

# 9

GENERAL DISCUSSION

Wall shear stress is known to play an important role in many processes involved in vascular biology, so as to regulate temporal and structural changes in the vascular dimensions [1]. However, at low shear stress locations the endothelial function is disturbed creating a pro-atherogenic environment. There is ample evidence that in the presence of risk factors atherosclerotic plaques are generated at low shear stress locations in the arterial system [2]. Studies on the relationship between shear stress and the generation/ destabilization of vulnerable plaques, however, are limited [3,4]. Vulnerable plaques are a sub-type of atherosclerotic plaques and are characterized by a lipid-rich core, a thin fibrous cap with macrophages and decreased smooth muscle cells with expansive outward remodeling [5]. *In vivo* assessment of plaque composition in the human vasculature was until now hardly possible due to imaging resolution and sensitivity for different plaque components and is most likely the reason for this lack in information. Due to the advances in image processing, the number of studies relating the *in vivo* WSS and plaque composition are increasing. For instance, intravascular ultrasound derived virtual histology showed that plaques located at acknowledged low shear stress locations, this is at the inner curve close to a side branch, had a larger necrotic core than the ones located at other parts of the vasculature [6]. Furthermore, animal studies already showed that baseline low shear stress is related to the vulnerable plaque formation [3,4].

In advanced stages of (vulnerable) plaques, when encroaching into the lumen, high shear stress starts to act at the plaque. Ulcers, considered as the formal weakest parts of the plaque, are often seen at the upstream side of the plaque, which are supposedly the areas of the plaques exposed to the highest shear stress. However, until now limited information was available on the influence of high shear stress on plaque composition/ plaque rupture.

The aim of this thesis is to study the relation between WSS, plaque composition and plaque rupture. Therefore, 3 lines of research were pursued:

1. Study the relation between the location of plaque rupture and WSS;
2. Develop a method capable of studying plaque composition by histology and WSS assessment based on non-invasive *in vivo* imaging;
3. Study the relation between plaque composition and increased WSS.



First, the methods used for the different studies described in this thesis are discussed. Thereafter the main findings of this thesis are reflected against state-of-the-art studies in this field.

## **ASSESSMENT WALL SHEAR STRESS AND PLAQUE COMPOSITION**

### *Wall shear stress*

For our research we used computational fluid dynamics in order to assess the wall shear stress in atherosclerotic carotid arteries of patients. The main advantage of this technique over other techniques that derive the WSS from velocity measurements (**Chapter 1**) is that the WSS is known at each location in the 3D geometry. On the other hand, a number of assumptions had to be made for this off-line WSS assessment like the description of the 3D geometry, in- and outflow boundary conditions and the properties of the viscous blood.

### *Vessel lumen geometry*

In our studies on WSS calculations we used the patient-specific lumen geometry as can be obtained by using either CTA or MRI. However, the resolution of both techniques, especially at the location of lumen narrowing, is compromised in a clinical setting. CTA has a higher resolution than MRI (0.5 mm compared to 1.0 mm) and covers the entire neck but suffers from streak artifacts, blooming effects due to calcifications and the patient is exposed to radiation during scanning. MRI on the other hand does not involve radiation, but suffers from a limited resolution and the acquisition time is much longer. An advantage over CTA is that MRI can provide additional flow information. Although both imaging modalities have their limitations in assessing plaque composition and size [7], we are confident that the resolution of both modalities is sufficiently high to determine patient-specific general patterns in the shear stress distribution [8,9].

### *In- and outflow boundary conditions*

In order to obtain realistic WSS values using the validated technique of computational fluid dynamics, appropriate in- and outflow boundary

conditions are required. Patient-specific flow measurements are not often available since it simply is not a standard clinical protocol for certain type of patients. Furthermore, flow measurements cannot always be performed because they are time consuming or the used imaging technique, like CTA, does not allow such measurements. Therefore, assumptions had to be made for the in- and outflow conditions. In **Chapters 3 and 4**, we used flow conditions based on an assumed healthy WSS in the common carotid artery. Since in these studies the WSS at the site of rupture was compared with the WSS at the entire plaque the final results were minimally affected by the assumed inflow conditions. However, if absolute WSS values need to be compared among patients, more accurate models estimating the in- and outflow are needed. Therefore, we performed flow measurements in the common, internal and external carotid artery and derived an empirical relation (**Chapter 7**). Moreover, contrasting earlier studies [10] these measurements were stratified according to the degree of area stenosis and thus can be used in the presence of disease. However, due to study restrictions in the MRI measurements, only patients aged over 70 were used to derive this empirical relation. Since it is known that the flow through the carotid artery is gender and age-related in healthy subjects [11], further research is needed in order to validate and extend our empirical model with gender and age.

Furthermore, we used static inflow conditions in contrast to the time-dependent pulsatile flow behavior due to the contraction of the heart. It has been shown that simulation of the time-averaged WSS corresponds very well with the average WSS of a time-dependent simulation [12]. To be independent on the choice of inflow profile, the distance between the inflow boundary and the bifurcation was sufficiently long in our studies, i.e. 3 times the lumen diameter, to allow flow development [13,14].

### ***3D plaque composition/ulceration***

Assessment of ulcers has been shown to be highly accurate using multislice CT (MSCT) imaging in comparison with histology [15]. Therefore, the location of ulcers with respect to the upstream and downstream side of the plaque (**Chapter 2**) or in relation to WSS (**Chapter 3**) could be sufficiently studied using CTA.

For studying other plaque features and expression of proteins or genes and distribution of various cell types, histology is still considered the golden standard. However, folding and stretching artifacts of tissue cross-sections during tissue processing lead to inhomogeneous deformation of the tissue. This hampers the 3D reconstruction of the tissue, hereby limiting accurate mapping of the WSS values to histology. In our opinion the best approach to link histology to WSS was to map the histology on *in vivo* imaging data by accounting for all possible deformations using advanced image processing techniques. **Chapter 5** describes the methodology for this advanced challenging task. We tackled this problem by using additional imaging steps during the tissue processing to be able to correct for these deformations in a step-wise manner. Still, some large deformations, for instance due to the surgical removal of the plaque, are currently not corrected for in our method. Also, the quality of the final histological sections can also be improved by optimizing the decalcification process. Furthermore, techniques need to be added to optimize the *in vivo* and *ex vivo* CT registration taking into account the *in vivo* blooming-effect of calcifications. Despite these limitations, the developed method can be used to further study the 3D plaque composition in respect to the *in vivo* patient-specific WSS.

### ***Wall shear stress and plaque composition/ destabilization and rupture***

For studying the relation between WSS, advanced plaque composition and plaque destabilization we were limited to symptomatic patients who, by definition, have already a destabilized plaque responsible for the symptoms. In **Chapter 3** we used the location of ulcerations as imaged with CTA and “restored” the lumen to analyze the relation between rupture location and WSS. Ideally, patients having a scan pre- and post plaque rupture should be used for this study, as described in **Chapter 4**, where we showed that the location of plaque rupture coincided with high WSS. Unfortunately, these cases are slim. In a larger patient group (n=20) we showed that plaque ulceration was associated with high WSS, although this association did not reach statistical significance (**Chapter 3**). Other studies in both human carotid and coronary arteries have shown that high WSS is co-localized with plaque weakening and rupture as we demon-

strated in **Chapter 4** [16-18]. This strengthens the hypothesis that high WSS is involved in plaque destabilization in the advanced stages of the disease, although the blood pressure probably provides the force needed for actual rupture [19-21]. In contrast to our results, other groups advocates a role for low WSS in further plaque destabilization [3,22,23], such that low WSS leads to excessive expansive remodeling perpetuating a vicious cycle of inflammation and matrix degradation leading. However, recent work shows a wide variety in vascular response to low shear stress conditions [24].

## FLOW INCREASE AT A VULNERABLE PLAQUE

The results of our studies showing plaque rupture occurring predominantly at the upstream location (**Chapter 2**) and the association of plaque rupture and WSS (**Chapter 3 and 4**) combined with results from other studies [16-18] indicate that high WSS is involved in plaque destabilization. Since these studies do not show a direct cause-and-relation between plaque destabilization and high WSS, we aimed at artificially increasing the WSS in an *in vivo* animal model of a vulnerable plaque [4,25]. The advantage of this model is that the environment and conditions are more controlled and the causal relation between plaque stability and WSS can be studied in detail. However, the atherosclerotic plaques in mice are not fully comparable to those seen in humans as they develop more rapidly. Furthermore, plaques in mice show less calcifications and the absolute WSS values are approximately 10 times higher compared to humans [26]. Despite these limitations, we doubled the flow at an artificially induced vulnerable plaque in the carotid artery of ApoE<sup>-/-</sup> mice. Contrasting previous work who used a six times increase of flow [27], we did not measure plaque size reduction but did find a significant increase in lipid content of the plaque. This result implicates an association between high WSS and enhanced plaque vulnerability (**Chapter 8**).

## FUTURE PERSPECTIVE

### *Use of 3D histology*

The 3D histology reconstruction method based on non-invasive imaging and histological cross sections as presented in **Chapter 5** provides the basis for research projects aiming at training and validating of wall segmentation algorithms of non-invasively acquired *in vivo* images. For example the Hounsfield plaque classification [28] could be extended with the analysis of lipids in the presence of large calcifications. Furthermore, automatic tissue classification algorithms can be trained by using multi-sequence MRI. The advantages of the 3D histology in these research questions is that the analysis is not biased by the user-selection of the “best-matching” slice and the entire plaque is taken into account instead of a single slice. This framework has also already been used and extended by Alic et al. (unpublished data) in the research of small-animal imaging. The framework enables to link *in vivo* MRI images, functional PET/SPECT data and histology of rat bearing tumors.

Another large research field could also benefit from this method, i.e. the study of mechanical properties of the atherosclerotic plaque. By combining the planar indentation tests developed by Cox et al. [29], a 2.5-dimensional mechanical characterization of the advanced plaques is possible, extending the knowledge of the plaque composition and related strength. By using this information, *in vivo* models of the plaques can be created, simulating the 3D stress distribution inside the plaque, providing a valuable tool for estimating the *in vivo* strength of the plaque.

### *Role of wall shear stress*

The role of WSS in the homeostasis of the vessel wall and the initiation in atherosclerosis is well established. In this thesis, we showed that also in the more advanced state of atherosclerosis, WSS is still capable of influencing the plaque composition. Whether high WSS is cause or consequence at the site of plaque rupture has to be investigated more thoroughly, but seems to be a likely candidate to spot sites at risks. Extending the knowledge on the actual strength of the plaque will provide additional information about the sites at risk, to either treat the plaque or follow the plaque progression closely over time.

### ***Role of (targeted) imaging of plaque components***

To follow plaque progression over time, non-invasive imaging techniques are required capable to assess the plaque composition and inflammation-state over time.

Currently, CT and MRI can assess anatomical information and plaque composition. Especially MRI research will probably gain more interest since the design of surface coils become more and more sophisticated as well as the MRI sequence protocols. Combined with molecular traces, labeled with MRI contrast agents will provide more functional information in the near future.

Already the first functional scans of metabolic activity using radio-active labeled glucose ( $^{18}\text{F}$ -FDG) in plaques are performed in patients [30], but it is currently unknown whether these techniques can safely be applied in longitudinal studies in patients with atherosclerosis. Furthermore, using the registration method presented in **Chapter 5**, detailed analysis of the localized activity has to be performed in conjunction with histology and *ex vivo* autoradiography to exclude potential non-specific binding of radioactive traces to, for instance, calcifications [31]. Recently, Menezes et al. [32] showed no correlation in enhanced  $^{18}\text{F}$ -FDG uptake and Hounsfield unit or calcifications at 5 years follow up. Combining the  $^{18}\text{F}$ -FDG uptake before carotid endarterectomy and the 3D-histological registration technique can provide evidence for this transient  $^{18}\text{F}$ -FDG uptake to check whether this phenomenon is related to plaque vulnerability or repair.

## **GENERAL CONCLUSIONS**

In this thesis, research is described that relate WSS to plaque composition and ulceration in atherosclerotic carotid bifurcations. The results of our studies implicate that shear stress plays a role in plaque destabilization at advanced stages of the atherosclerotic disease, but the underlying cellular and molecular mechanisms need more thorough investigation. In order to investigate those relationships in patients, a new 3D-histology reconstruction method was developed, that linked histological cross sections to non-invasive images allowing to assess the *in vivo* patient-specific shear stress distribution. In future experiments this effective tool can be used to further investigate the biomechanical stimuli in relation to plaque composition and rupture.

## REFERENCES

1. Malek AM, Alper SL, and Izumo S, Hemodynamic shear stress and its role in atherosclerosis. *Journal of the American Medical Association*, 1999. 282(21): p. 2035-42.
2. VanderLaan PA, Reardon CA, and Getz GS, Site specificity of atherosclerosis: site-selective responses to atherosclerotic modulators. *Arteriosclerosis, Thrombosis, and Vascular Biology*, 2004. 24(1): p. 12-22.
3. Chatzizisis YS, et al., Prediction of the localization of high-risk coronary atherosclerotic plaques on the basis of low endothelial shear stress: an intravascular ultrasound and histopathology natural history study. *Circulation*, 2008. 117(8): p. 993-1002.
4. Cheng C, et al., Atherosclerotic lesion size and vulnerability are determined by patterns of fluid shear stress. *Circulation*, 2006. 113(23): p. 2744-53.
5. Schaar JA, et al., Terminology for high-risk and vulnerable coronary artery plaques. Report of a meeting on the vulnerable plaque, June 17 and 18, 2003, Santorini, Greece. *European Heart Journal*, 2004. 25(12): p. 1077-82.
6. Rodriguez-Granillo GA, et al., Plaque composition and its relationship with acknowledged shear stress patterns in coronary arteries. *Journal of the American College of Cardiology*, 2006. 47(4): p. 884-5.
7. Kwee RM, et al., Multimodality imaging of carotid artery plaques: 18F-fluoro-2-deoxyglucose positron emission tomography, computed tomography, and magnetic resonance imaging. *Stroke*, 2009. 40(12): p. 3718-24.
8. Moore JA, et al., Accuracy of computational hemodynamics in complex arterial geometries reconstructed from magnetic resonance imaging. *Annals of Biomedical Engineering*, 1999. 27(1): p. 32-41.
9. Thomas J, et al., Reproducibility of image-based computational fluid dynamics models of the human carotid bifurcation. *Annals of Biomedical Engineering*, 2003. 31(2): p. 132-41.
10. Marshall I, Papathanasopoulou P, and Wartolowska K, Carotid flow rates and flow division at the bifurcation in healthy volunteers. *Physiological Measurement*, 2004. 25(3): p. 691-7.
11. Samijo SK, et al., Wall shear stress in the human common carotid artery as function of age and gender. *Cardiovascular Research*, 1998. 39(2): p. 515-22.
12. Lee SW, Antiga L, and Steinman D, Correlations among indicators of disturbed flow at the normal carotid bifurcation. *Journal of Biomechanical Engineering*, 2009. 131(6): p. 061013.1-7.

13. Wake AK, et al., Choice of in vivo versus idealized velocity boundary conditions influences physiologically relevant flow patterns in a subject-specific simulation of flow in the human carotid bifurcation. *Journal of Biomechanical Engineering*, 2009. 131(2): p. 021013.1-6.
14. Moyle KR, Antiga L, and Steinman D, Inlet conditions for image-based CFD models of the carotid bifurcation: is it reasonable to assume fully developed flow? *Journal of Biomechanical Engineering*, 2006. 128(3): p. 371-9.
15. Saba L, et al., Efficacy and sensitivity of axial scans and different reconstruction methods in the study of the ulcerated carotid plaque using multidetector-row CT angiography: comparison with surgical results. *American Journal of Neuroradiology*, 2007. 28(4): p. 716-23.
16. Gijssen FJ, et al., Strain distribution over plaques in human coronary arteries relates to shear stress. *American Journal of Physiology - Heart and Circulatory Physiology*, 2008. 295(4): p. H1608-14.
17. Tang D, et al., Sites of Rupture in Human Atherosclerotic Carotid Plaques Are Associated With High Structural Stresses. An In Vivo MRI-Based 3D Fluid-Structure Interaction Study. *Stroke*, 2009. 40: p. 3258-63.
18. Fukumoto Y, et al., Localized elevation of shear stress is related to coronary plaque rupture: a 3-dimensional intravascular ultrasound study with in-vivo color mapping of shear stress distribution. *Journal of the American College of Cardiology*, 2008. 51(6): p. 645-50.
19. Hoeks AP, et al., Local blood pressure rather than shear stress should be blamed for plaque rupture. *Journal of the American College of Cardiology*, 2008. 52(13): p. 1107-8; author reply 1108-9.
20. Li ZY and Gillard JH, Plaque rupture: plaque stress, shear stress, and pressure drop. *Journal of the American College of Cardiology*, 2008. 52(13): p. 1106-7; author reply 1107.
21. Li ZY, Taviani V, and Gillard JH, The impact of wall shear stress and pressure drop on the stability of the atherosclerotic plaque. *Conference proceedings - IEEE Engineering in Medicine and Biology Society*, 2008. 2008: p. 1373-6.
22. Chatzizisis YS, et al., Role of endothelial shear stress in the natural history of coronary atherosclerosis and vascular remodeling: molecular, cellular, and vascular behavior. *Journal of the American College of Cardiology*, 2007. 49(25): p. 2379-93.
23. Koskinas KC, et al., The role of low endothelial shear stress in the conversion of atherosclerotic lesions from stable to unstable plaque. *Current Opinion in Cardiology*, 2009. 24(6): p. 580-90.
24. Koskinas KC, et al., Natural history of experimental coronary atherosclerosis and vascular remodeling in relation to endothelial shear stress. A serial, in vivo intravascular ultrasound study. *Circulation*, 2010. 121(19):2092-101



25. Cheng C, et al., Shear stress affects the intracellular distribution of eNOS: direct demonstration by a novel in vivo technique. *Blood*, 2005. 106(12): p. 3691-8.
26. Cheng C, et al., Large variations in absolute wall shear stress levels within one species and between species. *Atherosclerosis*, 2007. 195(2): p. 225-35.
27. Castier Y, et al., High flow induces plaque regression in LDLR mice. *Vascular Pharmacology*, 2006. 45(3): p. e101.
28. de Weert TT, et al., In vivo characterization and quantification of atherosclerotic carotid plaque components with multidetector computed tomography and histopathological correlation. *Arteriosclerosis, Thrombosis, and Vascular Biology*, 2006. 26(10): p. 2366-72.
29. Cox MA, et al., Mechanical characterization of anisotropic planar biological soft tissues using finite indentation: experimental feasibility. *Journal of Biomechanics*, 2008. 41(2): p. 422-9.
30. Rominger A, et al., <sup>18</sup>F-FDG PET/CT identifies patients at risk for future vascular events in an otherwise asymptomatic cohort with neoplastic disease. *Journal of Nuclear Medicine* 2009. 50(10): p. 1611-20.
31. Laitinen I, et al., Non-specific binding of [18F]FDG to calcifications in atherosclerotic plaques: experimental study of mouse and human arteries. *European Journal of Nuclear Medicine and Molecular Imaging*, 2006. 33(12): p. 1461-7.
32. Menezes LJ, et al., What is the natural history of 18F-FDG uptake in arterial atheroma on PET/CT? Implications for imaging the vulnerable plaque. *Atherosclerosis*, 2010. 211(1):136-40



**SUMMARY**

**SAMENVATTING**

**LIST OF PUBLICATIONS**

**DANKWOORD**

**CV**

**PhD PORTFOLIO**

## SUMMARY

Atherosclerosis is an inflammatory disease affecting the main arteries in humans, resulting in thickening of the vessel wall (the plaque) and eventually obstructing the arteries. When the vessels become occluded, or thrombus formation occurs due to rupture of the obstructing plaque, the organs distal to the obstruction will be deprived of nutrients and oxygen. An occlusion or rupture in the carotid arteries (that supply the brain with blood) may lead to a transient ischemic attack or stroke. Therefore, the initiation, progression and final rupture of atherosclerotic plaques need to be elucidated in order to diagnose and treat patients in the early phase of the disease, before rupture occurs.

Despite systemic risk factors that increase the risk for plaque development, the disease has a focal nature, i.e. it affects mainly side branches and the inner curves of the arteries. At these particular locations, the average dragging force of the flowing blood acting on the vessel wall area, i.e. the wall shear stress (WSS), is known to be low. At these locations lipids can enter the vessel wall, initiating an inflammatory response. During plaque growth, the vessel wall will maintain the lumen size by outward remodeling. Unfortunately, when the size of the plaque is too large, lumen narrowing can occur, potentially changing the flow patterns and finally reducing the flow. As such, the WSS distribution will also change at the location of the growing plaque, with high shear stress at the upstream side and low shear stress at the downstream side of the plaque.

The aim of the work in this thesis was to investigate whether high WSS plays a role in destabilization of advanced atherosclerotic carotid plaques. To answer this question, different image modalities, such as computed tomography angiography (CTA) and magnetic resonance imaging (MRI), were used to visualize the *in vivo* plaques in patients. Furthermore, these image modalities provided the basis to estimate patient-specific WSS distribution. The WSS was calculated using computational fluid dynamics (CFD) estimating the solution of the Navier-Stokes equations for an incompressible flow and rigid walls defined by the lumen boundaries as assessed by *in vivo* imaging techniques.

First, in **Chapter 2**, we investigated the possibilities of *in vivo* CTA imaging to examine the lumen surface irregularities and location and type of ulcers at the atherosclerotic plaque in carotid arteries. In this study we found

that plaque ruptures can be studied with CTA and that these ruptures are found more frequently at the upstream side of the plaque, which is in line with previous studies. As the upstream side of the plaque is suggestive for locations with higher WSS, high WSS could be involved in plaque destabilization. To test this hypothesis, we studied the WSS and location of plaque rupture in a patient group (n=20) imaged with CTA (**Chapter 3**). We found that ulcers occur at the thicker parts of the diseased vessel ( $p < 0.05$ ) and have a tendency to occur at locations with a two times higher WSS ( $p = 0.11$ ). A similar result was obtained in a unique case where serial imaging was performed. After baseline carotid plaque assessment by MRI, 10 months later a second MRI was obtained from the plaque. This second MRI scan revealed an ulceration of the plaque, appearing exactly at the location with baseline high WSS (**Chapter 4**).

To study the relationship between biomechanical forces like WSS (as computed from 3D reconstructions based on non-invasive imaging) and plaque composition in greater detail, we developed and validated a method that registers histological cross-sections to *in vivo* non-invasive imaging techniques. Using this method, histology of excised carotid plaques can be spatially registered with *in vivo* CTA images obtained prior to surgery (**Chapter 5**). Furthermore, based on this method, image-based quantification of the carotid plaque composition can be extensively validated. In addition, we applied the registration technique to show that transglutaminases (a class of enzymes with pleiotropic function) are present in human carotid plaques, co-localizing with macrophages (white-blood cells) and calcifications inside the plaque (**Chapter 6**).

In order to estimate the patient-specific WSS distribution, beside the lumen boundaries, inflow and outflow measures of the blood flow are required. Since obtaining this flow information in a clinical setting can be difficult, we investigated the influence of lumen narrowing due to atherosclerosis on the inflow and outflow of the bifurcation in patients (**Chapter 7**). We found that with up to 65% lumen area stenosis, plaque growth does not seem to influence the blood flowing through the carotid bifurcation. After this cut-off point, however, flow through the internal carotid artery decreases in a linear fashion to zero at a 100% lumen stenosis, while flow through the external carotid artery remains unchanged. This empirical relation between the amount of blood flow and area stenosis can be used for CFD simulations when patient-specific flow measurements are unavailable.

To determine whether there is a causal relationship between high WSS and plaque vulnerability, we used a vulnerable plaque mice model. In this model, we artificially increased the flow, and thus the WSS, in a carotid artery with an advanced atherosclerotic plaque. We found that, due to the increase in flow, the lipid content of the plaques doubled. This result implied that advanced atherosclerotic plaques do respond to changes in WSS and that an increase in WSS may result in a more vulnerable phenotype (**Chapter 8**).

In conclusion, in this thesis the relationship between WSS and plaque composition and ulceration was investigated in carotid bifurcations. The results implicate that WSS plays a role in plaque destabilization at the advanced stages of the atherosclerotic disease. However, the underlying cellular and molecular mechanisms need more thorough investigation. To investigate those relationships in patients with atherosclerosis, a new 3D-histology reconstruction method was developed. This method allows to study histological cross-sections of excised plaques together with non-invasive images obtained prior to surgery, which can be used to assess the local WSS distribution. In future experiments this effective tool can be used to further investigate the biomechanical stimuli in relation to plaque composition and rupture.



## SAMENVATTING

Aderverkalking is een ontstekingsziekte van de vaatwand van slagaders. De ziekte manifesteert zich door een verdikking van de vaatwand (de plaque) waardoor het vat vernauwd raakt. Wanneer dit gebeurt, of wanneer er een bloedstolsel ontstaat bij het scheuren van de plaque, kunnen de organen die door het aangedane bloedvat gevoed worden te weinig voedingsstoffen en zuurstof krijgen. Wanneer dit gebeurt in de halsslagaders, kunnen er (tijdelijk) uitvalsverschijnselen ontstaan in de hersenen. Het is daarom van groot belang om het ontstaan, de groei en uiteindelijk het scheuren van aderverkalking plaques te begrijpen om patiënten in een vroeg stadium te kunnen diagnosticeren en behandelen, voordat de plaque scheurt.

Naast algemene factoren die het risico op het ontstaan van aderverkalking verhogen, ontstaat aderverkalking op typische plekken in de circulatie, namelijk in zijtakken of splitsingen van bloedvaten en in binnenbochten van vaten. Het is bekend dat op deze plaatsen de gemiddelde wandschuifspanning (WSS), een afschuifspanning veroorzaakt door het stromende bloed op de vaatwand, laag is. Op deze plekken kunnen vetten de vaatwand in dringen waardoor een ontstekingsreactie wordt veroorzaakt. Tijdens de groei van deze plaque zal het bloedvat de groeiende vernauwing compenseren door naar buiten te groeien zodat het vat voldoende open blijft voor de doorbloeding. Echter wanneer de plaque te groot wordt, kan het vat vernauwen waardoor het patroon van bloedstroming verandert en de bloedstroming uiteindelijk ook zal verminderen. Door de verandering in bloedstroming zal ook het patroon van de WSS veranderen op de locatie van de groeiende plaque waarbij hoge WSS aan de voorkant van de plaque ontstaat, en lage WSS aan de achterkant van de plaque.

Het doel van dit proefschrift was om te bekijken of hoge WSS een rol speelt in het verlagen van de stabiliteit van plaques in de halsslagaders. Om hierop een antwoord te kunnen geven zijn verschillende beeldvormende technieken gebruikt, zoals computer tomografie angiografie (CTA) en magnetische resonantie (MRI) om de aderverkalking bij patiënten in beeld te brengen. Deze beeldvorming vormde tevens de basis om patiënt-specifieke WSS te bepalen. Het berekenen van de WSS werd gedaan door middel van numerieke stromingsleer (ook wel computational fluid dynamics (CFD) genoemd) die de oplossing van de Navier-Stokes



vergelijkingen benadert voor een onsamendrukbare vloeistof die door een rigide vaatwand heen stroomt, waarvan de vorm bepaald werd met behulp van de beeldvormende technieken.

In **Hoofdstuk 2** hebben we de mogelijkheid onderzocht of met behulp van *in vivo* CTA beeldvorming het oppervlakte van het vat en de locatie en type ulcers (plaque rupturen) van de aderverkalking onderzocht kon worden. In deze studie vonden we dat gescheurde plaques goed met behulp van CTA bestudeerd kunnen worden en dat de plaques vaker scheuren aan de voorzijde van de plaque, wat in overeenstemming is met voorgaande studies. Omdat de voorkant van de plaque waarschijnlijk een hogere WSS ervaart, zou hoge WSS betrokken kunnen zijn bij de destabilisatie van de plaque. Om dit te onderzoeken hebben we de WSS en de locatie van ulcers bestudeerd in een groep patiënten (n=20) die met behulp van CTA in beeld zijn gebracht (**Hoofdstuk 3**). Hieruit bleek dat de ulcers voorkomen in het dikke gebied van het zieke vat ( $p < 0.05$ ) en dat er een trend is dat de WSS twee keer hoger is op de plek van ruptuur ( $p = 0.11$ ). Eenzelfde resultaat werd gevonden in een unieke casus waarbij seriële beeldvorming was uitgevoerd. Nadat een eerste beeldvorming van de plaque in de halsslagader was uitgevoerd met behulp van MRI, was er 10 maanden later een tweede MRI gemaakt van dezelfde plaque. Bij deze tweede MRI bleek dat de plaque gescheurd was en dat deze scheur precies was ontstaan op de locatie met hoge WSS die berekend was aan de hand van de eerste MRI zonder de ruptuur (**Hoofdstuk 4**).

Om de relatie tussen biomechanische krachten, zoals de WSS berekend met behulp van 3D reconstructies van niet-invasieve beeldvorming, en de compositie van aderverkalking, in detail te bestuderen is een nieuwe techniek ontwikkeld. Met deze gevalideerde methode is het mogelijk om histologische coupes te registreren met *in vivo* niet-invasieve beeldvorming. Door middel van deze methode kan de histologie van geopereerde plaques uit de halsslagader ruimtelijk geregistreerd worden met *in vivo* beeldvorming van vóór de operatie (**Hoofdstuk 5**). Daarbij kan met deze methode beeldgestuurde kwantificatie van de plaque compositie uit de halsslagader gevalideerd gaan worden. In **Hoofdstuk 6** hebben we gebruik gemaakt van deze registratie techniek om aan te tonen dat transglutaminases, een klasse van enzymen met diverse functies, aanwezig zijn in humane plaques uit de halsslagaders en co-lokaliseren met macrofagen (witte bloedcellen) en gecalcificeerde gebieden in de plaque.

Om patiënt-specifieke WSS te bepalen is naast de vorm van het vat, ook informatie over de doorbloeding van het vat nodig. Binnen een klinische omgeving kan het lastig zijn om deze metingen uit te voeren, daarom hebben we onderzocht wat de relatie is tussen de mate van vernauwing, als gevolg van de aderverkalking, en de doorbloeding van de halsslagader bij patiënten (**Hoofdstuk 7**). Het bleek dat tot een oppervlakte vernauwing van 65%, de plaque geen invloed lijkt te hebben op de doorbloeding van de halsslagader. Na dit punt neemt de doorbloeding door de interne halsslagader lineair af tot nul bij een 100% lumen vernauwing, terwijl de doorbloeding door de externe halsslagader onveranderd blijft ten opzichte van de instroming. Deze empirische relatie tussen de hoeveelheid doorbloeding en oppervlakte vernauwing kan gebruikt worden voor CFD simulaties wanneer patiënt-specifieke metingen van de doorbloeding niet beschikbaar zijn.

Om het causale verband te onderzoeken tussen hoge WSS en plaque instabiliteit, hebben we gebruik gemaakt van een muizen model met een instabiele plaque. In dit model hebben we kunstmatig de doorbloeding, en daardoor ook de WSS, verhoogd in de halsslagader waar een vergevorderde atherosclerotische plaque in aanwezig was. Hieruit bleek dat als gevolg van de verhoogde doorbloeding, het vetgehalte in de plaque verdubbelde. Dit resultaat geeft aan dat geavanceerde plaques kunnen reageren op veranderingen in WSS en dat een verhoogde WSS mogelijk resulteert in een meer instabiele plaque (**Hoofdstuk 8**).

Samengevat, in dit proefschrift is de relatie tussen de WSS, plaque samenstelling en plaque ruptuur onderzocht in de halsslagader. De resultaten impliceren dat WSS een rol speelt bij het destabiliseren van de plaque in het vergevorderde stadium van de ziekte. Echter, de onderliggende cellulaire en moleculaire mechanismen moeten nog verder onderzocht worden. Om dit te onderzoeken bij patiënten met aderverkalking is er een nieuwe 3D-histologie reconstructie methode ontwikkeld. Met behulp van deze methode is het mogelijk om histologische coupes van uitgenomen plaques te bestuderen naast niet-invasieve beeldvorming. Doordat deze beeldvorming gemaakt is vóór de operatie, kunnen deze beelden gebruikt worden voor het berekenen van de WSS. In vervolg experimenten kan deze methode gebruikt gaan worden om de invloed van biomechanische krachten op plaque samenstelling en ruptuur te onderzoeken.



## LIST OF PUBLICATIONS

### *Journal Papers*

**Harald Groen**, Frank Gijsen, Aad van der Lugt, Marina Ferguson, Thomas Hatsukami, Antonius van der Steen, Chun Yuan, and Jolanda Wentzel, Plaque rupture in the carotid artery is localized at the high shear stress region: a case report, *Stroke*, 2007;38(8):2379-81

**Harald Groen**, Frank Gijsen, Aad van der Lugt, Marina Ferguson, Thomas Hatsukami, Chun Yuan, Antonius van der Steen, and Jolanda Wentzel, High shear stress influences plaque vulnerability, *Netherlands Heart Journal*, 2008;16(7-8):280-3

Thomas de Weert, Sander Cretier, **Harald Groen**, Philip Homburg, Hamit Cakir, Jolanda Wentzel, Diederik Dippel, and Aad van der Lugt, Atherosclerotic plaque surface morphology in the carotid bifurcation assessed with multidetector computed tomography angiography, *Stroke*, 2009;40(4):1334-40

Hanke Matlung, **Harald Groen**, Judith de Vos, Theo van Walsum, Aad van der Lugt, Wiro Niessen, Jolanda Wentzel, Ed vanBavel, and Erik Bakker, Calcification locates to transglutaminases in advanced human atherosclerotic lesions, *American Journal of Pathology*, 2009;175 (4):1374-9

Alina van der Giessen, Michiel Schaap, Frank Gijsen, **Harald Groen**, Theo van Walsum, Nico Mollet, Jouke Dijkstra, Frans van de Vosse, Wiro Niessen, Pim de Feyter, Antonius van der Steen, and Jolanda Wentzel, 3D fusion of intravascular ultrasound and coronary computed tomography for *in vivo* wall shear stress analysis – A feasibility study, *International Journal of Cardiovascular Imaging*, 2009 Nov, *in press*

**Harald Groen**, Theo van Walsum, Sietske Rozie, Stefan Klein, Kim van Gaalen, Frank Gijsen, Piotr Wielopolski, Heleen van Beusekom, Rini de Crom, Hence Verhagen, Antonius van der Steen, Aad van der Lugt, Jolanda Wentzel, and Wiro Niessen, Three-dimensional registration of histology of human atherosclerotic carotid plaques to *in vivo* imaging, *Journal of Biomechanics*, 2010;43(11):2087-92

**Harald Groen**, Lenette Simons, Quirijn van den Bouwhuisen, Marielle Bosboom, Frank Gijsen, Alina van der Giessen, Frans van de Vosse, Antonius van der Steen, Jacqueline Witteman, Albert Hofman, Aad van der Lugt, and Jolanda Wentzel, MRI-based quantification of outflow boundary conditions for computational fluid dynamics of stenosed human carotid arteries, *Journal of Biomechanics*, 2010;43(12):2332-8

**Harald Groen**, Sietske Rozie, Frank Gijsen, Wouter Edeling, Thomas de Weert, Johan Reiber, Antonius van der Steen, Aad van der Lugt, and Jolanda Wentzel, Atherosclerotic plaque rupture in carotid arteries is associated with higher wall shear stress and plaque thickness, *submitted*

Jolanda Wentzel, **Harald Groen**, Alina van der Giessen, Rose van der Giessen, Gaston Rodriguez-Granillo, Frank Gijsen, Hans Schuurbijs, Antonius van der Steen, and Pim de Feyter, Plaque Free Wall Determines Positive Remodeling at 3 Year Follow-up: an IVUS Study, *submitted*

### *Conference Papers and Abstracts*

**Harald Groen**, Thomas de Weert, Frank Gijsen, Antonius van der Steen, Aad van der Lugt, and Jolanda Wentzel, Plaque Ulceration is Associated with High Shear Stress in Severely Stenotic Carotid Bifurcations, *JACC*, Chicago 2008;51(10 Suppl A):A135

**Harald Groen**, Thomas de Weert, Frank Gijsen, Antonius van der Steen, Aad van der Lugt, and Jolanda Wentzel, Plaque ulceration is associated with high shear stress in severely stenotic carotid bifurcations, *Proceedings of the 2008 Summer Bioengineering Conference ASME SBC 2008*, Marco Island, 2008

Jolanda Wentzel, **Harald Groen**, Rose van der Giessen, Gaston Rodriguez-Granillo, Frank Gijsen, Alina van der Giessen, Hans Schuurbijs, and Pim de Feyter, Vascular Remodeling During Atherosclerotic Plaque Build Up is Controlled by the Plaque Free Part of the Vessel Wall, *Proceedings of the 2008 Summer Bioengineering Conference ASME SBC 2008*, Marco Island, 2008

Alina van der Giessen, Frank Gijsen, Jolanda Wentzel, **Harald Groen**, Antonius van der Steen, and Frans van de Vosse, Comparison of Out-flow Condition Models on the Effect of Wall Shear Stress Calculations in Patient-specific Coronary Arteries, Proceedings of the 2008 Summer Bio-engineering Conference ASME SBC 2008, Marco Island, 2008

Jolanda Wentzel, **Harald Groen**, Rose van der Giesen, Gaston Rodriguez-Granillo, and Pim de Feyter, Plaque Free Wall Determines Positive Remodeling at 4 Year Follow-up: an IVUS Study, ESC 2008, Munchen. European Heart Journal 2008, 29 (Abstract Supplement), 237

Jolanda Wentzel, Hans Schuurbijs, Nieves Gonzalo Lopez, Frank Gijsen, Jurgen Ligthart, Alina van der Giessen, **Harald Groen**, Jouke Dijkstra, and Patrick Serruys, Abstract 4712: Necrotic Core Touching the Lumen is Most Frequently Exposed to High Shear Stress in Advanced Disease, Circulation 2010, 120: S990

Hanke Matlung, **Harald Groen**, Judith de Vos, Theo van Walsum, Aad van der Lugt, Wiro Niessen, Jolanda Wentzel, Ed vanBavel, and Erik NTP Bakker, Transglutaminases locate to calcified areas in advanced human atherosclerotic lesions, FASEB Journal 2010, 24: 116.2

### *Book Chapters*

Jolanda Wentzel, Frank Gijsen, Hans Schuurbijs, **Harald Groen**, Alina van der Giessen, Antonius van der Steen, and Patrick Serruys, "Why do we need flow measurements? Role of flow and shear stress in atherosclerotic disease", Handbook of OCT, Eds. Evelyn Regar, Ton van Leeuwen and Patrick Serruys 2007, ISBN: 978-1-84184-611-2

Jolanda Wentzel, Frank Gijsen, Rob Krams, Rini de Crom, Caroline Cheng, **Harald Groen**, Alina van der Giesen, Antonius van der Steen, and Patrick Serruys, "Vulnerable plaque and shear stress", Handbook of the Vulnerable Plaque (2nd ed), Eds. Ron Waksman, Patrick Serruys and Johannes Schaar, 2007, ISBN: 978-1-84184-621-7



## DANKWOORD

Dit proefschrift zou niet mogelijk zijn geweest zonder de inzet, hulp, ideeën, kritiek, steun en aanmoediging van heel veel verschillende mensen: van directe begeleiding tot aan hulp van verschillende afdelingen en studenten.

Als eerste wil ik Jolanda bedanken voor je direct en dagelijkse begeleiding, inclusief je nauwlettendheid op de voortgang van het project. Dit kwam dan vaak neer op het stoppen van mijn gepiel om sommige aspecten (te) perfect te krijgen. Bedankt voor al je tijd, energie en ideeën, een betere begeleiding van mijn project had ik me niet kunnen voorstellen. Ook Aad heel erg bedankt voor jouw visie en input voor het project, hierdoor bleef ik een sterke band houden met de klinische aspecten. Wiro, ook jou wil ik heel graag bedanken voor je inhoudelijke bijdrage en het rotsvast vertrouwen dat je gaf dat we een mooie “tool” gemaakt hadden. Ton heel erg bedankt voor jouw supervisie, nuchtere en praktische blik op mijn gehele promotie traject en de afronding ervan!

Vooraf tijdens de opstartfase van het project zijn Hans Reiber, Rini de Crom en Allard van der Wal nauw betrokken geweest waardoor de richting en invulling van het project vorm kon krijgen. Bedankt voor jullie (praktische) hulp en ideeën. Ook alle leden van de promotie- en leescommissie wil ik graag bedanken voor jullie tijd en dat jullie in mijn commissie plaats hebben willen nemen.

Ruim 4 jaar lang is het biomechanica “lab”(oratory) de plek geweest waar ik iedere dag met plezier naartoe ging. Frank, bedankt dat ik altijd terecht kon met vragen over de CFD, praktische vragen over (choco)flowmetingen of om te sparren over welke analyse methode “het beste” was. Alleen je koffie was wat aan de straffe kant voor mij... Hans, omdat jij zo’n beetje ervaring hebt met alle software die er maar is, kon ik bij jou altijd terecht met software problemen zoals Gambit (is niet gemaakt voor mm) of voor praktische oplossingen in Matlab (squeeze is erg handig), bedankt hiervoor! Alina, super bedankt voor jouw gezelligheid en levendigheid in het lab en je kritische vragen tijdens onze gezamenlijk promotietijd! Ik heb grote waarding voor je doorzettingsvermogen en veerkracht. En zeker, ook



ik heb warme herinneringen aan ons avontuur in Miami, het staat nog haast ingebrand in m'n rug! Een van de beste dingen tijdens mijn promotie is wel de komst van Kim geweest. Zonder jouw verse koffie 's ochtends, uitgebreide en gezellige verhalen en het vele labwerk wat je hebt verricht was het project niet zover gekomen als dat het nu is. Ondanks het gekraak denk ik met veel plezier terug aan onze snijacties! Helemaal super leuk dat je mijn paranimf wil zijn, wat moet ik zonder je!? Ali, many thanks for your (hovering) contribution in the lab the last year! It has been a privilege to meet you and to have the opportunity to "see" the Netherlands through your eyes. Ook wil ik graag Lambert bedanken, zeker voor de gezelligheid in Barcelona! Kim senior ;), al hebben we fysiek niet tegelijk in het lab gewerkt, graag wil ik je bedanken voor je bijdrage voor het laatste hoofdstuk! Verder is een hoop uitzoekwerk uitgevoerd door enthousiaste studenten, ik wil jullie graag bedanken voor je inzet, ideeën en oplossingen welke direct of indirect een bijdrage hebben geleverd.

Mieke heel erg bedankt voor het in goede orde laten verlopen van o.a. alle secretariële zaken die om de hoek komen kijken bij het promoveren. Miranda, Hans, Nico, Mike, Robert, Paul, Klazina, Annemiek en de alle andere medewerkers van de afdeling biomedical engineering, bedankt voor jullie interesse, vragen tijdens de dinsdagochtend presentaties, hulp waar nodig/mogelijk en gezellig labuitjes!

Het voordeel van een multidisciplinair project is dat je kan (en mag) samenwerken met mensen van verschillende afdelingen. De input van de afdeling radiologie is enorm geweest. Bij zo'n beetje ieder project was radiologie wel betrokken met de beeldvorming. Thomas, vooral in het begin heb je mij meegenomen in de wondere wereld van CT en contouren. Bedankt voor je gezellige samenwerking, jouw oplossingen en je contouren. Sietske heeft later het stokje overgenomen en aangevuld met MRI, weer een vak apart! Dank je wel voor de gezellige uurtjes (geknutsel) bij de MRI, je geregistreerde plaques en samenwerking. Philip bedankt voor het uitpluizen van alle patiënten statussen! Quirijn, enorm bedankt voor al jouw geïnvesteerde MRI uren en de overzichten waarmee je ons kon helpen patiënten te includeren.

Het hebben van een MRI scanner is geen garantie om (mooie) plaatjes te krijgen. Hiervoor heb je mensen nodig die in sequenties en k-space kunnen denken. Piotr, bedankt voor het maken van alle sequenties en meehelpen bij het scannen van de plaques! Gavin, many thanks for all your help in understanding the flow measurements and post processing!

Het maken van mooie beelden is één, maar het verwerken van de data is een heel ander vakgebied. Helemaal omdat deze beelden vaak meer informatie bezitten dan dat we zo met het oog kunnen zien. Theo bedankt voor de goede samenwerking en al je uren die je gependeed hebt in het meedenken, het maken van Mevis programma's voor de registratie taken en het registeren van plaques! Stefan, bedankt voor het verfraaien van dit mooie framework door het toevoegen van de niet-lineaire deformaties, met behulp van "enige" reverse-engineering. Ik heb fijn met je samengewerkt en hoop dat we dit in de toekomst kunnen herhalen! Het (automatisch) segmenteren van de vaten uit CTA data is geen makkie, zeker niet als ze erg vernauwd zijn... Rashindra, enorm bedankt voor al jouw uren scripten om jouw segmentatie algoritme ook voor deze data geschikt te krijgen. Verder wil ik ook graag alle andere collega's van de BIGR-groep bedanken voor alle hulp die ik van jullie gekregen heb.

Naast de intensieve samenwerking met de radiologie en de medische-informatica heb ik ook heel veel hulp gekregen van mensen van andere afdelingen. Beste Hencé Verhagen en collega's van de vaatchirurgie, bedankt voor jullie inzet om de plaques er heel uit te krijgen. Bedankt Jon Laman voor (praktische) immunologische hulp, Heleen van Beusekom bedankt voor jouw bijdrage in het project, zowel het meedenken als het gebruik van jullie apparatuur. Harrie Weinans, bedankt voor het gebruik van jullie  $\mu$ CT scanner, deze data blijken cruciaal in het registratie proces. Patricia bedankt voor je hulp tijdens de verbouwing zodat onze experimenten door konden gaan. Janine bedankt voor je tijd en hulp om mij te leren echoën. Dolf en Dennie, heel erg bedankt voor alle hulp (en scholing van mij) bij de labwerkzaamheden. Bedankt Pieter voor je hulp met immunohistologisch werk. Peter bedankt voor het gebruik van de NanoZoomer, dit heeft veel monnikenwerk voorkomen! Ed en Erik, ook jullie bedankt voor de goede samenwerking. Also, I would like to thank Chun Yuan and his group in Seattle for the corporation with the case report.

Ton, heel erg bedankt voor het in elkaar zetten van mijn proefschrift en het maken van de voorkant. Je hebt mij veel werk (en waarschijnlijk ook frustraties) uit handen genomen. Laraine, many thanks for reading and adjusting parts of my thesis, it made those sections much more readable!

Naast werk is er soms ook even tijd voor ontspanning op het werk, Cindy bedankt voor de gezellige koffiepauzes en lunches! Ook de koffiepauzes met de dames van de art-9 cursus waren aangenaam, zeker gezien de introductie van de Koekela, bedankt!

Ook alle (nieuwe) collega's van Nucleaire geneeskunde bedankt voor jullie interesse en de mogelijkheid om naast mijn nieuwe onderzoek nog de laatste dingen af te kunnen ronden van mijn proefschrift.

Mathieu super dat je mijn paranimf wil zijn, zelfs zonder dat je helemaal wist wat het precies was toen je "ja" zei! Een betere vriend kan ik me niet voorstellen, bedankt! Brenda ook jij heel erg bedankt voor je gezelligheid en interesse, hopelijk kunnen we de volgende vakantie(s) wel gewoon met jullie mee! Niek, bedankt voor de oude koeien die we zo nu en dan zitten te vissen uit het kanaal, ik kijk daar altijd naar uit!

Zonder een lieve familie die altijd achter je staat is promoveren eigenlijk een onbegonnen zaak. Lieve paps, bedankt dat je altijd geïnteresseerd bent in mijn werk en de artikelen die daaruit voortkomen en ook voor de mooie tekeningen in dit boekje! Lieve mams, bedankt dat je altijd voor me klaar staat en me helpt daar waar nodig en mogelijk is (zoals de punten en komma's). Zus, super leuk dat je er ook bij wilt zijn ondanks de afstand van ¼ maal de wereldomtrek, dat betekent veel voor me! Dank jullie wel!!! Juke, bedankt dat je altijd goed voor de (mijn) inwendige mens zorgt en Frank, bedankt voor al je goede verhalen!

Het is fijn als je 's ochtends met plezier naar je werk kan gaan, maar het is nog veel fijner als je aan het einde van de dag ook met veel plezier naar huis kan gaan. Lieve Hanke, dank je wel voor je liefde, gezelligheid, meedenken (en doen) en het vertrouwen dat het allemaal goed komt! Zonder jou was het een stuk zwaarder geweest, dat weet ik zeker. Volgend jaar jij nog en dan zijn we samen toe aan de volgende stap, we gaan er samen een mooi leven van maken lief!

## CURRICULUM VITAE

Harald Groen was born on August 24th 1978 in Haarlem. In 1997 he obtained his pre-university diploma at the Atheneum College Hageveld.

He studied Biomedical Engineering at the Eindhoven University of Technology (TU/e). For his master's thesis he investigated the remodeling of uterine vessels during pregnancy in mice. This project was carried out at the imaging group of the TU/e supervised by Bart ter Haar Romeny, in close collaboration with the department of Biophysics at Maastricht University supervised by Marc van Zandvoort, and the department of Vascular Pharmacology at Maastricht University supervised by Jo de Mey. In September 2005 he graduated from Eindhoven.

In July 2005 he started his PhD research project under the supervision of Jolanda Wentzel and Ton van der Steen at the department of Biomedical Engineering and Aad van der Lugt at the department of Radiology, both at the Erasmus MC in Rotterdam. In his project, he investigated the role of high wall shear stress in patients with advanced atherosclerotic plaques in the carotid bifurcation.

In February 2010 he started to work as a post-doc researcher at the department of Nuclear Medicine at the Erasmus MC in Rotterdam.



## PHD PORTFOLIO

<b>Courses</b>	<b>Date</b>	<b>ECTS</b>
NHS Vascular Biology (Papendal)	2005-09	2.0
Introduction to CFD, von Karman Institute	2006-01	1.5
Atherosclerosis Research	2006-04	1.5
Cardiovascular Imaging and Diagnostics	2006-04	1.5
CFD II, TU Delft	2006-11	1.5
Molecular Biology in Atherosclerosis and Cardiovascular Research	2007-06	1.5
English Biomedical Writing & Communication	2007-07	3.0
Proefdierkunde	2007-12	4.5
COEUR Research Seminar	2008-06	0.4
NHS Molecular Cardiology Program	2008-09	0.4
Regression Analysis ESP09	2008-10	1.5
Intensive <i>In Vivo</i> Imaging Course on Doppler & Vascular Imaging, Visual Sonics	2008-12	0.4
COEUR Research Seminar: Imaging of Carotid Bifurcation	2008-12	0.4
COEUR Research Seminar: PhD day	2009-05	0.4
<b>Supervision</b>	<b>Date</b>	<b>ECTS</b>
Internship HLO student (3 months)	2007-01	1.0
Graduation Project BSc Student InHolland (6 months)	2007-07	2.0

Graduation Project BSc Student InHolland (6 months)	2008-01	2.0
Graduation Project BSc Student InHolland (6 months)	2009-06	2.0

<b>Lectures</b>	<b>Date</b>	<b>ECTS</b>
3 <sup>rd</sup> International Symposium on Biomechanics in Vascular Biology and Cardiovascular Disease (Rotterdam)	2008-04	0.1
Presentation ICIN Project Day	2008-04	0.1
COEUR Research Seminar	2008-12	0.1
Dutch Conference of Bio-Medical Engineering (Egmond aan Zee)	2009-01	0.1

<b>Symposia and Congresses</b>	<b>Date</b>	<b>ECTS</b>
Wetenschapsdag NH (Amsterdam)	2005-10	0.4
1 <sup>st</sup> symposium on Biomechanics in Cardiovascular Disease: Shear Stress in Vascular Biology (Rotterdam)	2006-01	0.8
Dutch Atherosclerosis Society Cardiovascular Biology Meeting (Ermelo)	2006-03	0.8
Vascular Pharmacology (Noordwijkerhout)	2006-06	1.2
Dutch Conference of Bio-medical Engineering (Egmond aan Zee)	2007-01	0.8
Dutch Atherosclerosis Society Cardiovascular Biology Meeting (Ermelo)	2007-04	0.8

2 <sup>nd</sup> Symposium in Biomechanics in Cardiovascular Disease: Shear Stress in Vascular Biology (Rotterdam)	2007-04	0.8
Dutch Atherosclerosis Society Cardiovascular Biology Meeting (Ermelo)	2008-04	0.8
3 <sup>rd</sup> International Symposium on Biomechanics in Vascular Biology and Cardiovascular Disease (Rotterdam)	2008-04	0.8
American College of Cardiology (Chicago)	2008-06	0.8
ASME Summer Bioengineering Conference (Marco Island, Florida)	2008-06	1.2
Dutch Conference of Bio-Medical Engineering (Egmond aan Zee)	2009-01	1.6
4 <sup>th</sup> International Symposium on Biomechanics in Vascular Biology and Cardiovascular Disease (Rotterdam)	2009-04	0.8
European Society of Cardiology (Barcelona)	2009-08	1.2
5 <sup>th</sup> International Symposium on Biomechanics in Vascular Biology and Cardiovascular Disease (Rotterdam)	2010-04	0.8



